ABSTRACT

LIANG, HUIXUAN. The Specificity Protein 2 (Sp2) in the Proliferation and Cell Cycle Progression of the Neural Progenitors. (Under the direction of Dr. Troy Ghashghaei).

Neural progenitor cells give rise to neurons in the embryonic brain. Additionally, a few progenitor cells persist and are neurogenic in restricted regions of the postnatal and adult brain. Mechanisms that control the proliferation of progenitors are important for appropriate production of new neurons in the embryonic and postnatal brain. The longevity and developmental potential of stem cells is closely linked to molecular mechanisms that control the rate and fidelity of the cell cycle. Using neural stem cells as a platform with genetic, cellular, and biochemical assays I demonstrate that a zinc-finger transcription factor Specificity Protein 2 (Sp2) is a key regulator of the cell cycle. Conditional genetic loss-of-function approach was employed to delete Sp2 in neural progenitors, revealing a specific disruption in G2/M transition, M phase duration and rate of cell cycle exiting. Cell autonomous function of Sp2 was identified by mosaic deletion of Sp2 using Mosaic Analysis of Double Markers on chromosome 11 (MADM-11) in combination with time-lapse imaging, which clearly establishes Sp2 as a key regulator of progression through the M phase. Sp2 localizes to the nucleus but surprisingly is also a stable component of the centrosomal complex. Sp2-bound centrosomes are shuffled between perinuclear loci and the intercellular bridge during cytokinesis. In the absence of Sp2 this shuffling is excessive and abscission at the final stage of cytokinesis is defective. Importantly, conditional deletion of Sp2 leads to a decline in the generation of intermediate neural progenitor cells and neurons in the developing and postnatal brains. Our findings implicate Sp2-dependent mechanisms as novel

regulators of cell cycle progression, the absence of which disrupts neurogenesis in the embryonic and postnatal brain.

The Specificity Protein 2 (Sp2) in the Proliferation and Cell Cycle Progression of the Neural Progenitors

by
Huixuan Liang

A dissertation submitted to the Graduate Faculty of
North Carolina State University
in partial fulfillment of the
requirements for the degree of
Doctor of Philosophy

Physiology

Raleigh, North Carolina

2013

APPROVED BY:

_____	_____
Dr. Troy Ghashghaei Committee Chair	Dr. Jonathan Horowitz
_____	_____
Dr. David Threadgill	Dr. Marcelo Rodriguez-Puebla

BIOGRAPHY

Huixuan Liang was born in Zhongshan, China in 1984. In 2008, she got her bachelor's degree in Veterinary Medical Sciences from Nanjing Agricultural University in China. She then joined the graduate program in Molecular Biomedical Sciences, College of Veterinary Medicine at North Carolina State University to pursue a doctoral degree. Her thesis dissertation was under the direction of Dr. Troy Ghashghaei.

ACKNOWLEDGMENTS

I would like to give special thanks to my advisor Dr. Ghashghaei for his guidance and continuous supports. This work would not have been possible without the generous gift of genetic mice developed by my committee member Dr. Jon Horowitz and his graduate student Haifeng Yin. I also would like to thank my other committee members Drs. David Threadgill and Marcelo Rodriguez-Puebla for their insightful suggestions to my projects. Finally I am very grateful to my family and friends for having given me support and encouragement.

TABLE OF CONTENTS

LIST OF FIGURES

LIST OF ABBREVIATIONS

SP2: Specificity Protein 2

NSC: Neural stem cell

NPC: Neural progenitor cell

NE: Neuroepithelial cell

RG: Radial glial

IPC: Intermediate progenitor cell

TAP: Transit amplifying progenitor

VZ: Ventricular zone

SVZ: Subventricular zone

MZ: Marginal zone

PPL: Preplate layer

SEZ: Subependymal zone

RMS: Rostral migratory stream

OB: Olfactory bulb

ICB: Intercellular bridge

BrdU: Bromodeoxyuridine

BACKGROUND

Cell cycle regulation and neural development

The cell cycle is an essential process in proliferation and differentiation of eukaryotic cells. Timely and coordinated progression through the cell cycle requires complex signaling networks controlling duration of its distinct compartments as well as rate of cell cycle exiting and re-entering. The eukaryotic cell cycle comprises of four successive phases: Gap 1 (G1), synthesis (S), Gap 2 (G2) and the mitotic (M) phases. G1 is a critical stage in which cells assess whether to proceed through the cell cycle or to exit based on intrinsic and environmental cues (reviewed by Foster et al., 2010; Zetterberg et al., 1995). DNA is replicated during S and the replicated genetic material is later segregated into the nascent daughter cells during M (reviewed by Takeda and Dutta, 2005; Walczak et al., 2010). G2 serves as a safeguard against aberrant DNA replication and preserves genomic integrity before commitment into M (reviewed by Wang et al., 2009b).

In the developing brain, cell cycle regulation is required for proper growth of neural progenitor pools through control of cellular proliferation and expansion. On the other hand, timely control of cell cycle exiting is required for neuronal generation and differentiation. Disruption of the cell cycle often causes abnormal brain development, as exemplified in conditions such as microcephaly, and is implicated in various other neurodevelopmental disorders that result in mental retardation (reviewed by Wang et al., 2009a; Woods et al., 2005). Less severe or subtle defects in cellular proliferation or neuronal expansion result in other neurodevelopmental disorders such as the spectrum of autism disorders and

schizophrenia (Fan et al., 2012; Ito and Rubin, 1999; Katsel et al., 2008). Despite its important functional implications, how cell cycle progression is regulated during normal brain development and how disturbances of cell cycle machinery lead to neuronal disorders remains remarkably understudied.

Embryonic and adult neural stem cells are proposed as promising therapeutic targets for regenerative and/or repair in future therapeutic approaches. However, prior to utilization of stem cells it is imperative that we understand the molecular mechanisms that govern neural stem cell proliferation and diversification. The primary goal of the research conducted in this dissertation is to determine the regulation of proliferation and cell cycle progression in embryonic and adult neural progenitors.

To understand mechanisms underlying brain development one must understand the intricate organization of this tissue during various ages. Descriptive cellular organization in the rodent brain has been thoroughly studied as a model for mammalian brain development over the last century. Rodents are particularly useful because of their short gestation period and rapid establishment of the general organization of the brain. It is noteworthy that the general temporal and spatial patterns of developmental events are closely related in rodents and higher mammalian species (reviewed by Lui et al., 2011).

Active neurogenesis occurs predominantly during embryonic development in all mammalian species. After birth, the vast majority of progenitor domains become dormant (except in two restricted regions, see later) (reviewed by Kriegstein and Alvarez-Buylla, 2009). Function and lineage progression in both embryonic and postnatal progenitors will be introduced with particular emphasis on neural progenitors in the developing cerebral cortex,

a system that has drawn intensive investigation and is relatively well characterized. However, it is important to mention that basic principles underlying progenitor proliferation and neuronal expansion are highly conserved during embryonic and postnatal neurogenesis (reviewed by Ming and Song, 2011), and that our understandings in the developing cerebral cortex can be applied to other regions of the central nervous system in general (reviewed by Kriegstein and Alvarez-Buylla, 2009).

Neural progenitors during embryonic cortical development: keeping the balance between proliferation and differentiation

The central nervous system including the brain and spinal cord is derived from the neural tube, a structure formed by closure of the ectoderm in the early vertebrate embryo (Sadler, 2005) (Fig. 1). Prior to neurogenesis, the neural tube contains pseudostratified neuroepithelial cells (NEs) which extend thin processes to the apical ventricular surface facing the lumen of neural tube and to the basal outer surface of neural tube (Fig.1). However, the cell bodies of NEs are retained in the apical aspect of the ventricular zone (VZ) (Fujita, 1960) (Fig. 1).

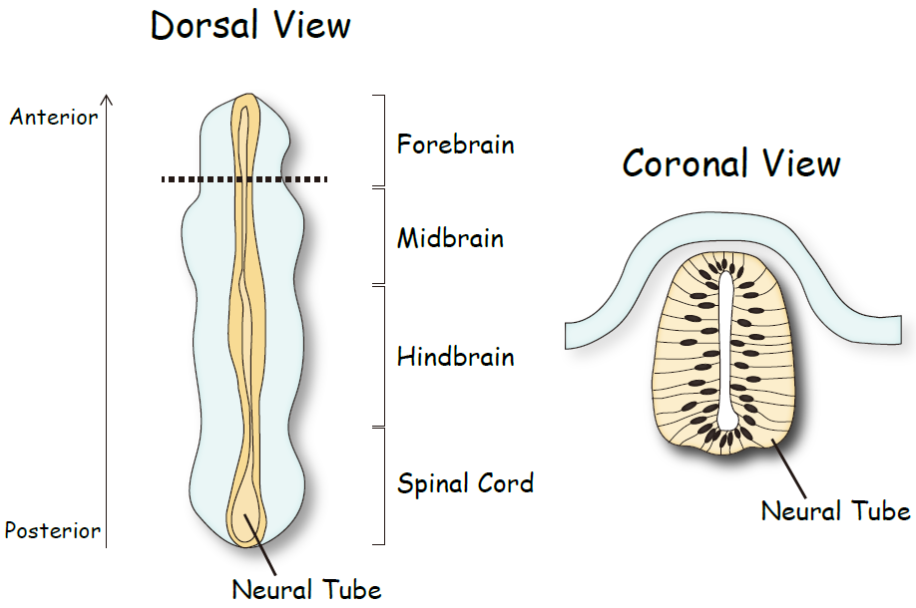

Figure 1: Neural tube formation. Dorsal view of the neurulating embryo (left) and coronal view of the neural tube (right). The position of the coronal view is indicated by dash line in the dorsal view.

During early growth of the neural tube, NEs primarily divide symmetrically to generate two NEs which facilitate rapid expansion in neural progenitor pools during early brain development (Fig.2) (Cayouette, 2003; Saito et al., 2003). NEs essentially function as embryonic neural stem cells and undergo a differentiation process throughout embryonic development. By birth, most of these cells transform into glial and ependymal cells which perform important barrier functions at the ventricular and endothelial interphases of the postnatal and adult brain (reviewed by Kriegstein and Alvarez-Buylla, 2009).

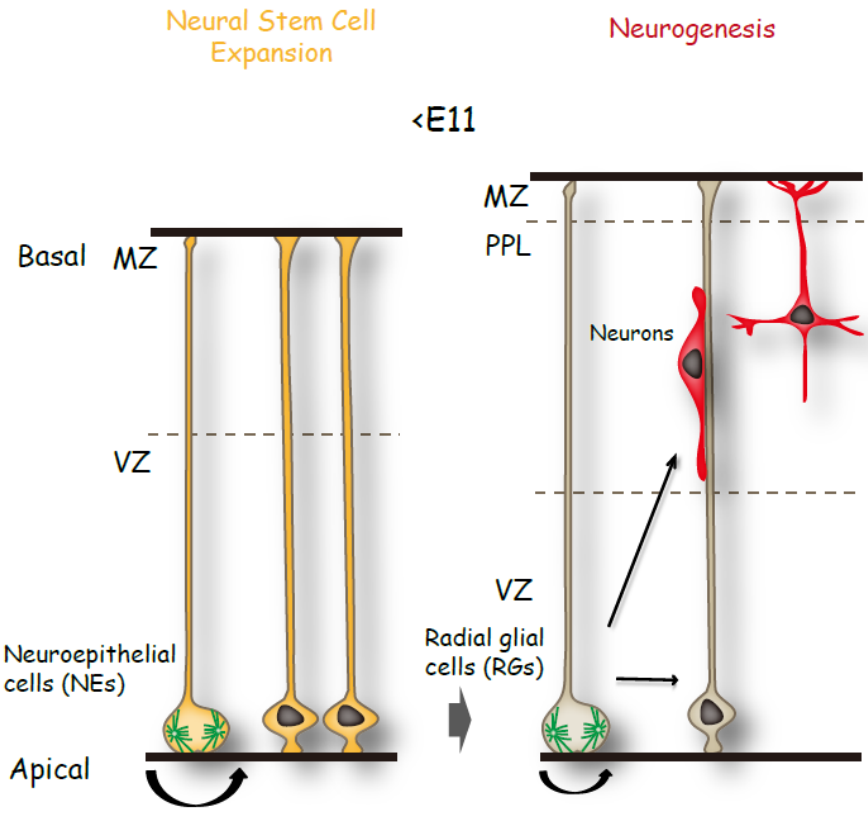

Figure 2: NE and RG division during cortical development. NEs undergo symmetric division to generate two NEs. During the onset of neurogenesis, NEs transform into RGs, which begin asymmetric divisions to generate neurons. NEs: neuroepithelial cells; RGs: radial glial cells; VZ: ventricular zone; MZ: marginal zone; PPL: preplate layer

Following an expansive round of divisions during early brain development, NEs transform into radial glial cells (RGs) and begin the first set of neurogenic divisions in the developing central nervous system (Fig. 2). Both cell types contain a number of common molecular features, such as expression of the intermediate filament protein Nestin, which is

commonly present in many progenitors throughout the developing body (Anthony et al., 2004; Lendahl et al., 1990). Moreover, RGs continue to display an apico-basal polarity similar to NEs, with processes expanding through the entire thickness of developing brain tissue (Fig. 2) (Malatesta et al., 2000; Noctor et al., 2002). Unlike early NEs, RGs begin to express several other proteins that can be used as markers for this more differentiated stage such as the brain lipid-binding protein (BLBP) and the glutamate transporter (GLAST) (Hartfuss et al., 2001; Kurtz et al., 1994). The most prevalent difference that emerges between the two cell types is the lineally restricted neurogenic potential of RGs compared to the more multipotent characteristic of NEs.

Given their typical morphology (radial processes spanning the entire wall of developing cortices), RGs were initially recognized as guide cells for neuronal migration during embryonic brain development (reviewed by Hatten, 1999). It was not until the end of the last century when RGs were shown to function as neural stem cells, possessing both neurogenic and gliogenic potential. Using fluorescence activated cell sorting for RGs followed by clonal analysis in vitro, Magdalena Gotz's group demonstrated that isolated RGs could generate neurons and glial cells (reviewed by Malatesta et al., 2000). Subsequent ex-vivo time-lapse imaging of cortical slices directly demonstrated that RGs generate both neurons and secondary neural progenitors (described below). RGs undergo a highly coordinated interkinetic nuclear migration during which their nuclei transition up and down the apico-basal axis of the VZ in remarkable coordination with different stages of the cell cycle. Specifically, RGs that enter G1 move from the apical toward the basal aspect of the VZ. Once there, RGs transition into S and G2 phases while diving back down toward the

apical VZ. Remarkably, mitotic round-up primarily occurs apically when the soma of RGs comes in contact with the lumen of the ventricles (Miyata et al., 2001; Noctor et al., 2001; Sauer, 1935). At this stage, RGs remain polarized with a basal process that extends to the pial surface (Fig. 2) (Götz et al., 2002; Miyata et al., 2001; Noctor et al., 2001; Weissman et al., 2003).

Generation of neurons from RGs begins around embryonic day E10.5 in the mouse cerebral cortex. Unlike NEs which mostly divide symmetrically, RGs largely undergo asymmetric divisions. Asymmetric neurogenic divisions generate a RG and a neuron while proliferative asymmetric divisions generate a RG and a secondary neural progenitor (Miyata et al., 2001, 2004; Noctor et al., 2001, 2004) (Fig. 2). Newborn neurons that are derived from RG divisions migrate towards the cortical plate along basal processes of RGs, which exhibit molecular characteristics that allow them to function as substrates for neuronal migration (Noctor et al., 2008; Schmid et al., 2004). Neurons in the developing cerebral cortex are diverse with many different neuronal cell types possessing unique morphological, molecular, and functional characteristics (reviewed by Molyneaux et al., 2007). Specific subsets of neurons occupy different layers of cerebral cortex and it had been documented for decades that early-born neurons occupy lower layers while late-born neurons settle in the upper layers (Fig.3) (Rakic, 1974). Previously, it was thought that subtypes of neurons are specified at the time of their birth through a progressive restriction in neurogenic potentials of various RGs (Frantz and McConnell, 1996; McConnell and Kaznowski, 1991; Mizutani and Saito, 2005). For example, early RGs are multipotent with the capacity to generate late-born neurons when transplanted into the older host brains (McConnell and Kaznowski,

1991). In contrast, older RGs are fate restricted and fail to generate early-born neurons when transplanted into younger embryonic brains (Frantz and McConnell, 1996; Mizutani and Saito, 2005). However, this model was recently challenged by findings from Ulrich Mueller's group using modern genetically based lineage tracing techniques in vivo. They found that a subset of RGs is restricted to generate late-born neurons even at the earliest stages of neurogenesis (Franco et al., 2012). These findings suggest that RGs can be intrinsically specified to generate certain subtypes of neurons, regardless of their birthdate. Finally, although RGs are multipotent with both neurogenic and gliogenic potential, neurogenesis largely precedes gliogenesis. In mice, neurogenesis massively declines upon birth concomitant with an increase in gliogenesis (reviewed by Kriegstein and Alvarez-Buylla, 2009). The differential timing for neural and glial production is likely to be cell-intrinsic, as isolated cortical progenitors generated neurons prior to glial cells (Qian et al., 2000).

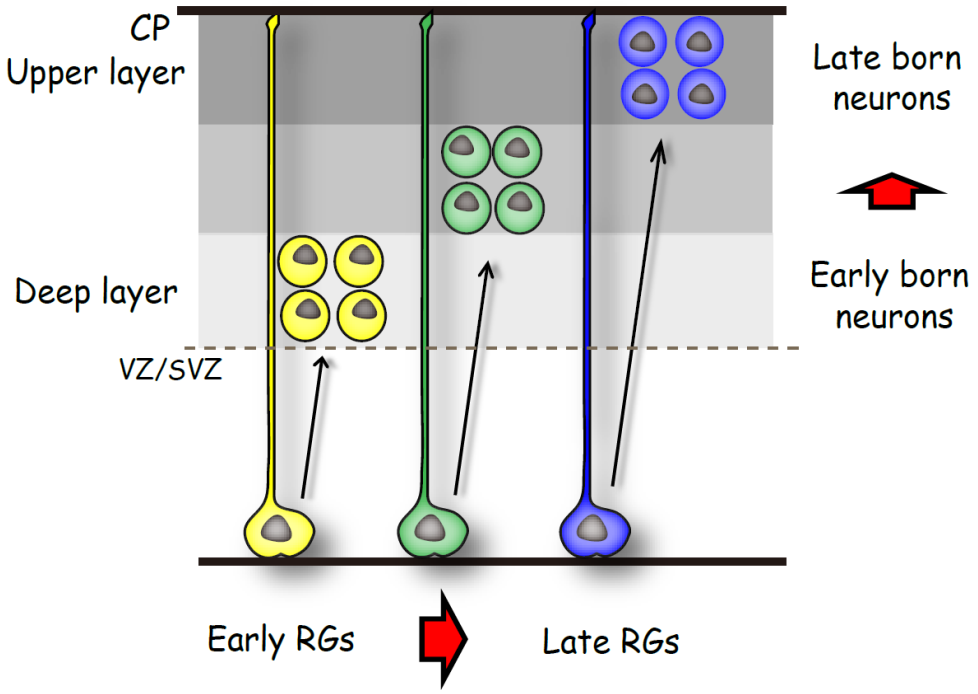

Figure 3: Laminar development of the cerebral cortex. Early-born neurons generated from RGs target deeper layers of the CP, and late-born neurons migrate past early-born neurons to settle in the upper layers. RGs: radial glial cells; VZ: ventricular zone; SVZ: subventricular zone CP: cortical plate

Past studies have established methods for isolation of cortical progenitors during embryonic neurogenic stages and analysis of their division patterns in vitro. These studies have clearly demonstrated the coexistence of symmetric and asymmetric neurogenic divisions in RGs (Qian et al., 1998, 2000; Shen et al., 2002). There is also evidence from evolutionary studies that the expansion of the mammalian cortex likely involved the

expansion of an intermediate population of progenitors, which are postulated to have helped rapidly generate large pools of neurons through terminal symmetric divisions (reviewed by Kriegstein et al., 2006). These intermediate progenitor cells (IPCs) divide in the subventricular zone (SVZ), as was reported decades ago (Smart, 1972, 1973). Using retro-viral labeling/Dil labeling followed by time-lapse analysis, several groups found that IPCs arise from RG divisions in the apical VZ, migrate basally, and unlike RGs, undergo mitosis in the SVZ (Haubensak et al., 2004; Miyata et al., 2004; Noctor et al., 2004) (Fig.4). In addition to their location, several features distinguish IPCs from RGs and NEs. IPCs display multipolar processes and do not form adherent contacts with the ventricular or pial surfaces. Moreover, IPCs almost exclusively undergo symmetric divisions during which one IPC either self-renews to generate two IPCs or generates two neurons (Fig.4). In the developing mouse cortex, the vast majority of symmetric divisions from IPCs (90%) are neurogenic (Noctor et al., 2004; Wu et al., 2005). Thus generation of neurons from a single parent neural stem cell are amplified through IPCs and this process is proposed to largely determine the size of distinct neuronal populations, which ultimately impact cortical size and evolutionary expansion in higher mammal brains (reviewed by Kriegstein et al., 2006).

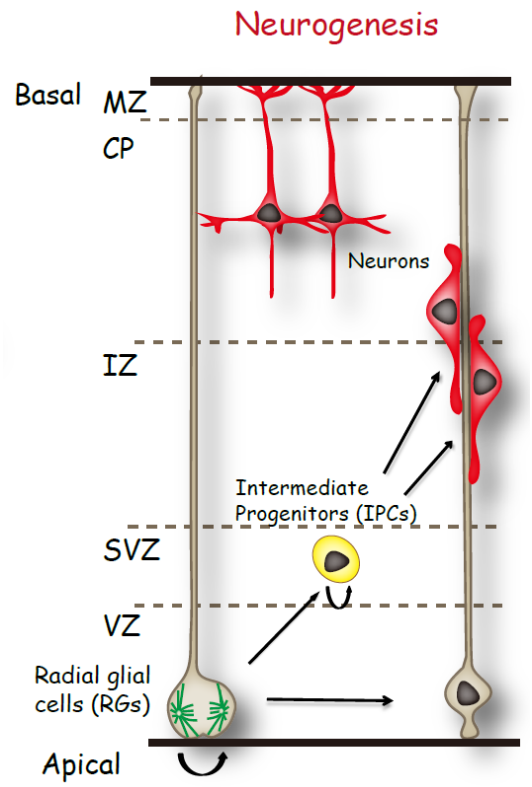

Figure 4: Generation of IPCs during cortical development. RGs can undergo asymmetric division to generate one RG and one IPC. Majority of IPCs undergo symmetric division to generate two neurons. RGs: radial glial cells; IPCs: intermediate progenitors; VZ: ventricular zone; SVZ: subventricular zone; IZ: intermediate zone; CP: cortical plate; MZ: marginal zone

Subcellular events underlying cell cycle progression in neural progenitors

A delicate balance between proliferation and differentiation of neural progenitors is critical for appropriate production and specification of neurons (reviewed by Farkas and

Huttner, 2008). Maintenance of this balance is tightly linked to cell cycle machinery. Proliferation is essentially the process when neural progenitors proceed through the cell cycle for reproduction and cellular division. On the other hand, neural progenitors must exit the cell cycle in a timely manner for terminal differentiation. To begin to understand how the cell cycle couples with progenitor functions during brain development, one must first understand the core features associated with cell cycle progression.

Dramatic changes in structural components of cycling progenitors occur during cell cycle progression. These sub-cellular events initiate according to a precisely controlled schedule and are critical for transition within various cell cycle stages: when delays and errors occur in one event, subsequent events can be postponed or abolished (reviewed by Sullivan and Morgan, 2007). In mammalian neural progenitors, sub-cellular events underlying cell cycle progression have been relatively well characterized in the cortical progenitors and thus will be focused below. NEs and RGs undergo mitosis at the apical ventricular surface and therefore are collectively referred to as apical progenitors (Miyata et al., 2001; Noctor et al., 2001; Sauer, 1935). Apical progenitors possess a primary cilium at their apical surface which is in contact with the cerebrospinal fluid in the lumen of the neural tube and later the cerebral ventricles (Fig. 5) (Dubreuil et al., 2007; Hinds and Ruffett, 1971; Spear and Erickson, 2012).

Primary cilia are microtubule-based protrusions of the plasma membrane, and important organelles specialized to respond to environmental signals underlying brain development (Louvi and Grove, 2011; Pazour and Witman, 2003). The cilium undergoes a repeated cycle of assembly and disassembly during distinct stages of the cell cycle: it

assembles in the G1 phase and its disassembly initiates during S-phase entry and completes during the G2/M transition (Li et al., 2011; Spear and Erickson, 2012). The dynamics of cilia construction impact cell cycle progression. For example, ciliary disassembly is mediated by a subunit of cytoplasmic dynein called Tctex-1, and blocking recruitment of Tctex-1 to the cilium for initiation of ciliary disassembly inhibits S-phase entry and accelerated cell cycle exiting in RGs. Conversely, acceleration of cilium disassembly increases S-phase entry and progenitor proliferation (Li et al., 2011). These findings provide a novel perspective that molecular and structural changes in the cilium are sufficient to switch neural progenitors between cell cycle exiting and re-entering, although the mechanisms remain largely unknown. The primary cilium is assembled from mother centrioles during G1 (Seeley and Nachury, 2010). Prior to centrosome duplication, each centrosome contains an older "mother" centriole and a younger "daughter" centriole. Mother centrioles are synthesized earlier than daughter centrioles and possess structural components that bear specific proteins to anchor microtubules and support ciliogenesis (Anderson and Stearns, 2009; Bornens, 2002; Curtis et al., 2007). The centrosomes replicate once cells enter the S phase using the pre-existing centrioles as a template. This process generates two centrosomes, with each one retaining the original mother centriole (mother centrosome) and the other containing the original daughter centriole (daughter centrosome) (Nigg and Stearns, 2011). Prior to mitosis, the duplicated pair of centrosomes remains near the apical surface of progenitors, possibly through association of the primary cilium and the mother centriole from which they assemble (Fig. 5). Ciliary disassembly before mitosis releases centrosomes from the apical surface which allows the subsequent movement of centrosomes toward the nucleus (Spear and

Erickson, 2012). Progression through the M phase is highly complex and cells undergo dramatic and relatively rapid structural and molecular changes. These changes occur in a strict order which further divide M phase into different stages (Sullivan and Morgan, 2007).

The rapid movement of centrosomes toward the nucleus coincides with nuclear envelope breakdown, which together with chromosome condensation mark the initial stage of the M phase termed prophase (Spear and Erickson, 2012) (Fig. 5).

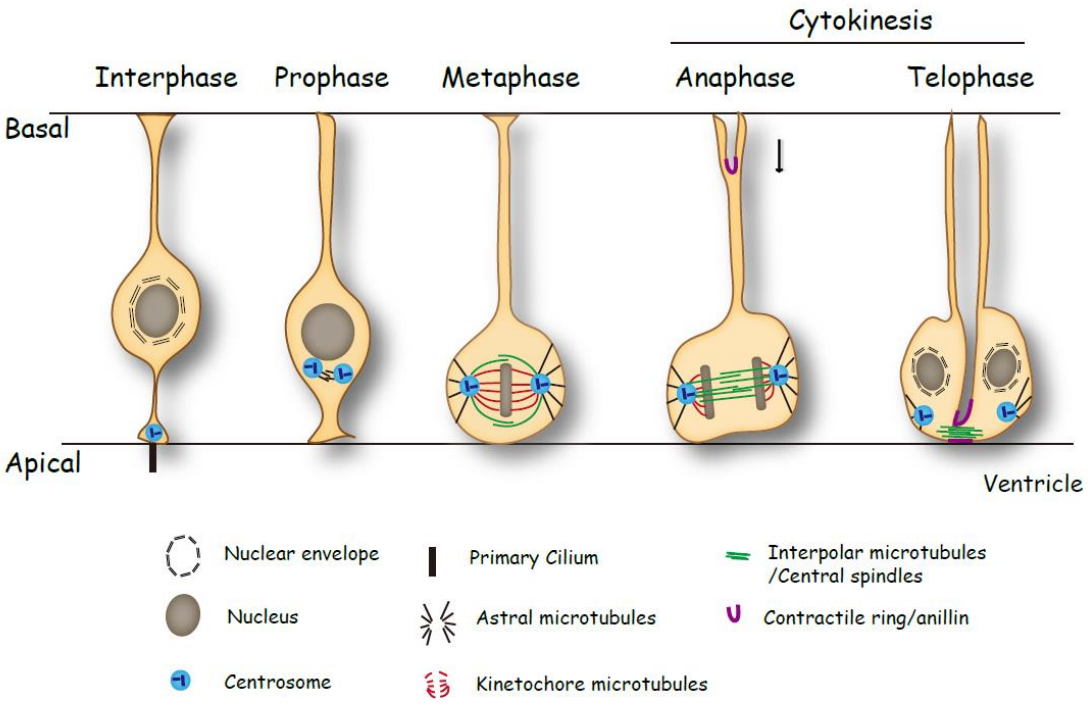

Figure 5: Subcellular events underlying neural progenitor cell cycle progression.

During prophase, microtubules gradually assemble from each duplicated centrosome resulting in the formation of a mitotic spindle, a microtubule/centrosome based machine that

physically mediates chromosome segregation (Sharp et al., 2000). For decades the centrosomes and their associated microtubules have been proposed to associate with nuclear envelope breakdown in mammalian somatic cells (Güttinger et al., 2009). Electron microscopy revealed that centrosomes, together with their associated microtubule bundles, protrude deeply into the nucleus during prophase (Georgatos et al., 1997; Robbins and Gonatas, 1964). During late G2 and prophase, a number of cytoplasmic dyneins are recruited to the invagination site, pulling apart the microtubules from both centrosomes and promoting mechanical shearing of the nuclear envelope (Beaudouin et al., 2002; Salina et al., 2002). Interestingly, the same outward pushing force on microtubules exerted by envelope-associated dyneins is also required for separation of duplicated centrosomes (Raaijmakers et al., 2012).

During the next progressive step of the M phase (prometaphase), centrosomes nucleate kinetochore microtubules which contact chromosomal centromeres and direct the alignment of duplicated chromosomes during metaphase (Fig.5). The centrosomes also generate astral microtubules that radiate out to anchor the inner face of the plasma membrane in the cell cortex. Additionally, interpolar microtubules from both centrosomes form antiparallel bundles in the center of mitotic cells (Fig.5) (Rusan et al., 2001). The dynamic polymerization and depolymerization of microtubules as well as their interactions with various proteins are required for proper alignment and ultimate separation of chromosomes during telophase. For example, the centrosome-associated proteins Abnormal Spindle-like Microcephaly-associated (ASPM), Magoh, and CDK5 regulatory subunit-associated protein 2 (CDK5RAP2) are required for microtubule assembly. Genetic deletion of each of these

proteins in neural progenitors disrupts mitotic spindle integrity and chromosome alignment (Fish et al., 2006; Silver et al., 2010; Yingling et al., 2008). In addition, interactions of astral microtubules with the cell cortex impact the positioning of chromosomes. For example, astral microtubules are anchored to the cell cortex in neural progenitors by a dynein associated complex of proteins (Yingling et al., 2008). Genetic deletions of dynein-associated proteins Lis1 and Nde1 cause spindle disorientation in cortical neural progenitors (Faulkner et al., 2000; Feng and Walsh, 2004a). Mechanism of this function may be extracted from studies in non-neural cells, in which the dynein complex Lis1 is first anchored to the cell cortex through the membrane bound G protein α subunit. Lis1 then mediates microtubule sliding towards the cell cortex, which in turn generates a pulling force on the microtubule attached chromosomes (Laan et al., 2012; Nguyen-Ngoc et al., 2007).

Separation of sister chromatids begins at anaphase and is completed during telophase (Fig.5) (Dubreuil et al., 2007; Kosodo et al., 2004). During the same period, the nuclear envelope reforms around segregated chromatids in each daughter cell to establish two distinct nuclear boundaries (Hebbar et al., 2008). During anaphase, interpolar microtubules reorganize to form a dense array of antiparallel microtubules termed the central spindle (Fig.5) (Dubreuil et al., 2007). How the central spindle is formed in neural progenitors is unknown, but likely utilizes mechanisms similar to those discovered in non-neuronal cells. Demonstrated in mammalian cell lines, factors that control central spindle assembly are recruited to interpolar microtubules during anaphase (reviewed by Glotzer, 2009). Such factors include a microtubule associated protein PRC1 (regulator of cytokinesis 1), which localizes to the central spindle and induces microtubule bundling (Fig.6) (Mollinari et al.,

2002; Zhu and Jiang, 2005). Another set of important factors that controls central spindle assembly is a motor complex termed Centralspindlin, which consists of a kinesin motor protein MKLP1 and a Rho GTPase-activating protein MgcRacGAP (Fig.6) (Mishima et al., 2002; Pavicic-Kaltenbrunner et al., 2007). Similar to PRC1, localization of Centralspindlin to interpolar microtubules induces robust bundling of antiparallel microtubules at the midzone (Mishima et al., 2002). In normal animal cells, assembly of central spindles utilizes preexisting microtubules as a template (Canman et al., 2000). However, central spindles can assemble *de novo,* when microtubule polymerization is inhibited by drugs or when centrosomes are physically removed by laser ablation (Alsop and Zhang, 2003; Canman et al., 2000). These findings suggest that in the absence of centrosomes, central spindle formation adopts self-assembling machinery, although the mechanisms involved in this process remain unknown.

Formation of the central spindle leads to initiation of cytokinesis, during which the cytoplasm and membrane between the two newly formed daughter cells are actively cleaved (reviewed by Green et al., 2012). Cytokinesis begins with specification of a cleavage initiation site, a narrow territory of the plasma membrane within the central spindle region. In the cleavage initiation site, the GTPase RhoA is switched from its GDP-bound inactivated state to a GTP-bound activated form (Kimura et al., 2000). Activation of RhoA can be mediated through the GTPase exchange factor Ect2, which is recruited by Centralspindlin to the central spindles near cleavage sites (Fig. 6) (Kimura et al., 2000; Nishimura and Yonemura, 2006; Su et al., 2011). Once activated RhoA directs assembly and constriction of a contractile ring that consists of a filamentous network of actin filaments and actin

associated proteins (Green et al., 2012) (Fig.6). For example, the actin scaffolding protein anillin is recruited to the contractile ring through interaction with the activated RhoA (Fig.6) (Hickson and O'Farrell, 2008; Piekny and Glotzer, 2008). Moreover, an effector enzyme Citron kinase is activated by RhoA, which in turn phosphorylates the regulatory light chain of myosin II to mediate further constriction of the contractile ring (Fig.6) (Bassi et al., 2013; Hickson and O'Farrell, 2008). The contractile ring constricts the plasma membrane and initiates cleavage furrow ingression (Green et al., 2012). Although the mechanisms that control neural progenitor cytokinesis remain largely unexplored, these regulatory molecules are likely to be conserved. For example, both RhoA and Citron kinase localize to the contractile ring of apical progenitors in the developing cortex (Sarkisian et al., 2002). Moreover, in citron kinase mutants localization of RhoA to the contractile ring is abolished and cytokinesis fails resulting in a multinucleated cellular phenotype (Sarkisian et al., 2002).

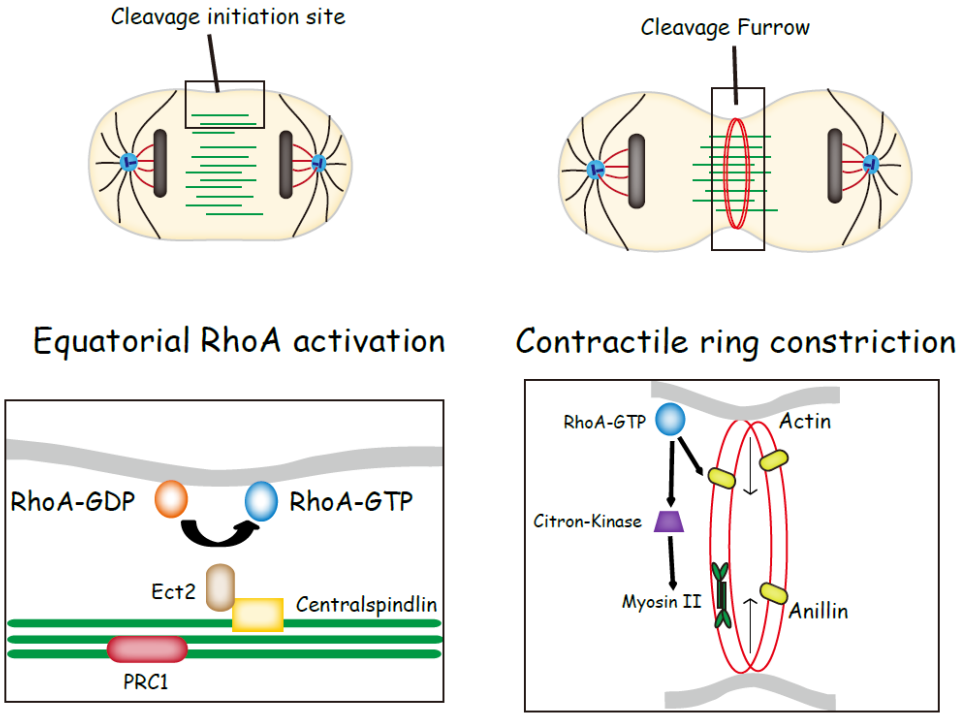

Figure 6: Cleavage site initiation and cleavage furrow formation in non-neural cells. Cytokinesis begins with specification of a cleavage initiation site, where RhoA is switched from its GDP-bound inactivated state to a GTP-bound activated state. Activation of RhoA can be mediated through the GTPase exchange factor Ect2, which is recruited by Centralspindlin to the central spindles. Once activated, RhoA recruits the actin scaffolding protein anillin to the cleavage site for contractile ring assembly. An effector enzyme Citron kinase is activated by RhoA, which in turn phosphorylates the regulatory light chain of myosin II to mediate further constriction of the contractile ring.

Despite postulated similarities in mechanisms of cytokinesis within neural and non-neural progenitors, there are also important differences. For example, the presence of a long ascending process in apical progenitors is an important differentiating factor between much

of what is known regarding cytokinesis in cell lines versus what happens in vivo in complex tissues such as the developing brain. Relatively recent studies utilizing time-lapse imaging of genetically labeled RGs have revealed that cytoplasmic division of the basal process of apical RGs precedes active cytokinesis in the cell body of the same cell during anaphase. This division of the basal process can be visualized by a branching point between the newly segregated processes (Fig.5) (Kosodo et al., 2008). Cytokinesis in basal processes and in cell bodies proceeds in a basal-to-apical direction (Fig.5) (Kosodo et al., 2008). The contractile-ring assembly factor anillin remains associated with the branching point during basal process division and localizes with the site of cleavage furrow ingression in the cell body during cytokinesis (Fig.5) (Hesse et al., 2012; Kosodo et al., 2008). These findings suggest that neural and non-neural cells might employ a similar cytokinesis machinery.

During late cytokinesis, continued constriction of the actin ring at the plasma membrane leads to the formation of a narrow intercellular bridge (ICB) that contains the midbody (Fig.5) (Dubreuil et al., 2007). The midbody contains components of the contractile ring and the microtubule bundles derived from the central spindle (Fig.5) (Dubreuil et al., 2007). Cytokinesis is finally completed during abscission when the intercellular bridge is cleaved (Fededa and Gerlich, 2012). Abscission is a complex event that relies on the coordination of multiple subcellular processes including reorganization of microtubules and the plasma membrane within the ICB. Cellular events and molecular regulators underlying neural progenitor abscission remain unexplored. In non-neural cells, the dense bundle of central microtubules needs to be dissembled and removed from the site of abscission (Fig.7) (Guse et al., 2005; Schiel et al., 2011). This process requires

inactivation of microtubule assembling factors such as the mitotic kinesin-like protein (MKLP1) and activation of microtubule severing factors such as Spastin (Connell et al., 2009; Guse et al., 2005; Yang et al., 2008). In addition, the plasma membrane at the site of severing undergoes major remodeling in preparation for abscission. For example, vesicles derived from the Golgi and recycling endosomes are transported to the ICB where they fuse at the site of abscission (Fielding et al., 2005; Goss and Toomre, 2008; Gromley et al., 2005; Schiel et al., 2011). Vesicle fusions reconstruct the surface area and stability of the plasma membrane that forms the ICB, a process proposed to enhance efficiency of abscission (reviewed by Chen et al., 2012).

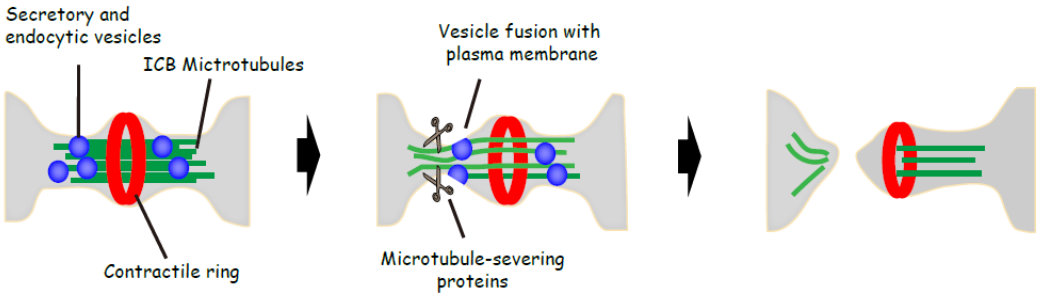

Figure 7: Abscission in non-neural cells. The midbody contains components of the contractile ring (red) and the microtubule bundles derived from the central spindle (green). During abscission, the dense bundle of central microtubules needs to be dissembled by microtubule severing factors. Vesicles (blue) derived from the Golgi and recycling endosomes (not shown) are transported to the ICB where they fuse at the site of abscission. ICB: intercellular bridge

In sum, subcellular events underlying cell cycle progression proceed through a strict schedule. These events are postulated to be highly conserved between neural progenitors and

non-neural cells. In neural progenitors, the molecules underlying initiation and progression of each cell cycle event still remain largely unexplored, however phenotypes observed from gene deletion experiments reveal a set of regulators that may display conserved functions.

The CDK/Cyclin complex as a key regulator in cell cycle progression: a matter of switching on and off in time

Molecular and cellular changes associated with various structural components occur in a sequential order, which in turn initiate the transition from one cell cycle stage into the other. In mammalian cells, the core engine driving these sequential sub-cellular events involves the cyclin-dependent kinases (CDKs). The activity of CDKs, as their name implies, requires binding to the Cyclin proteins (Pines, 1995). Cyclins are synthesized and destroyed periodically through different stages of cell cycle (Evans et al., 1983), which in turn regulates the activity of CDKs. Distinct cyclin isoforms preferentially form complexes with different CDKs, with each complex driving various transitions through specific stages of the cell cycle (reviewed by Malumbres and Barbacid, 2009). For example, CDK4/6-Cyclin D1 is required for the G1-S phase transition, whereas CDK1-Cyclin B activation is required for passage from the G2 to M phase (Gavet and Pines, 2010; Harbour et al., 1999; Lundberg and Weinberg, 1998). Temporal control of the coordinated action of CDK/cyclin is essential to trigger sequential incidence of sub-cellular events. Examples will later be given for CDK1/Cyclin B, the catalytic activity of which is at the heart of promoting mitotic events (reviewed by O'Farrell, 2001). Evidence presented in this section is based on experiments conducted in non-neural cells, in which the mechanism of CDK/Cyclin in cell cycle

regulation has been extensively studied. However, it should be noted that the functions and regulations involving the CDK/Cyclin-based machineries are likely to be conserved between neural and non-neural progenitors (reviewed by Dehay and Kennedy, 2007).

Entry into the M phase requires a network of proteins regulating activation of the CDK1/Cyclin B complex (reviewed by Lindqvist et al., 2009). Up-regulation of Cyclin B transcription and translation at the G2-M transition is critical to ensure sufficient association between CDK1 and Cyclin B (reviewed by Fung and Poon, 2005). In addition, CDK1 is subject to posttranslational modifications that affect its kinase activity. For instance, prior to mitosis CDK1 is inactivated partially through inhibitory phosphorylation by the Wee1 kinase (Gautier et al., 1991; McGowan and Russell, 1993). This inhibitory modification is later removed by the Cdc25B phosphatase resulting in activation of CDK1, which in turn is sufficient and required for initiation of mitosis (Russell and Nurse, 1987). Importantly, activation of the CDK1/Cyclin B complex relies on its centrosomal localization. For example, activated CDK1/Cyclin B complex first appears at the centrosomes during early mitosis, and interrupting this localization mimics the defects in mitotic entry as observed in CDK1 depletion (Jackman et al., 2003; Lindqvist et al., 2005; Löffler et al., 2011). These findings indicate that centrosomes may function as platforms for bringing CDK1 and its regulators together in a confined space in order to ensure their rapid interaction, resulting in timely induction of the transition into mitosis.

Upon activation, CDK1 phosphorylates a plethora of substrates to trigger subcellular alterations required for cell cycle progression (Errico et al., 2010). During prophase CDK1 phosphorylates the nuclear lamins, a network of intermediate filaments underneath the

nuclear envelope to stabilize the nucleus during interphase. This phosphorylation leads to depolymerization of the nuclear lamins, and breakdown of the nuclear envelope (Lüscher et al., 1991; Peter et al., 1990). Similarly, CDK1 phosphorylates the lamin B receptor on the inner nuclear membrane, decreasing its interaction with chromatids. This process partially dissociates chromatids from the periphery of nucleus in preparation for nuclear envelope breakdown (Tseng and Chen, 2011). In addition, a kinetochore associated protein Nsk1 is phosphorylated by CDK1 to stabilize the interaction between chromosomes and kinetochore microtubules in preparation for chromosome alignment (Chen et al., 2011). Substrates for CDK1 activation also include regulatory proteins required for the function of centrosomes during mitosis. For example, CDK1 phosphorylates a microtubule motor protein kinesins-5 for separation of duplicated centrosomes and bipolar spindle formation (Chee and Haase, 2010), and Nedd1 for recruitment of the γ-tubulin ring complex to centrosomes to promote microtubule polymerization (Zhang et al., 2009). Therefore once activated, the CDK1/Cyclin B complex then triggers the cascade of events leading to progression into M phase.

While progression within early mitosis requires activation of the CDK1/Cyclin B complex, events during late mitosis from chromosome separation to cytokinesis require inactivation of CDK1/Cyclin B at the onset of anaphase (reviewed by Nigg, 2001). CDK1 inhibition can be mediated by activation of the anaphase-promoting complex/cyclosome (APC/C), which is an E3 ubiquitin ligase that targets Cyclin B for degradation (Hershko et al., 1994; Irniger et al., 1995; King et al., 1996). Inactivation of CDK1 promotes sister chromatid separation in preparation for chromosome separation into nascent daughter cells.

Prior to anaphase, sister chromatids are held together by cohesion, a ring-shaped complex around the chromatids (Nasmyth and Haering, 2009). For chromosome separation, cohesion is cleaved by the protease separase, which the CDK1/Cyclin B complex binds to and inhibits (Gorr et al., 2006; Holland and Taylor, 2006). Interestingly, although cleavage of cohesin is sufficient to induce sister chromatids separation, additional regulation of CDK1 in interaction between microtubule and kinetochore is required to mediate efficient and faithful movement of separated chromatids (Oliveira et al., 2010; Pauli et al., 2008). This is demonstrated by a neat experiment in which the *Drosophila* syncytial embryos containing nuclear divisions in a common cytoplasm were first blocked in metaphase through inhibition of APC/C, which is required to activate separase and inhibit CDK1 (Hershko et al., 1994; Irniger et al., 1995). Subsequent injection of the tobacco etch virus protease, a plant derived protease that cleaves a subunit of cohesin, immediately induced chromosome separation. However in the presence of high CDK1, the speed of chromosome movement decreased and the bi-polar movement towards each centrosome was abolished. The abnormal chromosome separation was due to a failure to remove the mitotic kinase Aurora B from the kinetochores during anaphase, a process that requires inactivation of CDK1 (Oliveira et al., 2010). Aurora B localization to kinetochores during metaphase functions as a spindle assembly checkpoint to monitor the proper tension between kinetochores and microtubules. This tension is created by the counteracting forces between the microtubule pulling towards centrosomes and the cohesion of sister chromatids. When the tension is lost due to chromosome separation, Aurora B has to be removed from kinetochores to avoid reactivation of the checkpoint controls (reviewed by Kelly and Funabiki, 2009).

In addition to chromosome separation at the onset of anaphase, inactivation of the CDK1/Cyclin B complex is also required for initiation of cytokinesis. This was demonstrated by an experiment in which the mRNA of a nondestructible form of Cyclin B was injected during prometaphase in order to counteract CDK1 inactivation during anaphase. Cytokinesis failed to initiate under this condition, and central spindle assembly was absent (Wheatley et al., 1997). On the other hand, treatment of a CDK1-speicific inhibitor in mitotically synchronized cells is sufficient to induce premature cytokinesis (Niiya et al., 2005). Together, these findings suggest that CDK1 inactivation is both required and sufficient to promote cytokinesis. How CDK1 regulates cytokinesis initiation has been the subject of extensive investigations, and substrates for CDK1 include a variety of regulatory proteins required for central spindle assembly and RhoA activation. One such substrate includes the microtubule bundling protein PRC1, which is negatively regulated by CDK1 prior to anaphase for its function in central spindle assembly (Jiang et al., 1998; Mollinari et al., 2002). Another substrate is the kinesin-6 family motor protein MKLP1, a component of the centraspindllin complex which is required both for central spindle assembly and RhoA activation for cytokinesis initiation (reviewed by McCollum, 2004). Prior to anaphase, CDK1 phosphorylates MKLP1 and diminishes its kinesin motor activity for microtubule association and central spindle assembly (Mishima et al., 2004; Yüce et al., 2005). Interestingly, CDK1 inactivation mediates translocation of Aurora B to central spindles, in which Aurora B further phosphorylates MKLP1 to stabilize its association with central spindles (Guse et al., 2005; Oliveira et al., 2010). In addition to cytokinesis initiation, CDK1 inactivation is required for contractile ring formation during cleavage furrow ingression.

Phosphorylation of the regulatory light chains in myosin II by CDK1 early in mitosis inhibits interaction of myosin with actin filament; inactivation of CDK1 at anaphase relieved this inhibition for assembly and constriction of the contractile ring (Matsumura, 2005; Satterwhite and Pollard, 1992). Therefore the big picture emerging is that inactivation of CDK1 is a master regulatory pathway for cytokinesis initiation and progression, and this regulation is exerted in a highly complex and coordinated manner.

Compared to the role of CDK1 in early stage of cytokinesis, less is known about the function of CDK1 in abscission. Perhaps what complicates this issue is that early cytokinesis events are known to also impact abscission (reviewed by Green et al., 2012). For example, central spindles function as platforms that mediate transportation of the golgi- and endosome-derived vesicles to the cleavage site for abscission (Gromley et al., 2005). However, evidence suggests that CDK1 might be required for abscission, a process that is sensitive to the level of activated CDK1/Cyclin B present immediately prior to abscission. This is demonstrated by an experiment in which overexpression of the nondegradable Cyclin B at different levels arrested cells at different stage of cytokinesis. Overexpression of Cyclin B beyond physiological level arrests cells in metaphase, while overexpression of Cyclin B at moderate level and low level arrested cells in anaphase and abscission, respectively (Holloway et al., 1993; Wolf et al., 2006). These findings indicate that a gradual decline in CDK1 activity triggers sequential activation of events leading to the M phase exiting through initiation and completion of cytokinesis. Importantly, it is likely that the endogenous CDK1 activity beyond certain threshold is sufficient to repress the abscission machinery prior to completion of early cytokinesis events. Therefore, deciphering regulatory pathways

governing the gradual decline of CDK1 activity and interaction of CDK1 with abscission factors will be paramount to understanding how CDK1-based machineries are involved in abscission.

Role of cell cycle regulators in neural progenitor fate specification

Based on the information provided so far, it is not surprising that cell cycle regulation is tightly linked to neural progenitor proliferation and differentiation. Obviously, the overall length and rate of cell cycle exiting determines the size of progenitor pools and the amount of neuronal production (reviewed by Dehay and Kennedy, 2007). However, less obvious has been the link between the length of distinct cell cycle compartments and the fate of neural progenitor divisions. As described earlier, neural stem cells (NSCs) undergo either symmetric divisions resulting in daughter cells with the same cell fate, or they divide asymmetrically to generate cells with distinct fates (e.g., IPCs or neurons). Logically, symmetric divisions are important for expansion of NSC pools while asymmetric divisions increase cellular diversity. In this context, symmetry in NSC divisions is developmentally programed in a time- and cell-specific manner. For example, symmetric division of NSCs dominates during early cortical development, while RGs begin to adopt asymmetric divisions to induce neurogenesis (Miyata et al., 2001, 2004; Noctor et al., 2001, 2004). Remarkably, the duration of the cell cycle has been extensively shown to lengthen during the onset of asymmetric divisions and induction of neurogenesis. Multiple studies using cumulative BrdU labeling in mice have firmly established that total length of the cell cycle more than doubles from 8.1 hours during early symmetric divisions and NSC expansion, to 18.4 hours at developmental periods corresponding to the peak of asymmetric divisions and neuronal

production (Takahashi, 1995). Additionally, it is now well established that the increase in cell cycle duration is largely due to the increase in G1 length from around 3 to 12 hours (Arai et al., 2011; Calegari et al., 2005; Takahashi, 1995). Therefore, lengthening of the cell cycle through expansion of G1 is associated with the increase in neurogenic potential of NSCs and IPCs during development.

Interestingly, temporally regulated changes in cell cycle length are causatively rather than consequentially linked to the change from proliferative to neurogenic divisions in NSCs (reviewed by Salomoni and Calegari, 2010). For example, experimental lengthening of G1 through RNAi against CDK4/Cyclin D1 induced premature neuronal production (Lange et al., 2009). Conversely, shortening of G1 by CDK4/Cyclin D1 overexpression accelerates proliferative divisions leading to the expansion of NSCs and IPCs (Lange et al., 2009; Pilaz et al., 2009). Based on these observations a "cell cycle length hypothesis" has been proposed (Salomoni and Calegari, 2010). According to this hypothesis a certain length of time (especially during the G1 phase) is needed to ensure sufficient transcription and translation of cell fate determinants within dividing cells. For example, experimental lengthening of G1 induced a precocious expression of the proneural gene TIS21 prior to the onset of neurogenesis, and these changes coincides with a premature neuronal production (Calegari and Huttner, 2003). Similarly, expression of the proneural gene atoh7 in Xenopus is up-regulated when G1 lengthening was induced by overexpression of the CDK4 inhibitor p27, but down-regulated during G1 shortening induced by Cyclin E1 overexpression (Ohnuma et al., 2002).

The link between mechanisms that control cell cycle length and cell fate specification has been further demonstrated by direct interaction between molecular regulators of each process. For example, the proneural transcription factor neurogenin 2 (Ngn2) has been recently shown to be phosphorylated by CDKs and this phosphorylation progressively increased on multiple residues in response to rising levels of CDKs. Phosphorylation of Ngn2 by CDKs inhibits its DNA binding and transcriptional activation for a number of proneural genes (Ali et al., 2011). In parallel, activity of CDKs has been shown to decline during G1 lengthening, due to the progressive accumulation of endogenous CDK inhibitors (Cremisi et al., 2003; Vernon et al., 2003). Taken together, these findings indicate that molecular regulators of specific stages of the cell cycle either directly or indirectly impact mechanisms of fate-specification in NSCs, providing a paradigm-shift and a departure of existing paradigms that the two processes (cell fate specification and cell cycle regulation) are mutually exclusive.

Tempting as the cell cycle length hypothesis may be, several outstanding questions remain to be addressed. The mode of cell division is likely to be determined by the counteracting effects between proliferative (symmetric) and proneural (asymmetric) genes. How proliferative genes are regulated during prolonged duration of G1 remains largely unknown. Additionally, while this model has thus far emphasized the duration of G1 as a key regulator of fate in NSCs, changes in duration and integrity of other cell cycle compartments may also impact mechanisms of fate specification. A longer S phase and shorter G2 have been reported in proliferative progenitors compared to neurogenic progenitors in the developing cortex (Arai et al., 2011; Calegari et al., 2005). Importantly,

lengthening of G2 through reduction of Cdc25B without altering the total cell cycle length is associated with a reduction in neuron production from NSCs (Peco et al., 2012). In another report, shortening of G2 with up-regulation of Cdc25B was demonstrated to induce an elevation in mitotic entry and premature neuronal specification (Gruber et al., 2011). Therefore, a causative link is likely to exist between fate determination and regulation of cell cycle compartments outside G1. Further investigation is critical to better understand how these novel paradigms are regulated and whether or not the manipulation of these mechanisms can be used in reprogramming of NSCs in various cell-based therapies in the future.

Neural progenitors in the postnatal subependymal zone

As previously mentioned, although the vast majority of progenitor domains in the central nervous system become dormant by birth, the subependymal zone (SEZ) of the lateral ventricles and the rostral migratory stream (RMS) continue to harbor NSCs and NPCs in postnatal and adult mice (Ghashghaei et al., 2007; Kriegstein and Alvarez-Buylla, 2009). Cellular organization in SEZ stem cell niche differs from the embryonic stem cell niche. In the SEZ niche, ependymal cells form an epithelial-like barrier lining the wall of the lateral ventricle. SEZ NSCs are displaced from the VZ regions and are situated underneath the ependymal layers (Fig.8). Despite the differences in cellular organization, postnatal SEZ NSCs are highly related to embryonic RGs. Lineage tracings demonstrated that perinatal RGs give rise to postnatal SEZ NSCs (Merkle et al., 2004). Moreover SEZ NSCs maintain astroglial characteristics including expression of glial fibrillary acidic protein (GFAP) (Doetsch et al., 1999a).

SEZ NSCs give rise to transit amplifying progenitors (TAPs), which in turn generate neuroblasts. Neuroblasts continue to divide as they actively migrate tangentially along the rostral migratory stream (RMS) (Fig.8). After reaching the olfactory bulb (OB), neuroblasts differentiate into interneurons (Lois et al., 1996; Luskin, 1993). SEZ NSCs are slow dividing cells and are largely quiescent while TAPs and neuroblasts are actively dividing cells (Costa et al., 2011; Doetsch et al., 1999a; Garcia et al., 2004; Ponti et al., 2013). The quiescent nature of adult NSCs is proposed to maintain the stem cell repertoire and to support lifelong neurogenesis (Furutachi et al., 2013). Following the initial division of SEZ NSCs, TAPs and neuroblasts undergo more than one round of division before committing into their next lineage (Costa et al., 2011; Ponti et al., 2013). Conceptually TAPs and neuroblasts correspond to the embryonic IPCs, divisions of which can amplify the progenitor pool and the neuronal output. Similar to embryonic progenitors, SEZ neural progenitors are heterogeneous. Different subsets of progenitors are found to reside in different regions of the SEZ, express different transcription factors, and are required to generate different subsets of OB interneurons (Kohwi et al., 2007; Stenman et al., 2003; Waclaw et al., 2006; Young et al., 2007). For example, the transcription factor Paired box gene 6 (Pax6) is expressed by a subset of progenitors situated in the dorsal SEZ and is required for specification of dopaminergic neurons in the olfactory bulb (Kohwi et al., 2005). However, compared to embryonic NSCs and NPCs, the lineage progression and cell cycle profiling in postnatal neural progenitors are less elucidated.

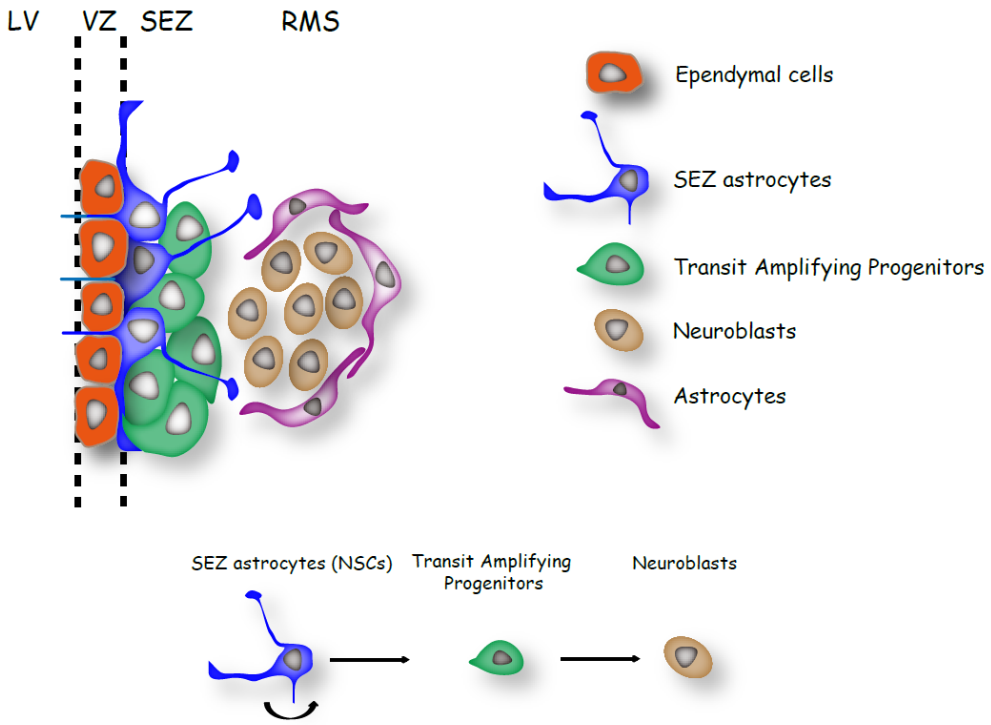

Figure 8: SEZ neural stem cell niche in the postnatal brains. In the SEZ niche, ependymal cells form an epithelial-like barrier lining the wall of the lateral ventricle. SEZ astrocytes (NSCs) are displaced from the VZ regions and are situated underneath the ependymal layers. SEZ NSCs give rise to transit amplifying progenitors (TAPs), which in turn generate neuroblasts. LV: lateral ventricle; VZ: Ventricular zone; SEZ: Subependymal zone; RMS: Rostral migratory stream

Introduction to the dissertation

The specificity protein (Sp) family of transcription factors has been associated with progenitor functions including regulation of the cell cycle (Baur et al., 2010; Black et al., 2001; Krüger et al., 2007; Marin et al., 1997). Although Sp family members are co-expressed broadly, developmental defects exhibited by subtype-specific knockout mice indicate that their functions may only partially overlap (Bouwman et al., 2000; Göllner et al., 2001; Loo et al., 2003; Marin et al., 1997; Nguyên-Trân et al., 2000; Supp et al., 1996). A couple of studies published during my thesis work illustrated that Sp2 is required for early embryonic development in mice and zebrafish (Baur et al., 2010; Xie et al., 2010), and that Sp2 over-expression in skin stem cell and progenitor populations is oncogenic (Kim et al., 2010). Specifically, acute loss of Sp2 was shown to negatively regulate the proliferation of immortalized mouse fibroblasts (Baur et al., 2010). However, whether Sp2 functions as a bona fide transcription factor has remained unclear; past reports have indicated that Sp2 has little, if any, transcriptional activity or DNA-binding capacity in mammalian cells (Moorefield et al., 2004), whereas a more recent report has claimed widespread DNA binding by Sp2, targeting regulatory regions of a wide range of vital genes (Terrados et al., 2012). Importantly, the cell biological relevance of Sp2 had remained relatively unknown prior to my thesis work.

MATERIALS AND METHODS

Animals

Animals were used under Institutional Animal Care and Use Committee and North Carolina State University regulations. Animals were housed at Laboratory Animal Research facilities at the College of Veterinary Medicine. The Sp2 floxed mice were generous gifts from Dr. Horowitz (Department of Molecular Biomedical Sciences, College of Veterinary Medicine, North Carolina State University). Sp2 floxed mice were generated using the homologous recombination with targeting vectors including two LoxP sites flanking Sp2 exon 3 and 4. To conditionally delete Sp2 in NSCs and NPCs Sp2 floxed mice were crossed to the transgenic *Nestin-cre* (B6.Cg-Tg (Nes-cre)1Kln/J; Jackson Lab, # 003771) or knock-in $Emx1^{cre}$ mice (B6.129S2-Emx1tm1(cre)Krj/J; Jackson Lab, #005628). To track cre-mediated recombination, *Nestin-cre* or $Emx1^{cre}$ mice were crossed to mice expressing the reporter tdTomato (tdTom) (B6.129S6-Gt (ROSA) 26Sortm14 (CAG-tdTomato) Hze/J; Jackson Lab, # 007908) or LacZ (B6.129S4-Gt (ROSA) 26Sortm1Sor/J; Jackson Lab, #003309). Sp2 deleted floxed alleles were detected by PCR using the following primers: SAF-3 5' GAGATTCAGATTTAGAGGGCTACCAGTGTCCA 3' and TAR-2 5' CGCTCAAGCCCCATTGCTGGGCCTGGTGACAA 3'.

For mosaic analyses, *MADM11-GT/TG:Sp2 F/+ :Nestin-cre* mice were generated using breeding schemes previously described (Hippenmeyer et al., 2010). In brief, the *Nestin-cre* or $Emx1^{cre}$ mice were first crossed to the MADM11-GT line while Sp2 floxed mice were crossed to the MADM11-TG line. The resulting *MADM11-GT: Nestin-cre* or *MADM11-GT:* $Emx1^{cre}$ mice were then crossed to the MADM11-TG:Sp2 F/+ mice to

generate the *MADM11-GT/TG:Sp2 F/+ :Nestin-cre* or *MADM11-GT/TG:Sp2 F/+:Emx1^{cre}*. For examination of cre-mediated recombination, *MADM11-GT/TG:Nestin-cre* or *MADM11-GT/TG:Emx1^{cre}* mice were generated without the Sp2 flox background.

Mice expressing the enhanced green fluorescent protein EGFP fused to the human Centrin-2 (CENT2::EGFP) (CB6-Tg (CAG-EGFP/CETN2)3-4Jgg/J; Jackson Lab, # 008234) were used for tracking centrioles.

For embryonic analyses, the morning of observed vaginal plug was designated as embryonic day 0.5 (E0.5). Embryos were harvested from time-pregnant females following Avertin overdose (7.5 mg/g body weight), their brain removed and fixed with 4% paraformaldehyde for a minimum of 24 hours prior to processing. For fixed analyses of postnatal brains, mice were sacrificed at multiple developmental stages by Avertin overdose (7.5 mg/g body weight) followed by transcardial perfusion with 4% paraformaldehyde in 0.1 M phosphate buffered saline (PBS).

Tissue processing and immunohistochemistry

After perfusion, brains were removed and post fixed in 4% paraformaldehyde in 1x PBS overnight at 4°C. Brains were then sectioned at 50 μm on the vibratome (Leica VT 1000 S). Brain sections were blocked in 10% goat serum with 1% Triton X in 1x PBS for 1 hour at room temperature (RT), followed by overnight incubation with primary antibodies in 1x PBS at 4°C. Sections were washed three times with 1x PBS followed by incubation with appropriate secondary antibodies conjugated to Alexa 488, Cy3 or Alexa 647 (diluted at 1:1000 in 1x PBS) for 1 hour at RT.

Primary antibodies used were as follows: rabbit anti-RFP (Abcam; 1:1000), chicken anti-GFP (Abcam; 1:1000), rabbit anti-cre (Covance; 1:500), rabbit anti-Ki67 (Vision Biosystems; 1:500), rabbit anti-PH3 (Millipore; 1:500), mouse anti- PH3 (Abcam; 1:500), mouse anti-BrdU (BD Bioscience; 13:1000), rat anti-BrdU (Abcam; 1:200), guinea pig anti-DCX (Chemicon; 1:1000), mouse anti-GFAP (Millipore; 1:1000), , mouse anti-NeuN (Millipore; 1:1000), rabbit anti-S100β (Sigma; 1:1000), rabbit anti-Dlx2 (Dr. D. Eisenstat, Manitoba Institute of Cell Biology, Winnipeg, MB, Canada; 1:1000), rabbit anti-Gsx2 (Dr. K. Campbell; 1:4000), rabbit anti-Pax6 (Millipore; 1:500), rabbit anti-cleaved caspase3 (Cell Signaling; 1:1000), rabbit anti-BLBP (Chemicon; 1:500), rabbit anti-Tbr2 (Chemicon; 1:1000), rabbit anti-NG2 (Millipore; 1:1000), mouse anti-Tuj1 (Covance; 1:1000), rabbit anti-Cux1 (Santa Cruz; 1:500), rabbit anti-Ctip2 (Abcam; 1:500), mouse anti α-tubulin (Sigma; 1:1000), rabbit anti γ-tubulin (Sigma; 1:1000). When needed, sections were counterstained with the Nissl stain (Invitrogen; 1:1000), TO-PRO-3 Iodide (Invitrogen; 1:2000) or DAPI (VECTASHIELD mounting medium, Vector labs) for cytoarchitectonic characterization of sections.

Staining the whole embryos for the beta-galactosidase gene lacZ was as described previously (Nagy et al., 2007). Whole embryos at E12.5 were harvested, with the extraembryonic membranes removed. Embryos were fixed in the fixative solution (5mM EGTA, 0.2% Glutaraldehyde and 2mM $MgCl_2$ in 1x PBS) at RT for 15 minutes. The fixed embryos were then rinsed in the detergent solution (2mM $MgCl_2$ and 0.02% NP-40 in 1x PBS) at RT for 15 minutes. The embryos were then incubated in the staining solution (2mM $MgCl_2$, 0.02% NP-40, 5mM Potassium ferricyanide, 0.01% Sodium deoxycholate and

1mg/ml X-gal in 1x PBS) at 37 °C for 3 hours in the dark. After staining, the embryos were dehydrated through a graded series of ethanol (70%, 90%, 95% and 100%, prepared in xylene). For sectioning, the embryos were cryopreserved with 30% sucrose in 1x PBS overnight at 4°C followed by overnight freezing in tissue freezing medium (Triangle Biomedical Sciences) at -80°C. Embryos were then sectioned at 20 µm on a cryostat (Leica).

In situ hybridization

The probe used for in situ hybridization corresponded to the Sp2 type I transcript variant, which is predicted to encode the full length Sp2 protein. This probe was generated from the 489-bp portion at the 5' end of mouse Sp2 exon 4 as described previously (Yin et al., 2010). Amplified DNA fragments were sub-cloned into vector pSC-A (Promega) at the TOPO binding site using the Zero Blunt® TOPO® PCR Cloning Kit (Invitrogen). The construct was singly digested with restriction enzymes XhoI and HindIII to create the sense and anti-sense strands respectively. To prepare digoxigenin-labeled probes for in situ hybridization, 4 µl of 5X transcription buffer (Roche), 2 µl DIG RNA Labeling Mix (Roche), 2 µl of RNase Out (RNasIn), and RNA polymerase (T7 or Sp6; Roche) were mixed with 2 µg of linearized probe DNA and incubated for 2 hours at 37°C. Labeled probes were purified from unincorporated nucleotides with NucAway Spin Columns (Ambion), according to the manufacturer's instructions. Antisense or sense probes were synthesized in these reactions depending on the orientation of the cDNA insert within pSC-A.

For tissue preparation, tools for perfusion were cleaned with the RNase Away (Molecular Bioproducts). Brains were removed and kept in 4% paraformaldehyde in 1x PBS/0.1% DEPC H2O at 4°C for 2 hours. Brains were placed in 10% RNase free sucrose

solution (Sigma) with sterilized 1x PBS for 2 hours at 4°C and then placed in 30% RNase free sucrose with sterilized 1x PBS overnight at 4°C. Brains were immersed in tissue freezing medium (Triangle Biomedical Sciences) overnight at -80°C, sectioned at 15 µm by the cryostat and stored at -80°C.

In situ hybridization of brains sections was performed as previously described (Yin et al., 2010). For pretreatment, slides with the brain sections were pre-warmed at RT for 10 minutes followed by fixation with the 4% paraformaldehyde at RT for 15 minutes. Sections were washed twice in 1xPBS in 0.1% diethylpyrocarbonate (DEPC) at RT for 15 minutes, and then equilibrated in 5x standard saline citrate (SSC) (750 mM NaCl and 75 mM sodium citrate in 0.1% DEPC, adjust PH=7.0) at RT for 15minutes. Pre-hybridization of the sections was performed in the hybridization buffer (50% Dehionized formamide, 0.02g Ficoll, 0.02g Polyvinylpyrrolidone, 0.02g Bovine serum albumin and 0.1% Tween-20 in 5x SSC) at 60°C for 2 hours. Sections were then incubated in the hybridization buffer with the probe at 20 mg/ml, at 65°C overnight. For fluorescent in situ hybridization (FISH), after the overnight hybridization, sections were blocked with 10% goat serum in 1x PBS at RT for 1 hour. Blocking solutions were then replaced with the chicken anti-digoxigenin (Abcam; 1:1000) and other primary antibodies in 1x PBS at 4°C overnight. Sections were washed three times with 1x PBS followed by incubation with appropriate secondary antibodies conjugated to Alexa 488, Cy3 or Alexa 647 (diluted at 1:1000 in 1x PBS) for 1 hour at RT.

Ex utero electroporation

Ex utero electroporation was performed as previously described (Hand et al., 2005). 0.4 µm tissue culture inserts (Falcon) were placed on top of 6 well dishes (Falcon). 2 ml of

the sterile tissue culture grade water was added to the bottom of the dish and each culture insert was incubated with 1 ml coating solution containing 8.3 µg/ml Laminin (Sigma) and 83.3 µg/ml Poly-D-lysine (Sigma) in the sterile tissue culture grade water overnight at 37°C/5% CO2. 4 µg/µl of the construct pCAG-cre (Addgene) was mixed with the fast green FCF (sigma) at a dilution of 1:20. Embryonic brains were harvested and kept in the ice cold complete HBSS (2.5 mM Hepes, 30 mM D-glucose, 1 mM CaCl2, 1 mM MgSO4 and 4mM NaHCO3 in the 1x Hank's Buffered Salt Solution (HBSS)). 2 µl of the mixed solution was injected into each lateral ventricle of the isolated embryonic heads using the Picospritzer III microinjector. Electroporation was performed using the ECM 830 electroporator (BTX) and the parameters were set as follows: number of pulses = 6; pulse duration = 100 ms; voltage = 50 mv; interval = 100 ms; polarity = unipolar. Coronal brain sections were immediately collected at 250 µm by vibratome and plated in the Laminin/Poly-D-lysine coated culture inserts. Sections were then cultured in the slice culture medium (20 mM D-glucose, 1 mM L-glutamine, 25% Complete HBSS, 1% Penicillin-streptomycin and 5% Fetal bovine serum in the Basal Medium Eagle) at 37°C with 5% CO2.

Neurosphere growth and differentiation assay

For the neurosphere growth assay, brains were rapidly collected from P0 and P21 cWT and cKO mice. SEZ and RMS were microdissected in the ice cold complete HBSS, followed by enzymatic dissociation as described (Jacquet et al., 2009a). In brief, the microdissected tissue was enzymatically digested in the dissociation medium (100 mM Na2SO4, 30 mM K2SO4, 6 mM MgCl2, 0.25 mM CaCl2, 1 mM Hepes, 20 mM glucose) with 3% Cysteine and 1% Papain). Dissociation was performed twice, 20 minutes each, at

37° C with 5% CO2. Cells were then washed and 1 million viable cells were cultured in the NEP basal medium (2% B-27 supplement, 1% N-2 supplement and, 1% L-glutamine and 1% penicillin-streptomycin in the Neurobasal medium). Cells were cultured at 37°C/ 5% CO2 and were supplemented with growth factors EGF (100 µg/ml, Invitrogen) and bFGF (10 µg/ml, Invitrogen) every 2 days. The neurospheres were passaged every 5 days by mechanical dissociation, as previously described (Jacquet et al., 2009a). Measurements of the neurosphere numbers were obtained on a C1 confocal microscope equipped with incubated stage for culture dishes. The number of neurospheres was counted in 5 random spots (each with the area of 1.62 mm2) from each culture well, once a day throughout all passages.

For the differentiation assay, neurospheres were plated in the 8-well glass coverslips coated with laminin (8.3 µl/ml in sterile H_2O) and Poly L-lysine (80 µg/ml in sterile H_2O). Cultured neurospheres were allowed to differentiate for 6 days, followed by immunostaining for TuJ1, Ng2 and GFAP. Individual cells were visualized by the DAPI nuclei acid stain (VECTASHIELD mounting medium, Vector labs), and the percentage of TuJ1 (+), Ng2 (+) and GFAP (+) cells in the cell culture was quantified to assess the differentiation capacity from the culture neurospheres.

BrdU and IdU Administration

Mice at various developmental stages were administered intraperitoneal injections of bromodeoxyuridine (BrdU) or iodinated deoxyuridine (IdU) (Sigma) at 100 µg/g body weight. For pulse-chase experiments, a single pulse of BrdU was followed by sacrifice at

0.5, 1, 4, or 12 hours after the last BrdU injection. For assessment of cell cycle exiting, 3 pulses of BrdU were administered at 2-hour intervals and injected mice were perfused 48 hours after the last pulse.

For estimation of the cell cycle duration, BrdU/IdU dual labeling was performed as described before (Martynoga et al., 2005). IdU was injected initially followed by BrdU injection 3 hours later (Ti) and mice were perfused 0.5 hours later. Immunoflorescent staining was performed using the mouse anti-BrdU antibody (BD Biosciences) that recognizes both IdU and BrdU and the rat anti-BrdU antibody (Abcam) that only recognizes BrdU. Under this regiment, cells that exit the S phase during the interval between IdU injection and BrdU injection (Ti) are IdU+/BrdU- while the IdU+/BrdU+ cells are cells that remain in the S phase. Length of S phase (Ts) is calculated as: Ts= Ti/ (number of IdU+/BrdU- cells/ number of IdU+/BrdU+ cells). To estimate the total cell cycle length (Tc), immunofluorescent staining against Ki67 was performed to label cells that are in the active cell cycle and Tc is calculated as: Tc=Ts/ (number of IdU+/BrdU+/ numbers of Ki67+ cells).

Flow cytometry and cell sorting

SEZ and RMS regions were microdissected followed by enzymatic dissociation to generate single cell suspension. For cell cycle analysis, suspension was centrifuged at 1000 rpm for 5 minutes and supernatant was discarded. Cells were washed with 5 ml of ice cold 1x PBS and suspended by gentle vortexing for 5 seconds. Suspension was centrifuged at 1000 rpm for 5 minutes and the cell pellet was resuspended with 0.5 ml ice cold 1x PBS and

5 ml of 70% ethanol. After fixation, cells were washed with 5 ml ice cold 1x PBS and then stained with RNase A (Roche) at 1 mg/ml in 1x PBS and Propidium iodide (Sigma) at 1 µg/ml in 1x PBS at RT in the dark for 45 minutes. Cells with staining solution were gently vortexed for 5 seconds and then transferred to the round-bottom tube with nylon meshed cap (BD Biosciences). Samples were kept in ice to avoid cell clumping. DNA content of the sample was then analyzed by flow cytometry in the Flow Cytometry and Cell Sorting Laboratory, College of Veterinary Medicine, North Carolina State University.

For fluorescence-activated cell sorting, a single cell suspension from the *MADM11-GT/TG:Sp2 F/+ :Nestin-cre* SEZ and RMS regions was sorted by the Dako Cytomation MoFlo high speed sorter. Genomic DNA was then extracted from the sorted cells containing red only, green only or yellow fluorescence followed by PCR analysis for the Sp2 deleted floxed alleles.

Time-lapse Live imaging

For cultured neural progenitors, 35 mm glass bottom dishes (MatTek) were coated with 20 µl/ml Poly-D-lysine (Sigma) in the sterile tissue culture grade water at 37°C/5% CO2 overnight. Solution was removed by aspiration and dishes were washed three times with the sterile H2O. Enzymatically dissociated cells from the SEZ and RMS were plated on the dishes, at the density of 300 cells/ mm2. Cells were supplemented with growth factors EGF (100 µg/ml, Invitrogen) and bFGF (10 µg/ml, Invitrogen) every day. For live imaging, isolated cells were incubated in the LiveCell TM stage chamber (Pathology Devices) equilibrated in 5% CO2 at 37°C. Time-lapse imaging was performed on the Nikon Eclipse

C1 for the duration of 15-20 hours, with an interval of 10 or 30 minutes. Cellular divisions were analyzed with the Nikon EZ-C1 3.90 Freeviewer software.

For organotypic slice cultures, brains were harvested from the E14.5 embryos and coronal brain sections were immediately collected at 250 µm using a vibratome. Slices were then seeded onto cell culture inserts (Millipore) placed on top of 35mm glass-bottom dishes (World Precision Instruments). The dishes were incubated in a WSKM stage top incubator (Tokai Hit), with 5% CO_2 at 37°C. Time-lapse confocal imaging was conducted using an Olympus IX81 confocal microscope and the images were captured every 15 minutes for a duration of 20-24 hours. Mitotic and cytokinetic events were analyzed with the Olympus FV10-ASW 2.0 Viewer software.

Generation of the Sp2 constructs and transfection

cDNA for the fluorescent reporter EGFP was amplified by PCR from the existing constructs in the Ghashghaei lab. A forward primer was designed to contain an Xho I restriction site: 5'- TAT CTC GAG AGA GGT ACC GCC ACC ATG GTG AGC AAG GGC GAG GAG -3'. The reverse primer contained an EcoR I restriction site: 5'- GAA TTC ATA CTT GTA CAG CTC GTC CAT GCC G -3'. The amplified EGFP sequence was then inserted into a vector containing the CAG promoter, using the Xho I and EcoR I restriction digestion followed by ligation (T4 DNA Ligase, NEB). The vector was denoted as pCAG:EGFP.

The Sp2 open reading frame (ORF) was amplified by PCR from the mouse Sp2 cDNA (Invitrogen, # FL1002). A forward primer was designed to contain an EcoR I

restriction site: 5'- TAT GAA TTC ACT TGT ACT TGT ATG AGC GAT CCA CAG ATG AGC ATG GCC GCC ACT GCT GCT -3' and the reverse primer contained the Myc tag and a Not I restriction site: 5'- CGT TAT GCG GCC GCT TAC AGA TCT TCT TCA GAA ATA AGT TTT TGT TCC AAG CCC TTC GTG CCT AG -3'. The amplified fragment corresponds to Sp2 type I transcript variant (NM_001080964), which encodes the full length Sp2 protein. The Sp2 ORF was then inserted into the pCAG:EGFP vector, 21 bps downstream from the EGFP 3' end. Restriction digestion using EcoR I and Not I followed by ligation was performed for the cloning. The final vector was denoted as pCAG:EGFP::SP2.

The N-terminal half and C-terminal half of the Sp2 cDNA were amplified to encode the 1- 381 and 382-612 amino acids of Sp2, respectively. Amplification of the Sp2 N-terminal half used the forward primer containing the EcoR I restriction site: 5'- TAT GAA TTC ACT TGT ACT TGT ATG AGC GAT CCA CAG ATG AGC ATG GCC GCC ACT GCT GCT -3' and the reverser primer containing the Myc tag and Not I restriction site: 5'- GCG TTA GCG GCC GCT TAC AGA TCT TCT TCA GAA ATA AGT TTT TGT TCG ACG GTT GAT GTG GTT GC -3'. Amplification of the Sp2 C-terminal half used the forward primer containing the EcoR I restriction site: 5'- TAT GAA TTC ACT TGT ACT TGT ACC TGT AAC AGC CCT GCA -3' and the reverse primer containing the Myc tag and Not I restriction site: 5'- CGT TAT GCG GCC GCT TAC AGA TCT TCT TCA GAA ATA AGT TTT TGT TCC AAG CCC TTC GTG CCT AG -3'. The N- and C-terminal half containing fragments were inserted into the pCAG:EGFP vector, 21bps downstream from the EGFP 3' end. Restriction digestion using EcoR I and Not I followed by ligation was

performed for the cloning. The vectors were denoted as pCAG:EGFP::SP2 ΔC 382-612 for the Sp2 N-terminal half and pCAG:EGFP::SP2 ΔN 1-381for the Sp2 C-terminal half.

Cos7 and NIH3T3 cells were purchased from ATCC and cultured with DMEM (Cellgro) with 10% FBS (Gibco) and 1% penicillin-streptomycin (Invitrogen). Cells were passaged using Trypsin EDTA (Sigma) when they were 80% confluent. For transfection, 0.4 µg of the pCAG - EGFP::Sp2 was transfected into each well of the 6 well dishes using the Effectene Transfection Reagents (Qiagen). To monitor the co-localization of Sp2 with centrioles, co-transfection with the construct CETN2::RFP was performed.

Western Blotting and immunoprecipitation

SEZ and RMS microdissected tissues from cWT and cKO brains were collected in the ice-cold lysis buffer (50 mM Tris-HCL pH 8.3, 1% Triton X 100, 0.5 M EDTA pH 8.0, 100 mM NaCL, 50 mM NaF and one protease inhibitor tablet [Roche # 05892791001] per 10 ml of lysis buffer) followed by homogenization. Lysed tissue was then centrifuged for 20 minutes (12000 rpm at 4°C) and the supernatant was collected and protein concentration was determined using a BCA Protein Assay Kit (Pierce; Thermo Scientific). For immunoprecipitation, samples were incubated with appropriate antibodies (diluted at 1:100) overnight at 4°C under rotary agitation. The Dynabeads Portein A (Invitrogen) was added to samples at 50 µl/ml, and the lysate beads mixtures were incubated at 4°C for 1 hour under rotary agitation. Supernatants were removed from the beads and discarded. Beads were washed three times with the lysis buffer, and proteins were boiled at 95-100°C for 5 minutes in the denaturing buffer (0.1M Tris-HCL (pH 6.8), 4% SDS, 20% Glycerol, 0.2%

Bromophenol blue, and 0.2 mM B-mercaptoethanol). Samples were then run on a reducing SDS-PAGE gel followed by transfer to a nitrocellulose membrane (Bio-Rad). Membranes were blocked with 5% nonfat dry milk in 1x TBST for 1 hour at RT followed by overnight incubation with appropriate antibodies (diluted at 1:1000) at 4°C. Membranes were washed three times with 1x TBST and then incubated at RT for 1 hour with a goat anti-rabbit or goat anti-mouse secondary antibody conjugated to horseradish peroxidase (Millipore; 1:10000). Following thorough washing, membranes were developed with the Pierce ECL Western Blotting Substrate (Thermo Scientific). For loading control, membranes were stripped and re-probed with a mouse anti-actin antibody (BD Transduction Laboratories; 1:1000). Antibodies used for immunoprecipitation/western blotting were rabbit-anti Sp2 (Sigma), mouse-anti Myc tag (Millipore), mouse-anti Pan-CDC25 (Sigma). For loading controls, the western blotting with the mouse-anti Pan-actin (Sigma) was performed.

Centrosome isolation

Sucrose gradient centrifugation was used to isolate centrosomes from NIH3T3 cells essentially the same as previously described (Astrinidis et al., 2010). Cells were grown on two 100 mm plates with DMEM (Cellgro) with 10% FBS (Gibco) and 1% penicillin-streptomycin (Invitrogen). Cells at 75-80% confluence were treated with 70 ng/ml nocodazole (Sigma) in culture medium for 16 hours and then 20 µg/ml of cytochalasin B (Sigma) in culture medium for 90 minutes. Cells were washed one time with cold 1xPBS and lysed in cold lysis buffer (50 mM Tris-HCl PH8.3, 1% Triton X, 0.5 M EDTA PH8.0, 100 mM NaCl, 50 mM NaF and one protease inhibitor tablet (Roche # 05 892 791 001) per 10 ml buffer). Cells with lysis buffer were gently mixed on a rocker in 4°C for 30 minutes.

The mixed solution was centrifuged at 1,000 rpm for 5 minutes at 4°C. The cell pellets were saved for nuclear fraction analysis. The supernatant lysate was filtered through a 0.45 µm polyethersulfone membrane (VWR International) and loaded on top of a 1 ml sucrose cushion (10 mM PIPES-KCl PH6.8, 1 mM EDTA, 0.1% Beta-mercaptoethanol and 60% sucrose) in a thin-walled ultracentrifuge tube (# 344061, Beckman Coulter). Samples were centrifuged at 12,000 rpm at 4°C for 40 minutes in the SW28.1 swing-bucket ultracentrifuge rotor (Beckman Coulter) using the Beckman L8-80M ultra centrifuge. The sucrose cushion in the bottom was mixed with the lysate 2 ml above it to make a 20% sucrose solution and this mixed solution was enriched with centrosomes. A discontinuous sucrose gradient was made by gently overlaying the lighter sucrose solution onto the dense sucrose (1 ml of 70%, 50% and then 40% sucrose in 10 mM PIPES PH6.8, 1 mM EDTA, 0.1% Beta-mercaptoethanol and 0.1% Triton X). Tubes were laid down to allow diffusion of the solution for 2 hours before use. The 20% sucrose solution was overlaid on top of the discontinuous sucrose gradient and centrifuged at 25,000 rpm for 80 minutes at 4°C. Fractions, 250 µl each, were collected from the bottom and centrifuged at 13,000 rpm for 30 minutes at 4°C. The pellets were suspended in 25 µl denaturing buffer and analyzed by western blotting. Rabbit anti-Lamin B1 (Abcam; 1:1000) and mouse anti-γ tubulin (Abcam; 1:1000) antibodies were used to identify nuclear fraction and centrosomal fraction, respectively.

Microarray analysis

cWT and cKO mice at P7 and P21 were sex-genotyped by PCR amplification of the sex-determining region on the Y chromosome. Forward and reverse primers were used as

follows: 5’ TGGGACTGGTGACAATTGTC 3’ and 5’ GAGTACAGGTGTGCAGCTCT 3’, respectively. Total RNA was extracted from SEZ and RMS microdissected regions from males (n=3 per age) using TRIzol reagents (Invitrogen). Purification of total RNA (Qiagen RNeasy Mini Kit) and RNA integrity analysis (with Agilent RNA 1000 Nano reagents and the Agilent 2100 Bioanalyzer) were performed prior to expression profiling at the University of North Carolina Neuroscience Center, Functional Genomics Core Facility. The Affymetrix GeneChip Mouse Gene 1.0 ST array was used for gene profiling and microarray data analysis was performed using JMP Genomics 4.1. Expression values were normalized with RMA (Robust Multi-array Average) on the log2 scale. Differentially expressed genes across two different time points between cWT and cKO RNA were identified using p value < 0.05 from one way ANOVA analysis as the cutoff.

Data analysis

Confocal images of Sp2 cWT and cKO were labeled for the appropriate markers using identical antibody concentrations. Tissue analyses were performed using the confocal microscope (Nikon Eclipse C1 or Olympus IX81), followed by imaging analysis using the Nikon EZ-C1 3.90 Freeviewer software or the Olympus FV10-ASW 2.0 Viewer software. Data were quantified using standard stereological estimation as described previously (Jacquet et al., 2009a, 2009b). Significance was determined using Student’s t-test and all values were expressed as mean ± standard error of the mean (SEM).

CHAPTER 1

SP2 IS REQUIRED FOR PROLIFERATION IN NEURAL PROGENITORS

Results

1.1 Sp2 is expressed by embryonic and postnatal neural progenitors

In situ hybridization of the embryonic CNS revealed robust expression in germinal layers of the E14.5 embryo. Particularly strong expression was detected in the ventricular zones (VZ) and subventricular zones (SVZ) of the entire CNS including the cerebral cortex (CTX), the lateral ganglionic eminence (LGE), and the olfactory bulb (OB) (Fig. 9A). Sp2 expression continued after birth only in structures that remain neurogenic during postnatal and adult periods, including the subependymal zone (SEZ), rostral migratory stream (RMS), and the OB (Fig. 9B).

To determine the cell specificity of Sp2 mRNA expression, we conducted fluorescence in situ hybridization (FISH) in combination with immunohistochemistry for various cell types in the E14.5 cortex and LGE (Fig. 10A). The strongest expression was seen in mitotic progenitors expressing phosphorylated form of Histone H3 (PH3) in the VZ and SVZ of both progenitor domains (Fig. 10A). Correspondingly, VZ progenitors in the cerebral cortices immunoreactive for paired box gene 6 (Pax6), and genetic screened homeobox 2 (Gsx2) in the LGE, both expressed Sp2. Basal NPCs expressing T-box brain gene 2 (Tbr2) in the cortex, and LGE-specific NPCs expressing distal-less homeobox 2 (Dlx2) also expressed Sp2. Thus, Sp2 expression largely and ubiquitously overlapped with NSCs and NPCs in the embryonic CNS.

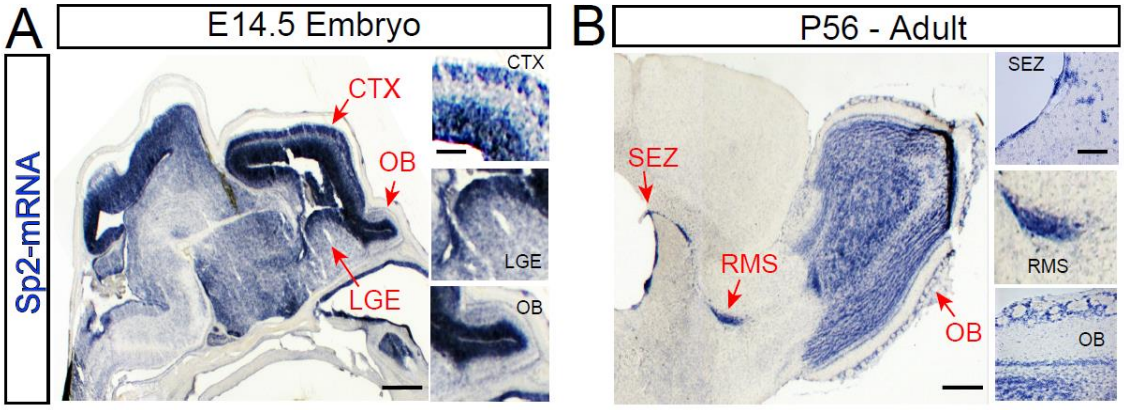

Figure 9. Sp2 expression in the brain. (A) In situ hybridization using a probe specific to the full length transcript of Sp2 revealed high expression in the germinal zones of the E14.5 cerebral cortex (CTX), lateral ganglionic eminence (LGE), and olfactory bulb (OB). **(B)** In situ hybridization for Sp2 in the P56 young adult brain revealed restricted expression in neurogenic regions including the subependymal zone (SEZ), rostral migratory stream (RMS), and OB. Scale bars: A, low mag, 200 µm; high mag, 60 µm; B, low mag, 200 µm; high mag, 60 µm.

FISH analysis in the SEZ and RMS of young adult (P56) mice indicated that Sp2 mRNA largely overlapped with cells within the cell cycle (e.g., PH3+), migrating neuroblasts expressing doublecortin (Dcx), and a small fraction of astrocytes positive for the glial fibrillary acid protein (GFAP+; Fig. 10B). Ependymal cells labeled with S100β, which are postmitotic and do not proliferate, were devoid of Sp2 mRNA (Fig. 10B). Sp2 was also expressed at low levels by some granule neurons in the olfactory bulbs (Fig. 10B). Thus, Sp2 is primarily expressed in NSCs, NPCs, and migrating cells within the germinal zones of the embryonic and adult brains, which suggested a potential role for Sp2 in neural progenitor proliferation.

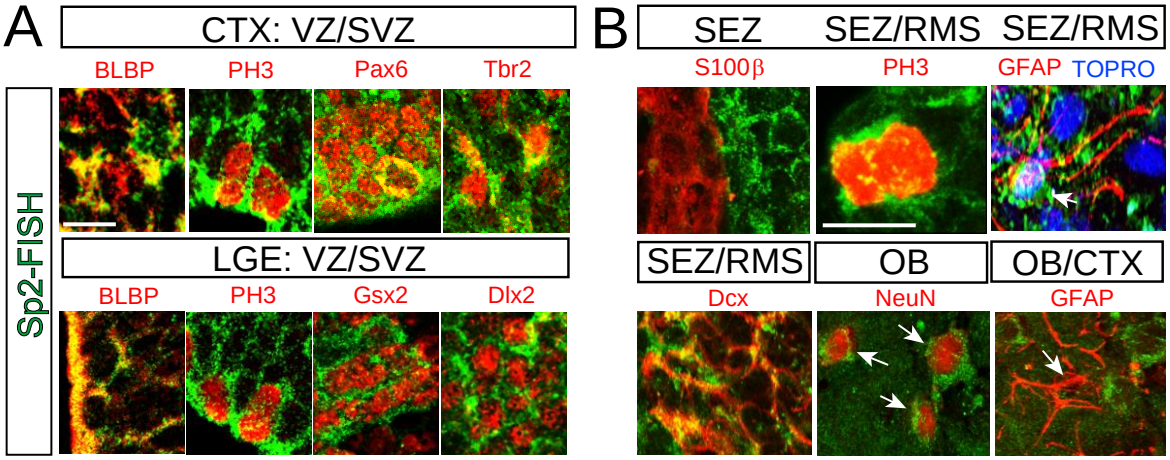

Figure 10. Cell specificity of Sp2 mRNA expression. (A) Fluorescence in Situ Hybridization (FISH) using the Sp2 probe (green) co-labeled with antibodies (red) against BLBP, PH3, and Pax6 in the VZ, and Tbr2 in the SVZ. Similar specificity for Sp2 expression was seen in the LGE where the labeled transcript overlapped with BLBP+, PH3+, and Gsx2+ progenitors in the VZ, and with Dlx2+ progenitors in the SVZ. **(B)** FISH characterization of Sp2+ cell types in the SEZ, RMS and OB. Sp2 mRNA (green) overlapped with cells labeled for PH3 and Dcx (red), which label mitotic progenitors and migrating neuroblasts in the SEZ and RMS, respectively. Subsets of neurons in the granule cell layer of the OB (NeuN+, red) also expressed Sp2. Ependymal cells labeled with S100β antibody (red) and parenchymal astrocytes labeled with GFAP antibody (red) largely failed to overlap with Sp2 mRNA. Scale bars: bar in BLBP in A applies to all except PH3 in B; both are 5 μm.

1.2 Conditional deletion of Sp2 in embryonic and postnatal neural progenitors

Based on the expression of Sp2 in both embryonic and postnatal NSCs/NPCs, we decided to examine the role of Sp2 at both developmental time points. We adopted a loss-of-function approach via the conditional deletion of Sp2, using the cre-lox system. Efficiency

of cre-mediated recombination varies in a cell type- and time point-specific manner. Cre-mediated recombination from a *Nestin-cre* transgenic line and a knock-in $Emx1^{cre}$ line will be examined in neural progenitors during developing and postnatal brains. The *Nestin-cre* lines had been broadly utilized to direct recombination in neural progenitors while $Emx1^{cre}$ mediates cre recombination in neural progenitors of the developing dorsal telencephalon. To track cre-mediated recombination, *Nestin-cre* or the $Emx1^{cre}$ mice were crossed to mice expressing the reporter genes tdTomato (*tdTom*) or β-galactosidase (*LacZ)* (Fig.11A). Similar to past reports on the same line, we found that *Nestin-cre* mediated recombination commences in the CNS during embryogenesis (Fig. 11B). However, much to our surprise, in mice on a tdTomato (tdTom) reporter background the recombination rate was extremely insufficient in the ventricular (VZ) and subventricular (SVZ) zones of the neocortex during early (E12.5) and mid stages of forebrain development (E14.5) (Fig. 11B). In contrast to the time point during cortical development, by P0 the robust tdTom expression was found throughout the cerebral cortices (Fig. 11B).

To test whether the insufficient *Nestin-cre* dependent reporter expression is due to a low level of cre expression, additional expression analyses using cre-specific antibodies were performed. The absence of cre expression in the proliferative regions VZ/SVZ in the embryonic cerebral cortices confirmed the observed patterns of tdTom at the various stages of development (Fig. 11C).

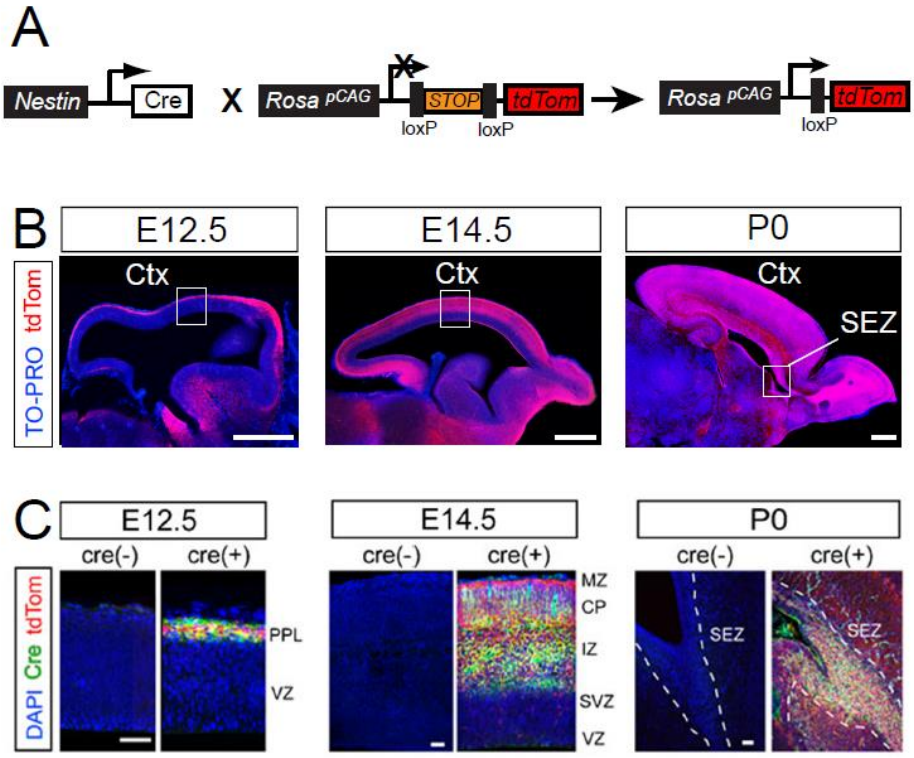

Figure 11. Recombination in NSCs and NPCs of *Nestin-cre* transgenic mice (A) tdTom reporter expression mediated by Nestin cre. **(B)** Sagittal view of tdTom expression in the developing CNS at embryonic stage E12.5, E14.5 and postnatal stage P0. **(C)** Cre expression (green) in combination with tdTom and DAPI (blue) in *Nestin-cre* (+) and *Nestin-cre* (-) brains. Expression of cre was largely absent in the E12.5 VZ proliferative region and E14.5 VZ/SVZ proliferative region. In P0 robust expression of Cre was present in SEZ. Scale bars: (B) 500 µm, (C) 30 µm.

High-magnification imaging revealed an extremely low recombination rate in PH3 or BrdU immunoreactive cycling NSCs and NPCs in the E14.5 lateral ganglionic eminence (LGE), olfactory ventricle (OV) and the cerebral cortex (Ctx) (Fig. 12A) (1.3 $\pm$ 0.7% at E12.5 and 7.4 $\pm$ 4% at E14.5 of PH3+ cells in the VZ and SVZ, respectively; n=3

mice/group). Consistent with these findings, *Nestin-cre* on a different reporter line (Rosa-lacZ) also yielded low levels of reporter activity in the VZ of E12.5 cerebral cortices (Fig. 12B). In both reporter backgrounds, the majority of recombined cells were situated in the preplate layer (PPL) of the E12.5 cortex as well as intermediate zone (IZ) and cortical plate (CP) of the E14.5 cortex, suggesting that recombination became sufficient during postmitotic stages of neuronal differentiation (Figs. 12A-B).

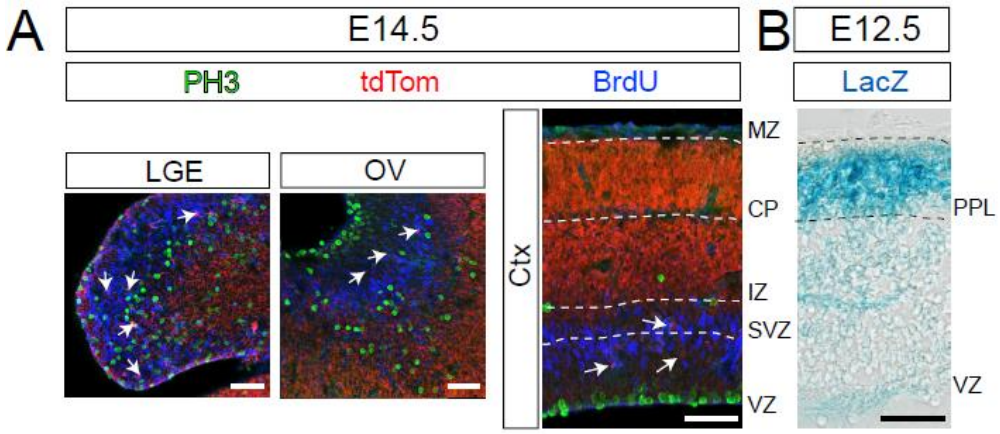

Figure 12. Insufficient rate of recombination in embryonic NSCs and NPCs of *Nestin-cre* transgenic mice. (A) Expression of tdTom in PH3 (+) (green) or BrdU (+) (blue) NSCs and NPCs in the LGE, OV the Ctx at E14.5. **(B)** Laminar pattern of *Nestin-cre* mediated recombination in NSCs and NPCs reported by LacZ expression in the E12.5 cerebral cortex. LacZ was predominantly expressed in the preplate (PPL), which consists of postmitotic cells, but not in the VZ, which consists of cycling NSCs. Scale bars: 40 µm.

In contrast, the rate of recombination in NSCs and NPCs increased dramatically in the subependymal zone (SEZ) and the rostral migratory stream (RMS) of newborn (P0) mice (Fig. 13). Nearly every BrdU-labeled NSC and NPC expressed tdTom (93 + 5% of BrdU+),

suggesting sufficient *Nestin-cre* mediated recombination in these cells. These findings suggest a gradual increase in the rate of *Nestin-cre* mediated recombination during perinatal development in NSCs and NPCs.

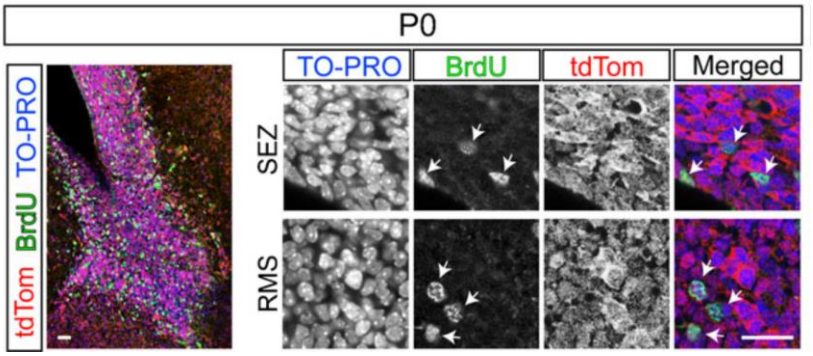

Figure 13. Sufficient rate of recombination in postnatal NSCs and NPCs of *Nestin-cre* transgenic mice. The rate of *Nestin-cre* mediated recombination in NSCs and NPCs reaches high levels at P0, revealed by expression of tdTom in nearly all cells (TO-PRO+, blue) and BrdU immunoreactive progenitors (green; arrows) of the subependymal zone (SEZ) and the rostral migratory stream (RMS). Scale bars: 20 µm.

For comparison we utilized a knock-in *Emx1*^{cre} line of mice, in which the cre-mediated recombination occurred in the dorsal telencephalic NSCs and NPCs (Gorski et al., 2002). In contrast to the *Nestin-cre* line, *Emx1*^{cre} mediated recombination was sufficient in the VZ/SVZ of the developing cortex at both E12.5 and E14.5 (Fig. 14A), which we confirmed again using antibody staining for cre (Fig. 14B). In addition, robust recombination was found in the majority (83 $\pm$ 8%) of PH3+ progenitors in the E12.5 VZ and SVZ of the cortex (Fig. 14C). The efficiency increased to nearly 100% by E14.5 (Fig. 14C). Thus, the low degree of recombination in *Nestin-cre* brains is not due to potential issues

associated with cre-loxP interactions in embryonic progenitors, but is most likely related to the transgene in this specific strain.

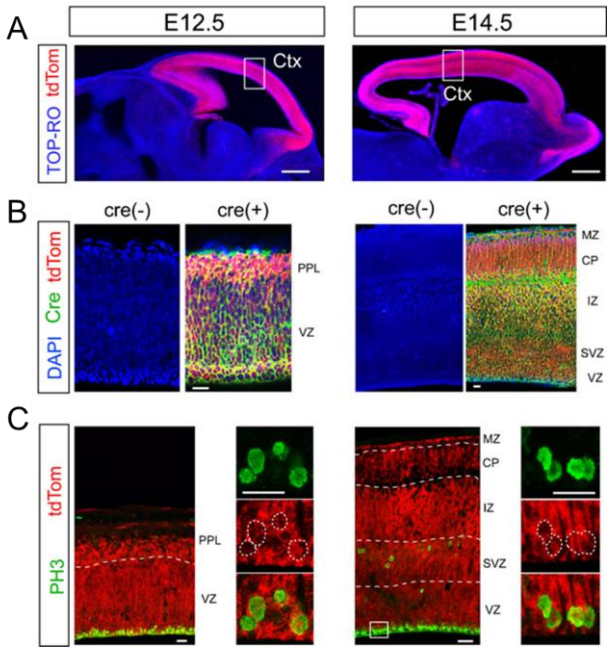

Figure 14. Sufficient rate of recombination in embryonic NSCs and NPCs of *Emx1^{cre}* knock-in mice. (A) Robust tdTom expression (red) was detected in the entire cortex at both E12.5 and E14.5. **(B)** Analysis of cre expression at ages corresponding to sections in A, using a cre-specific antibody (green), in combination with tdTom and DAPI (blue). Cre controls were obtained from brains of mice negative for *Emx1^{cre}*, but genetically positive for tdTom reporter. **(C)** High magnification of the *Emx1^{cre}* mediated tdTom expression (red) at ages corresponding to sections in A. tdTom was highly expressed in the VZ regions (box) and co-localized strongly with PH3+ mitotic NSCs (green). Scale bars: A, 300 µm; B, 30 µm; C, low mag (left panesl), 20 µm; high mag (right panels), 10 µm.

To conclusively confirm our surprising findings on the developmental patterns of cre-mediated recombination in NSCs and NPCs in the *Nestin-cre* lines, and to rule out possible

recombinogenic issues related to the Rosa locus in the reporter lines in the first part of the study, we crossed both cre lines into the Mosaic Analysis with Double Markers on chromosome 11 (MADM-11) line of mice (Hippenmeyer et al., 2010). In this line, cre-dependent mitotic recombination results in expression of GFP or tdTom independently or together resulting in various cells with three potential expression patterns (Fig. 15, red, green, yellow). Recombination can also occur in postmitotic cells during the G0 phase, but in this case only cells expressing both GFP and tdTom (yellow cells) will be obtained (Fig. 15).

Using this strategy we found recombined cells with all three colors (red, green, yellow) throughout all layers of the cerebral cortices in $Emx1^{cre}$ MADM11 brains at E12.5 (Fig. 16A). In addition, recombined NSCs and NPCs were co-labeled with the mitosis marker PH3 in the VZ region (Fig.16A). Thus, the $Emx1^{cre}$ knock-in allele is sufficient for driving mitotic recombination in NSCs and NPCs as early as E12.5.

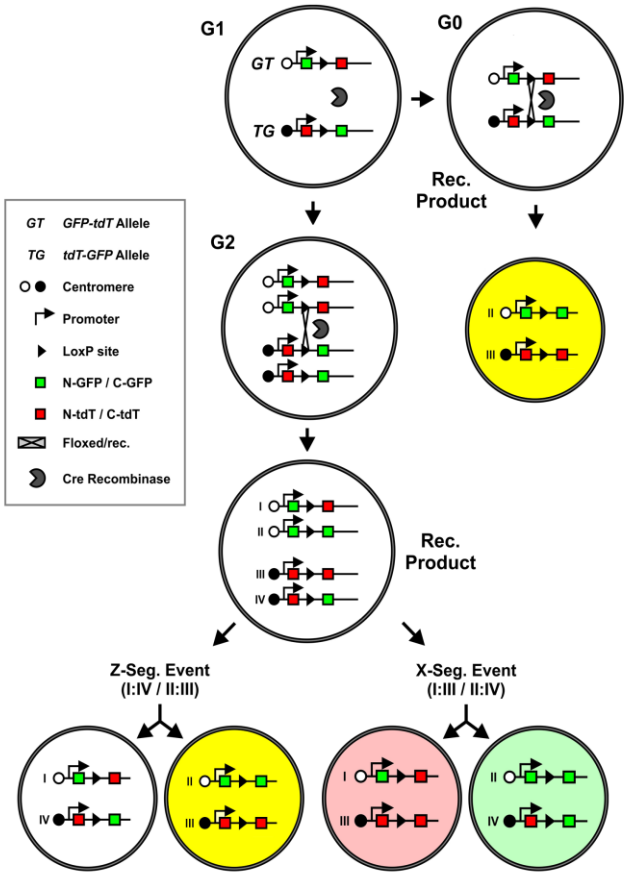

Figure 15. Scheme of cre-induced reporter expression in Mosaic Analysis with Double Markers on chromosome 11 (MADM-11) mice. Cre-dependent mitotic recombination results in expression of GFP or tdTom independently or together resulting in various cells with three potential expression patterns (red, green, yellow). Recombination can also occur in postmitotic cells during the G0 phase, but in this case only cells expressing both GFP and tdTom (yellow cells) will be obtained.

In contrast to the *Emx1*^{cre} line, *Nestin-cre* mediated recombination in the MADM-11 background was extremely infrequent in the cerebral cortices at E12.5, and the few recombined cells failed to co-label with PH3 in the VZ. Moreover, the few MADM-11 cells were predominantly situated in the preplate (PPL) and all of these cells expressed both GFP

and tdTom, suggesting that recombination had occurred during postmitotic stages of their development (Fig. 16A). At E14.5, a few more recombined cells could be found in *Nestin-cre:MADM-11* cerebral cortices, but fewer clones could be detected in the VZ/SVZ compared to IZ/CP situated cells. Moreover, the majority of VZ/SVZ recombined cells were largely devoid of PH3 immunostaining (Fig. 16B). By E17.5, recombination became sufficient in the entire cerebral cortex and PH3+ recombined cells in both VZ and SVZ regions could be readily detected (Fig. 16B). These data confirm our finding that mitotic recombination (i.e., recombination in NSCs and NPCs) only becomes sufficient during perinatal development in the specific *Nestin-cre* line we obtained from the Jackson laboratory.

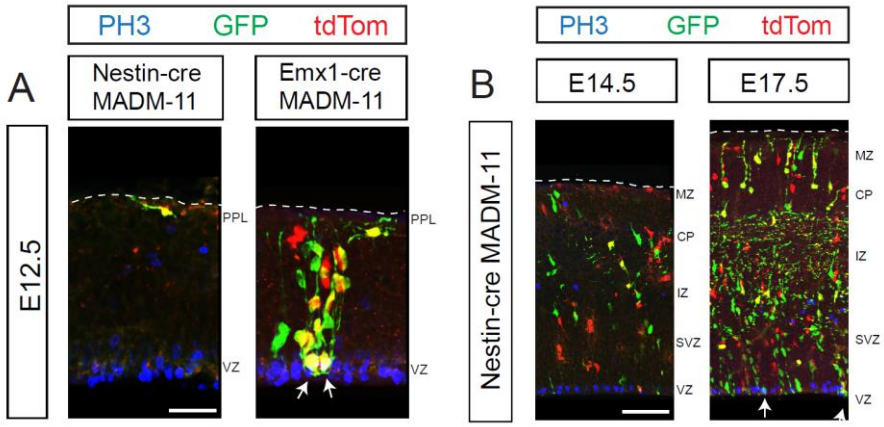

Figure 16. Analysis of mitotic and post-mitotic specificity of recombination in the cerebral cortices of *Emx1^{cre}* and *Nestin-cre* mice using the MADM-11 genetic system. (A) Scheme of cre-induced reporter expression in Mosaic Analysis with Double Markers on chromosome 11 (MADM-11) mice. **(B)** MADM-11 recombined cells in E12.5 *Nestin-cre* and *Emx1^{cre}* cerebral cortices. Co-localization of PH3 (blue) with recombined cells in VZ was labeled by arrows. **(C)** Nestincre:MADM-11 recombined cells in E14.5 and E17.5 cerebral cortices**.** Co-localization of PH3 (blue) with recombined cells in VZ was labeled by arrows. Scale bars: B, 30 µm; C, 60 µm.

Based on these findings, we utilized the *Emx1*^{cre} lines for the Sp2 conditional deletion during the embryonic brain development while the *Nestin-cre* lines were used to direct cre-mediated recombination to postnatal neural progenitors (Fig. 17A). The Sp2 floxed mouse was a generous gift from Dr. Horowitz (Department of Molecular Biomedical Sciences, North Carolina State University). In the Sp2 floxed mice two loxP sites were introduced to flank Sp2 exon3 and exon4 (Fig. 17B). Mice carrying "floxed" Sp2 alleles were crossed to the *Emx1*^{cre}or *Nestin-cre* lines to delete exon3 and 4, and prevent transcription of Sp2 due to a frame shift (Fig. 17B).

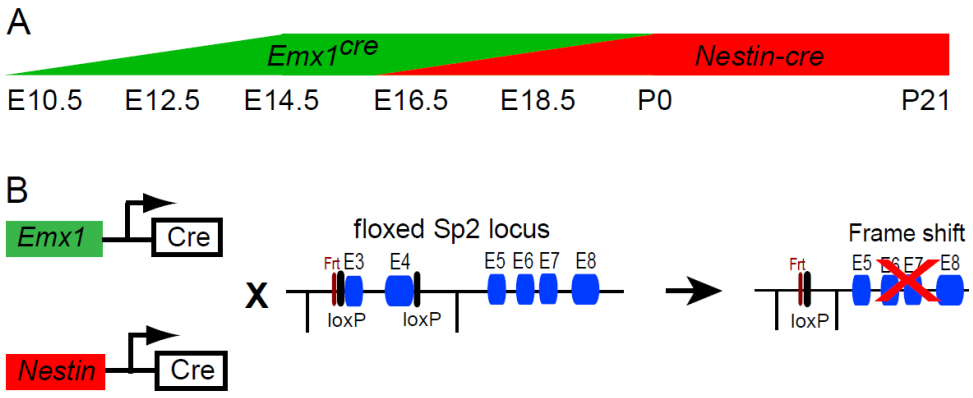

Figure 17. Generation of Sp2 Nestin:cKO and Emx1:cKO mice. (A) Time-graph illustrating the temporal efficiencies of the Emxcre and *Nestin-cre* lines which were used to differentially delete Sp2 in the embryonic and perinatal NSCs and NPCs. **(B)** Breeding scheme for generation of Nestin:cKO and Emx1:cKO mice.

1.3 Deletion of Sp2 causes growth retardation and histological anomalies in the brain

Mice with genotypes *Emx1^{cre}:Sp2 +/+*, *Nestin-cre:Sp2+/+*, *Sp2F/+*, and *Sp2F/F* served as conditional control mice (cWT), while *Emx1^{cre}:Sp2F/+* and *Nestin-cre:Sp2F/+* were conditional heterozygous (Emx1:cHET and Nestin:cHET, respectively) and *Emx1^{cre}:Sp2F/F* and *Nestin-cre:Sp2F/F* conditional homozygous (Emx1:cKO and Nestin:cKO, respectively) Sp2 "knock-out" mice. In a mating scheme to generate Emx1:cKO P0 pups in 25% of pups in each litter, only 16% were obtained at birth (n=19; three independent litters), suggesting Emx1-mediated deletion of Sp2 was partially selected against in utero (Fig. 18A). This data suggests that embryonic deletion of Sp2 is partially selected against in utero. Consistent with our previous findings that Nestincre is a poor driver for early embryonic neural progenitors, mendelian distribution of the Nestin:cHET and Nestin:cKO appeared normal at birth (progeny analyzed in 203 pups from 22 litters; P=0.82 from $\chi 2$ test; Fig. 18B).

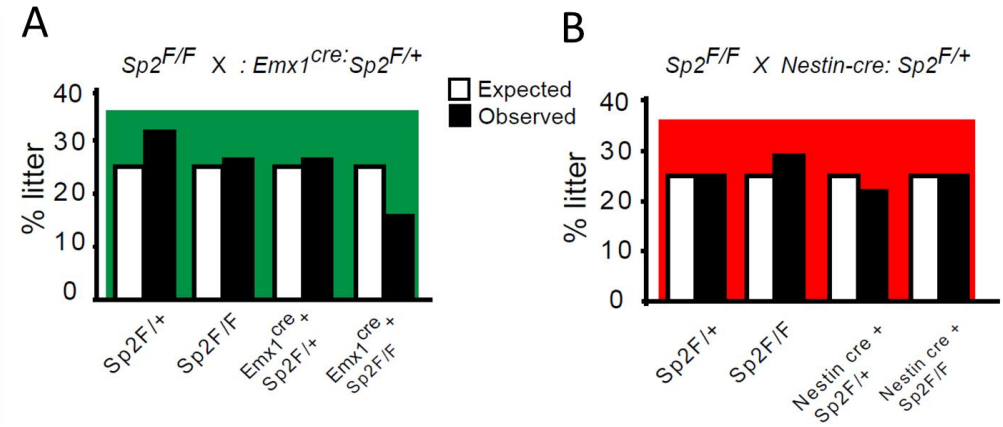

Figure 18. Birth distribution of Nestin:cKO and Emx1:cKO pups at P0. **(A)** P0 Emx1:cKO pups were retrieved at the ratio lower than expected according to medallion distribution. **(B)** Mendelian distribution of the Nestin:cHET and Nestin:cKO appeared normal at birth.

To confirm efficiency of the cre-mediated Sp2 deletion, we performed PCR analysis of genomic DNA and western blot analysis of protein extracts from P21 Nestin:cKO whole brains and SEZ/RMS. Near complete deletion of Sp2 was confirmed (Fig. 19A-B).

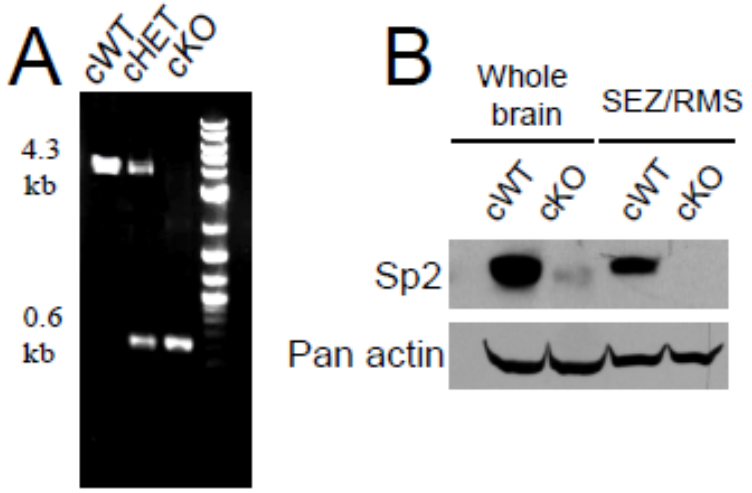

Figure 19. Near complete deletion of Sp2 in the Nestin:cKO brains. (A) PCR analysis of genomic DNA derived from P21 Nestin:cHET and Nestin:cKO brains to detect deletion of the Sp2 floxed alleles. Undeleted floxed allele yielded a 4.3 kb PCR product, whereas the deleted allele was 0.6 kb in size. **(B)** Western blotting against Sp2 in protein extracts from whole brains or from microdissected SEZ/RMS obtained from P0 mice indicated near complete absence of Sp2 in the Nestin:cKO brains.

Emx1:cKO embryos displayed growth retardation compared to control littermates. (Fig. 20A). Despite an apparently normal embryonic development, Nestin:cHET and Nestin:cKO mice grew more slowly during postnatal stages when compared to control cWT littermates (Fig. 20B).

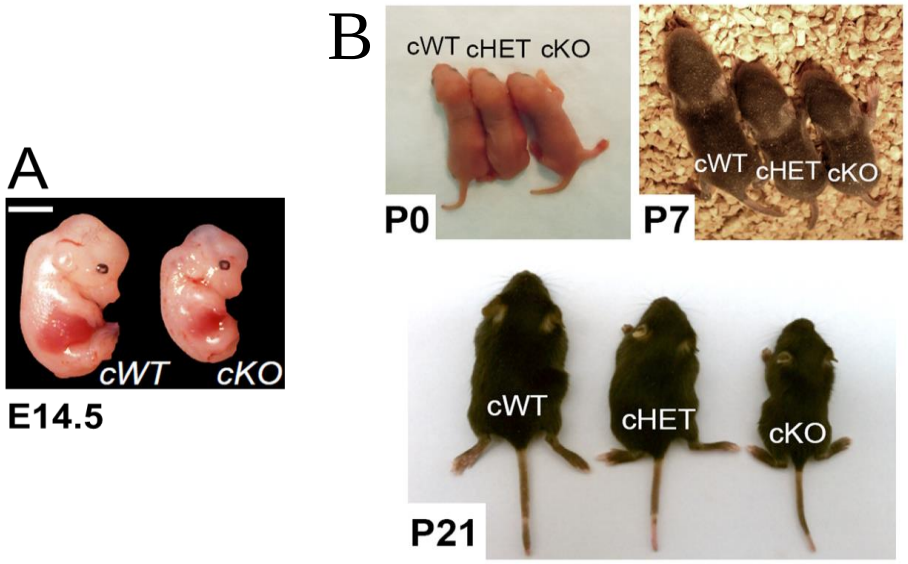

Figure 20. Growth retardation in Sp2 mutant mice (A) Emx1:cKO embryos failed to grow compared with littermate cWT controls. **(B)** Nestin:cHET and Nestin:cKO mice appeared normal at birth (P0), but failed to grow during early postnatal life (e.g. at P7 and P21) compared with littermate cWT controls. Scale bar: 300 µm.

Specific defects within the CNS became apparent during the first two weeks of postnatal life and were most profound between postnatal days 7 (P7) and P21. These included mild hydrocephalous in 32% of P21 Nestin:cKO mice (n=28) which indicated potential defects in maintenance of homeostasis in the periventricular tissue of the CNS. Ectopic cellular accumulations were observed in the P21 SEZ and RMS of both Nestin:cHET and Nestin:cKO mice (Fig. 21A). Stereological estimations of Nissl stained P21 brain sections revealed significant reductions in the volumes of the OB, hippocampus, and cerebellum in Nestin:cHET and Nestin:cKO brains (n=3 per genotype; Fig. 12B). Significant

expansions were noted in the initial segment of the RMS (RMS-i) in both Nestin:cHET and Nestin:cKO brains (Fig. 21B). These histological defects were never observed in brains from *Nestin-cre: Sp2+/+* (Fig. 21A), Sp2F/+, or *Sp2F/F* mice (data not shown), demonstrating that the identified morphological phenotypes were independent of potential cre-related or hypomorphic issues.

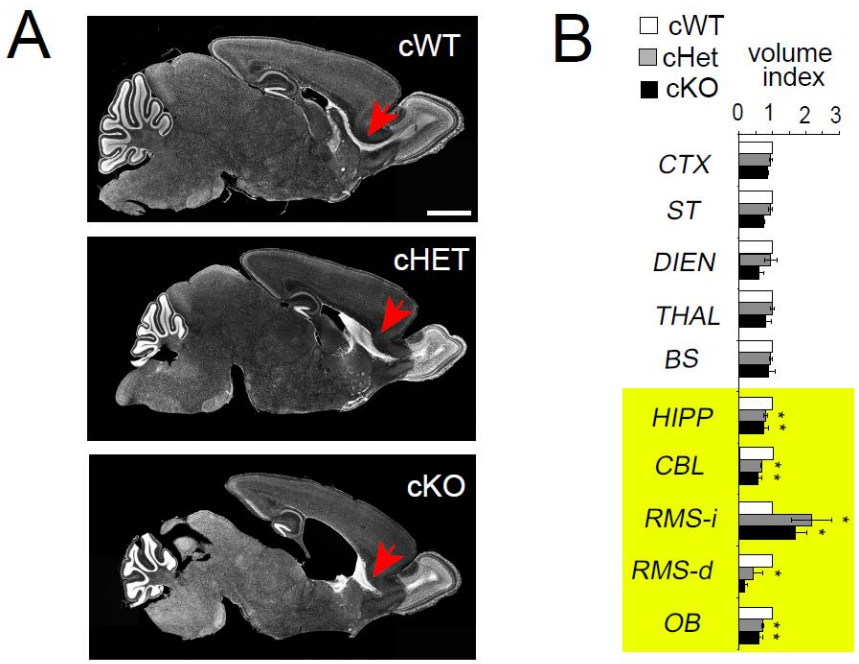

Figure 21. Histological anomalies in the brain of Nestin:cHET and Nestin:cKO. (A) Nissl-stained sagittal sections revealed ectopic cellular accumulations in the P21 SEZ and RMS of both Nestin:cHET and Nestin:cKO mice (red arrows). **(B)** Volume indices, calculated using stereological estimation methods, indicated significant reductions in the volumes of the Nestin:cHET and Nestin:cKO OB, hippocampal formation (HIPP) and cerebellum (CBL). Significant expansions were noted in the initial segment of the RMS (RMS-i) in both Nestin:cHET and Nestin:cKO brains. Scale bar: 300 µm. *P<0.05, Student's t-test, n=3/age group.

1.4 Sp2 is required for proliferation in postnatal neural progenitors

Upon closer examination, marker analysis revealed that the 'bulge' in the Nestin:cHET and Nestin:cKO RMS was largely occupied by Dcx+ neuroblasts (Fig. 22A). To determine if the neuroblast-filled bulges in Nestin:cKO SEZ and RMS corresponded to disruptions in proliferation of NSCs and NPCs, BrdU was administered to P0 and P21 mice followed by one hour of survival. Quantification of the number of BrdU+ progenitors revealed a significant reduction in the RMS in both Nestin:cHET and Nestin:cKO brains (Fig. 22B). Based on the consistent decline in proliferation of both Nestin:cHET and Nestin:cKO progenitors, we decided to focus on comparing cWT and Nestin:cKO brains hereafter.

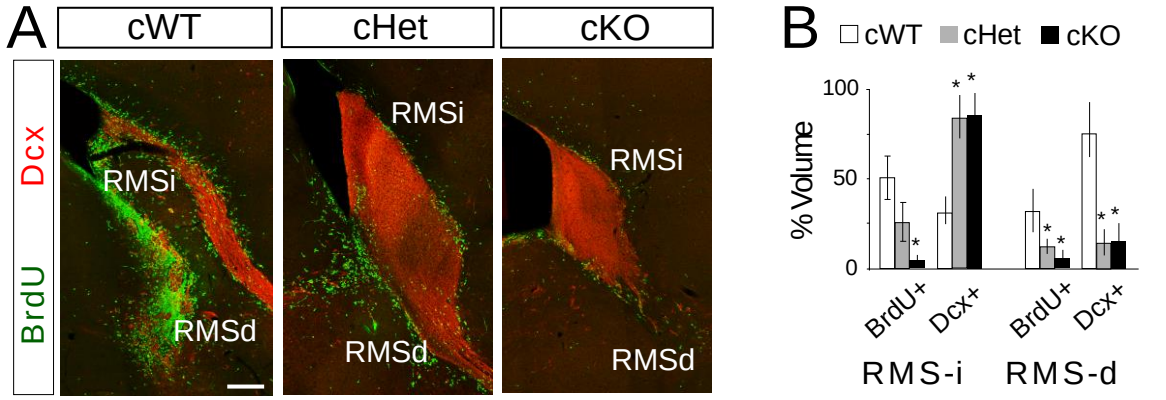

Figure 22. Accumulation of migrating neuroblasts and decreased proliferation in the Nestin:cHET and Nestin:cKO RMS. (A) Confocal micrographs of Dcx-labeled neuroblasts (red) and BrdU incorporated cells (green) in P21 RMS-i and RMS-d. **(B)** The expanded region in RMS-i was largely occupied by Dcx+ migrating neuroblasts in Nestin:cHET and Nestin:cKO brains, but the number of BrdU+ proliferating cells was significantly decreased throughout the RMS regions. Scale bars: 100 µm. *P<0.05, Student's t-test, n=3/age group.

We next examined proliferation of the dividing progenitors in SEZ. Under a single pulse of BrdU administration followed by 1 hour survival period, the BrdU incorporation in SEZ would largely label actively dividing transit amplifying progenitors (TAPs). The pan cell cycle marker Ki67 was also utilized to label cycling progenitors. Consistent with the proliferation defects in RMS, there was an overall reduction of BrdU+ and Ki67+ labeled progenitors in the Nestin:cKO SEZ (Figs. 23A-B).

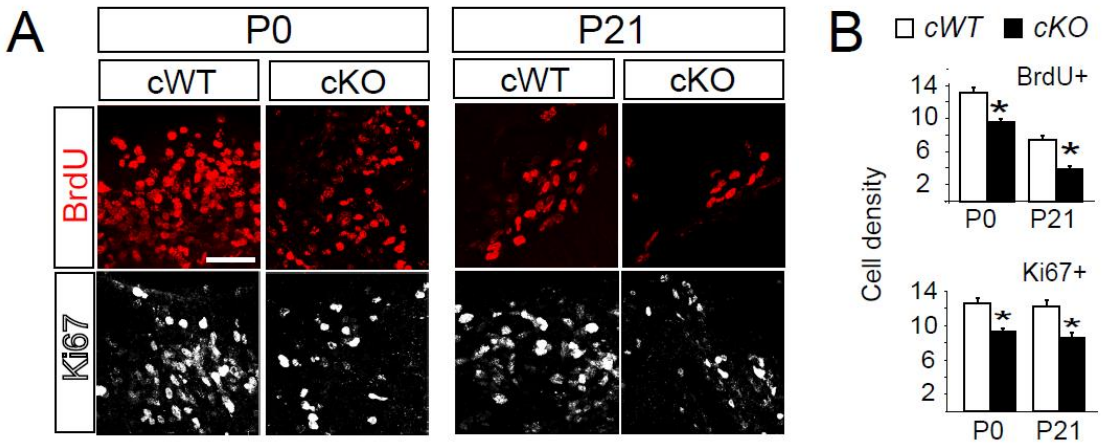

Figure 23. Reduction of cycling progenitors in the postnatal Nestin:cKO brains. (A) Confocal micrographs of Ki67+ and BrdU+ (red) cycling cells in the P0 and P21 cWT and Nestin:cKO SEZ. **(B)** Quantitative comparison of BrdU+ and Ki67+ cellular densities in the cWT and Nestin:cKO SEZ. Scale bars: 20 µm. *P<0.05, Student's t-test, n=3/age group.

The SEZ transit amplifying progenitor pool comprises different subsets of progenitors, which can be characterized by expression of the transcription factors Gsx2, Dlx2 and Pax6 (reviewed by Kriegstein and Alvarez-Buylla, 2009). To determine whether or not

Sp2 is required for proliferation in all subsets of progenitors, we next utilized progenitor type-specific markers in combined with the proliferation marker BrdU (Fig.24). We found that there was a universal reduction of BrdU labeling in all subsets of progenitors, indicating that Sp2 is required for proliferation of all cycling populations (Fig. 24).

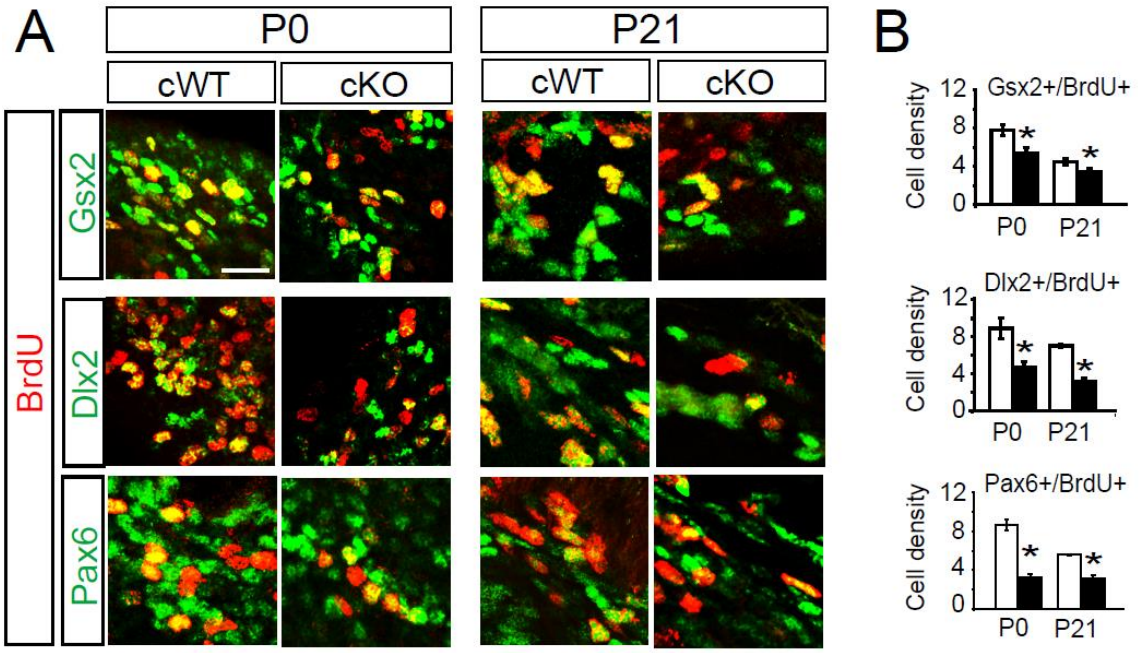

Figure 24. Sp2 is required for proliferation of all cycling progenitors in the postnatal brains. **(A)** The proliferating portions of progenitors expressing the transcription factors Gsx2, Dlx2 and Pax6 were identified by a 1-hour BrdU pulse. Representative confocal photomicrographs illustrating BrdU labeled (red) progenitors in the Gsx2, Dlx2 and Pax6 domain (green). **(B)** Universal reduction in BrdU (+) progenitors that co-labeled with Gsx2, Dlx2 and Pax6. Scale bars: 10 μm. *P<0.05, Student's t-test, n=3/age group.

Next to determine the self-renewing capacity of SEZ NSCs, the neurosphere assay was performed (Reynolds and Weiss, 1992). SEZ of P0 and P21 cWT and Nestin:cKO brains were microdissected and cultured to generate neurospheres. In line with our in vivo findings, the number of both primary and secondary neurospheres from Nestin:cKO progenitors were compromised and progressively worsened between P0 and P21 (Fig.25A-B). Taken together these results suggested that Sp2 is an important regulator of proliferation in postnatal NSCs and NPCs.

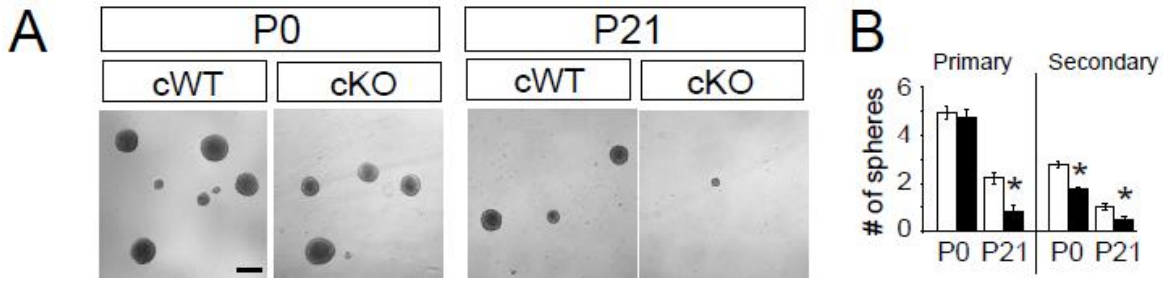

Figure 25. Neurosphere growth is retarded in the Sp2 mutant progenitors. (A) Primary neurospheres generated from cWT and Nestin:cKO SEZ and RMS progenitors harvested at P0 and P21. **(B)** Quantification of both primary and secondary neurospheres derived from P21 cWT and Nestin:cKO progenitors. *P<0.05, Student's t-test, n=3/age group. Scale bar: 200 µm.

1.5 Sp2 is required for proliferation in embryonic neural progenitors.

Consistent with our previous findings that *Nestin-cre* is an insufficient driver for cre recombination in embryonic NPCs, we failed to detect significant proliferation phenotypes in the embryonic cerebral cortical Nestin:cKO progenitors (Fig.26).

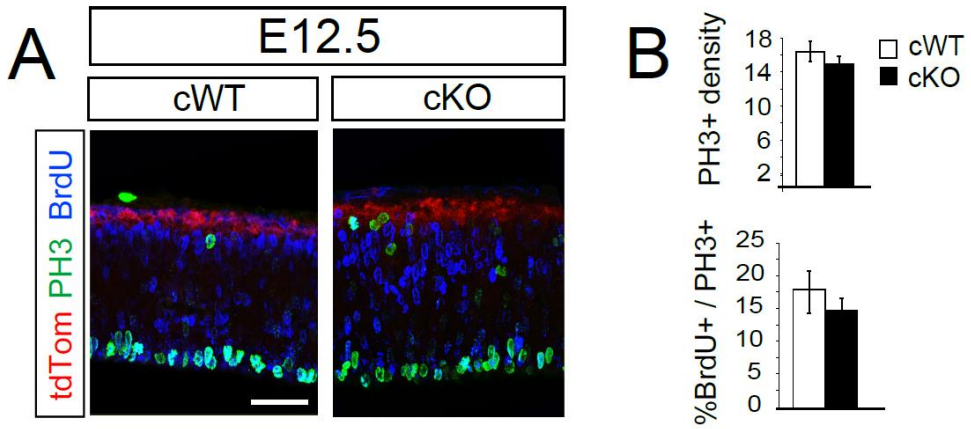

Figure 26. Lack of proliferation phenotype in the Nestin:cKO embryonic cerebral cortices. (A) Density of PH3+ (green) and BrdU+ (blue) nuclei was indistinguishable in the developing cortex of *Nestin-cre* driven cWT and Nestin:cKO brains at E12.5, owing to inefficient recombination (tdTom, red) in the VZ. **(B)** PH3+ densities were obtained in the VZ of Nestin:cKO and cWT mice and are presented as mean±s.e.m. Scale bar: 20 µm.

To assess if embryonic NSCs and NPCs require Sp2 for their proliferation, alternatively we expressed cre in Sp2F/F and Sp2+/+ embryonic brains with tdTomato cre recombination reporter (tdTom) by means of ex-utero electroporation using a pCAG-cre construct (Fig. 27A). The brains were harvested and organotypic slices were collected and maintained for two days in vitro (E13.5 + 2 DIV;Fig. 27B). The cultures were supplemented with BrdU for 1 hour followed by fixation and immunohistochemistry to visualize BrdU+ cells. Cre-mediated recombination in embryonic Sp2F/F brains resulted in a significant decrease in the percentage of BrdU+ cells in the tdTom+ population in the VZ and SVZ of

the developing cortex (Fig. 27B). These findings led us to conclude that akin to postnatal NSCs and NPCs, the proliferation of embryonic progenitors within the VZ and SVZ is Sp2-dependent.

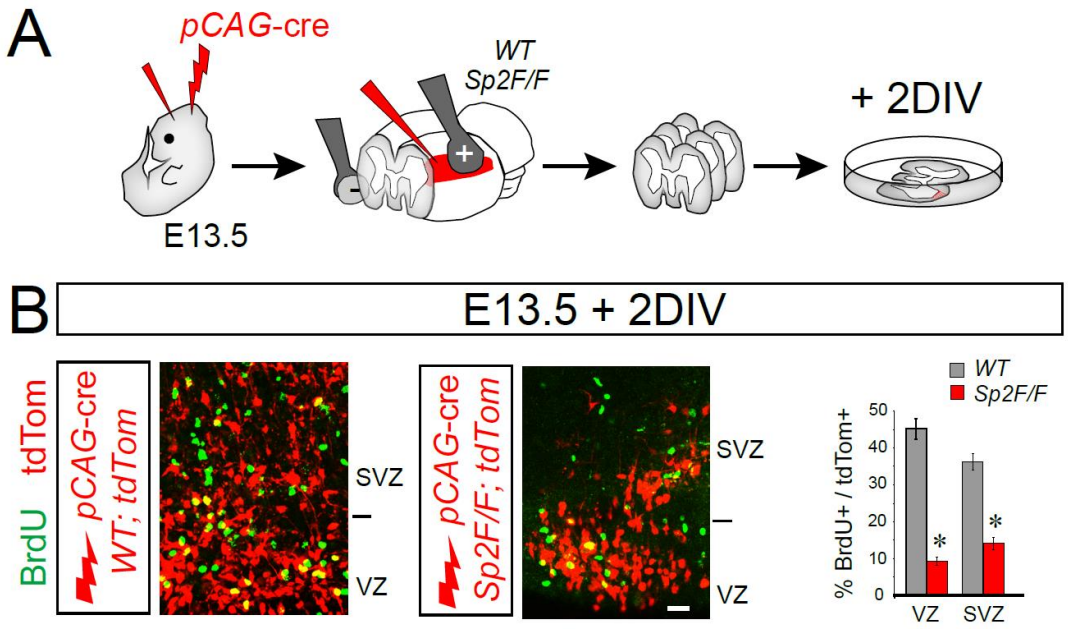

Figure 27. Sp2 is required for proliferation of embryonic NSCs and NPCs. (A) Ex vivo electroporation of a pCAG-cre construct into the embryonic brains of E13.5 tdTomato (tdTom) reporter mice on a Sp2+/+ and Sp2F/F backgrounds. **(B)** tdTom+ cells (red) reported on cre-mediated recombination. Fractions of proliferating tdTom+ cells were determined by staining for BrdU (green; BrdU applied to culture bath 1 hour prior to fixation). Charts illustrate differences in percentage of tdTom+ cells co-labeled with BrdU in the ventricular zone (VZ) and subventricular zone (SVZ) of the developing cerebral cortices. Scale bar: 10 µm. *P<0.05, Student's t-test, n=3/age group.

CHAPTER 2

SP2 IS REQUIRED FOR CELL CYCLE PROGRESSION IN NEURAL PROGENITORS

The findings in chapter 1 demonstrate that Sp2 is highly expressed by embryonic and postnatal NSCs and NPCs. Conditional deletion of Sp2 mediated by the time point specific drivers *Nestin-cre* and $Emx1^{cre}$ clearly demonstrate that Sp2 is required for proliferation of all cycling progenitors in both the embryonic and postnatal neural stem cell niche. The significant decline in BrdU incorporation in conditional Sp2-null NSCs and NPCs prompted us to investigate the role of Sp2 in cell cycle progression. We addressed this issue by a combination of approaches including a series of BrdU-tracing experiments, cell cycle analysis by flow cytometry and time-lapse live imaging.

Results

2.1 Sp2 deficiency causes elevated M phase labeling in neural progenitors

To address whether the dynamic of cell cycle progression is disrupted or not in the Sp2-null cells, we first use the presumptive M phase cells expressing the phosphorylated form of histone H3 (PH3). Surprisingly, we observed an elevated density of PH3+ progenitors in the postnatal Nestin:cKO SEZ and RMS despite the overall reduction of BrdU+ and Ki67+ cycling progenitor pool (Fig. 28).

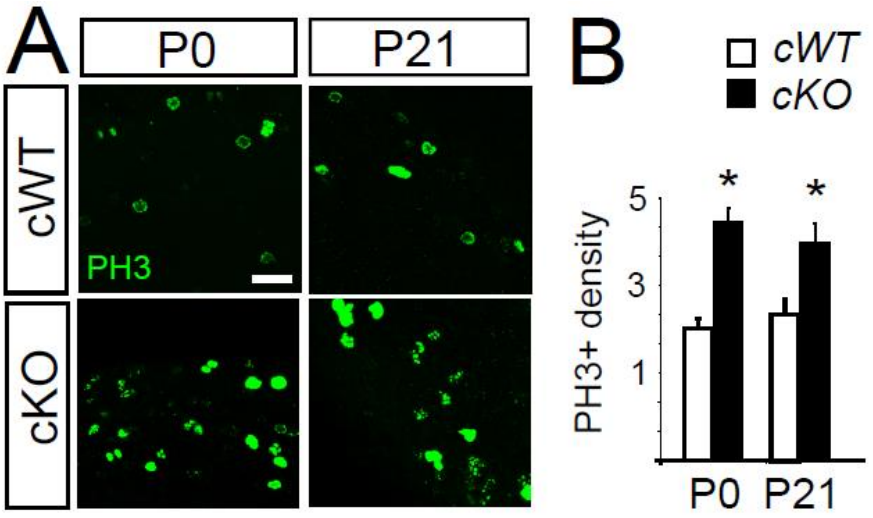

Figure 28. Elevated expression of the M-phase marker PH3 in the Sp2-null brains. (A) Confocal micrographs of PH3+ (green) labeled progenitors in the P0 and P21 SEZ/RMS**. (B)** Significant increase in density of PH3+ M-phase cells in the P0 and P21 Nestin:cKO. Scale bar: 10 µm. *P<0.05, Student's t-test, n=3/age group.

To test whether the elevated expression of PH3 in the Nestin:cKO NSCs/NPCs is cell intrinsic or not, we microdisected cWT and Nestin:cKO SEZ/RMS progenitors followed by cell culture *in vitro* for 5 days. We found that Nestin:cKO cultures expressed PH3 in significantly higher numbers than control cultures (Fig. 29), suggesting a potential M phase arrest in Sp2-null progenitors.

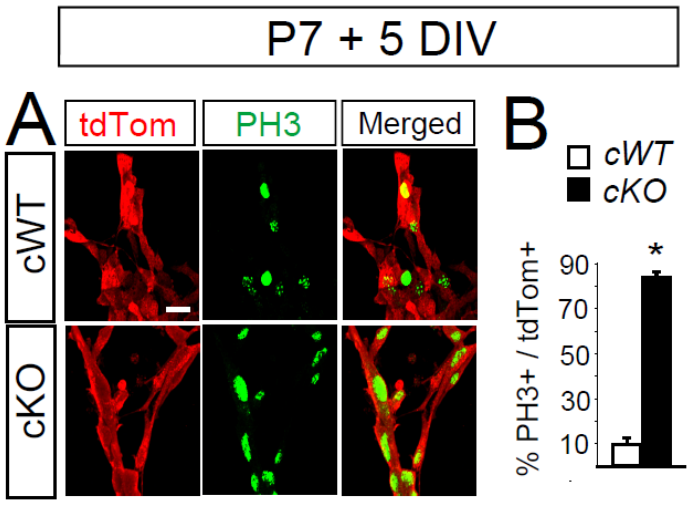

Figure 29. Elevated expression of the M-phase marker PH3 in cultured Sp2-null progenitors. **(A)** PH3 staining (green) in P7 SEZ/RMS cells (tdTom, red) plated on poly-d-lysine for five days. **(B)** Sp2-null cultured progenitors contained a higher percentage of cells colabled with PH3 (green) among the total population of tdTom+ cells. Scale bar: 10 µm. *P<0.05, Student's t-test, n=3/age group.

To conclusively exclude potential cell non-autonomous effects of Sp2 deletion in vivo, we next utilized Mosaic Analysis with Double Markers genetic mice with targeted 'MADM' insertions into the 3' region of chromosome 11 (MADM-11) (Fig. 30) (Hippenmeyer et al., 2010). Since chromosome 11 also carries the Sp2 gene in mice, progenitors carrying one floxed allele of Sp2 on the homozygous MADM-11 background will undergo cre-mediated mitotic recombination resulting in generation of cWT (tdTom+), Nestin:cHET (GFP+ tdTom+), and Nestin:cKO (GFP+) cells from clones of NSCs and NPCs that label distinctly with fluorescent reporters. However, cre-mediated mitotic recombination is not ubiquitous and only occurs in a small fraction of NSCs and NPCs, which allows for

mosaic and clonal analysis of progenitor functions in a mixed heterozygous and wildtype background.

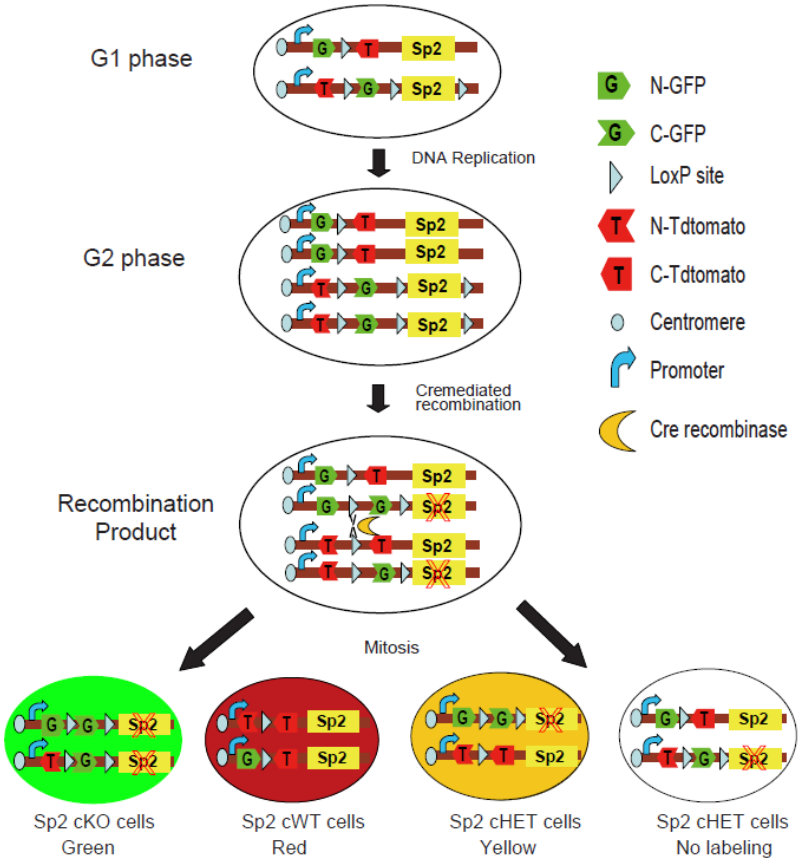

Figure 30. Diagram for the Mosaic Analysis of Double Marker (MADM). Mosaic Analysis with Double Markers genetic mice was utilized with targeted 'MADM' cassette inserted into the 3' region of chromosome 11 (MADM-11) (Hippenmeyer et al., 2010). Since chromosome 11 also carries the Sp2 gene in mice, progenitors carrying one floxed allele of Sp2 on the homozygous MADM-11 background will undergo cre-mediated mitotic recombination resulting in generation of cWT (tdTom+), Nestin:cHET (GFP+ tdTom+), and Nestin:cKO (GFP+) cells from clones of NSCs and NPCs that label distinctly with fluorescent reporters.

To confirm that cellular genotypes matched the expected reporter combinations, MADM cells were sorted subjected to PCR genotyping, which indicated that Sp2 genotypes (i.e., wildtype, heterozygous, or homozygous) were concordant with the expression of MADM reporters (Fig. 31).

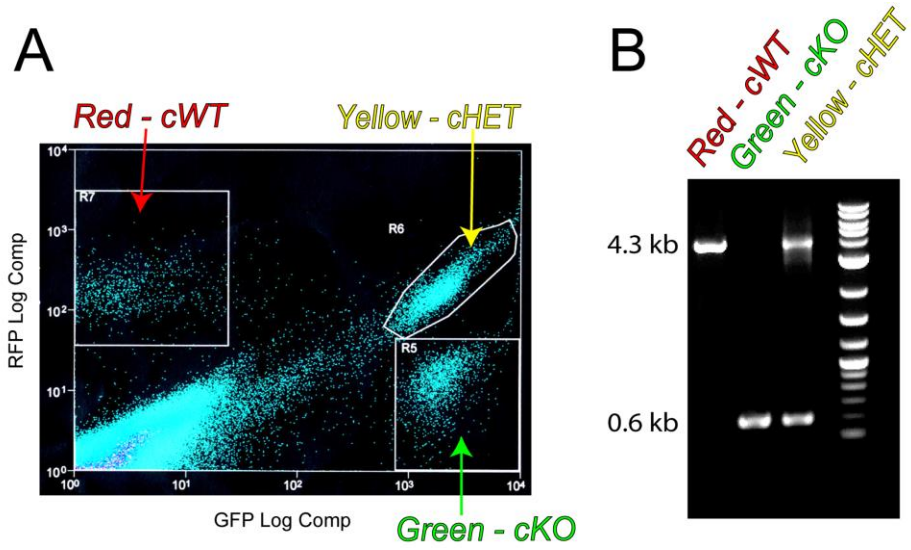

Figure 31. Distinctly labeled MADM-11 cells faithfully carry allelic deletion of Sp2 corresponding to their specific combinatorial expression of fluorophores. (A) *Nestin-cre:Sp2 F/+:MADM-11* cells from P0 mice were harvested and sorted using fluorescence activated cell sorting. **(B)** PCR analysis of DNA confirmed genotypes of distinctly sorted populations corresponding to Red = cWT, green = cKO, and yellow = cHET genotypes.

Subsequent in vivo analyses of *Nestin-cre:Sp2F/+:MADM-11* progenitors substantiated our findings that the percentages of PH3+ nuclei in Nestin:cKO and Nestin:cHET populations (green and yellow cells respectively; Fig. 32) were significantly higher than in the cWT progenitor pool (red cells; Fig. 32). Thus, the elevated density of

PH3+ (presumptive M phase) cells in the absence of Sp2 expression, despite the severe depletion of other proliferation indices, strongly favored a possible defect in cell cycle progression in postnatal neural progenitors.

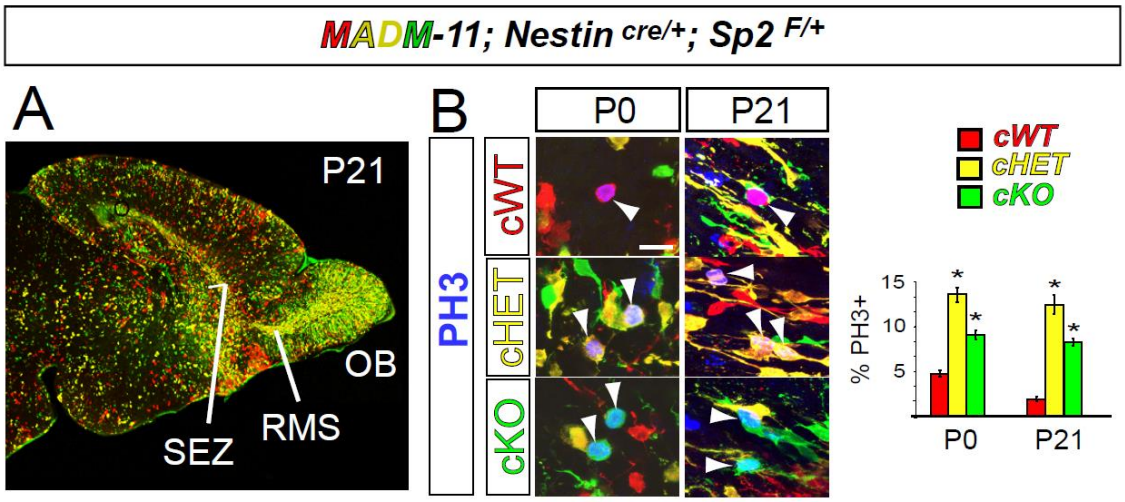

Figure 32. In vivo analysis of *Nestin-cre:Sp2 F/+:MADM-11* progenitors. (A) Sagittal sections of the P21 *Nestin-cre:Sp2 F/+:MADM-11* brains. **(B)** Percentages of PH3+ (blue) cells that were Nestin:cKO (green) and Nestin:cHET (yellow) were significantly higher than cWT (red) progenitors (PH3+ color labeled cells, arrow head). Scale bar: 10 µm.

Similarly, despite the overall reduction of BrdU incorporation upon the acute deletion of Sp2 in the embryonic progenitors, percentage of PH3+ labeled progenitor cells was significantly elevated in the VZ and SVZ of embryonic Sp2F/F cortical slices electroporated with pCAG-cre (Fig. 33).

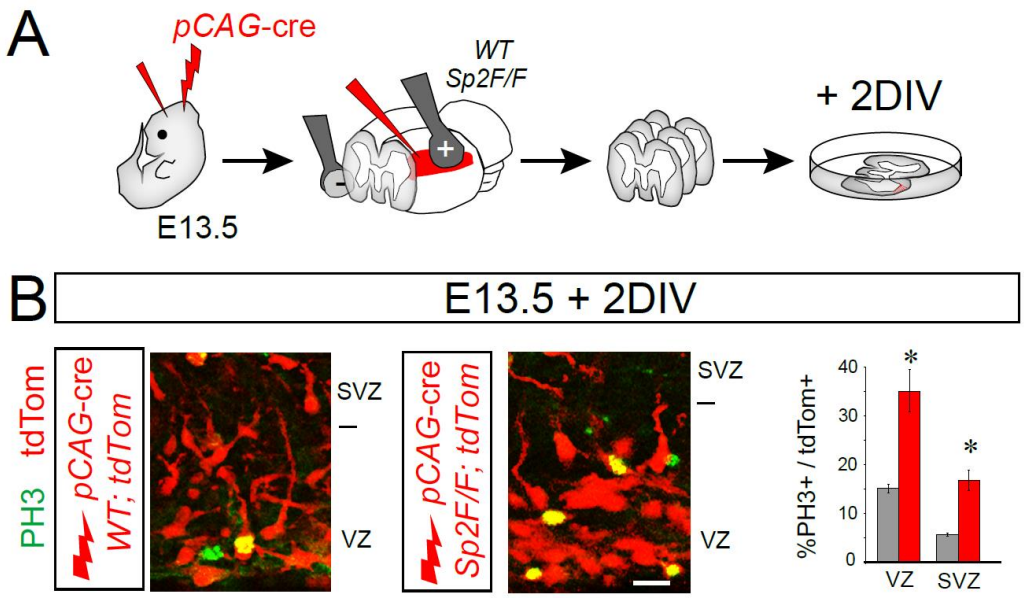

Figure 33. Acute deletion of Sp2 induces elevated M-phase labeling in embryonic NSCs and NPCs. (A) Ex vivo electroporation of a pCAG-cre construct into the embryonic brains of E13.5 tdTomato (tdTom) reporter mice on a Sp2+/+ and Sp2F/F backgrounds. **(B)** tdTom+ cells (red) reported on cre-mediated recombination. Fractions of proliferating tdTom+ cells were determined by staining for PH3 (green). Charts illustrate differences in percentage of tdTom+ cells co-labeled with PH3 in the ventricular zone (VZ) and subventricular zone (SVZ) of the developing cerebral cortices. Scale bar: 10 µm. *P<0.05, Student's t-test, n=3/age group.

We have established that the *Emx1*^{cre} line is a suitable in vivo model for sufficient cre-mediated recombination in embryonic NSCs and NPCs. In contrast to the lack of embryonic phenotype in the Nestin:cKO, a profound M-phase defects was detected in the Sp2-null brains mediated by the *Emx1*^{cre} lines. Every E14.5 Emx1:cKO cortex exhibited significant increase in density, and profound disruption in organization of PH3+ nuclei in the VZ and SVZ (Fig. 34). Together deletion of Sp2 caused elevated M phase labeling in

postnatal and embryonic neural progenitors despite the overall reduction in proliferation, which strongly favored an M phase defect in the absence of Sp2.

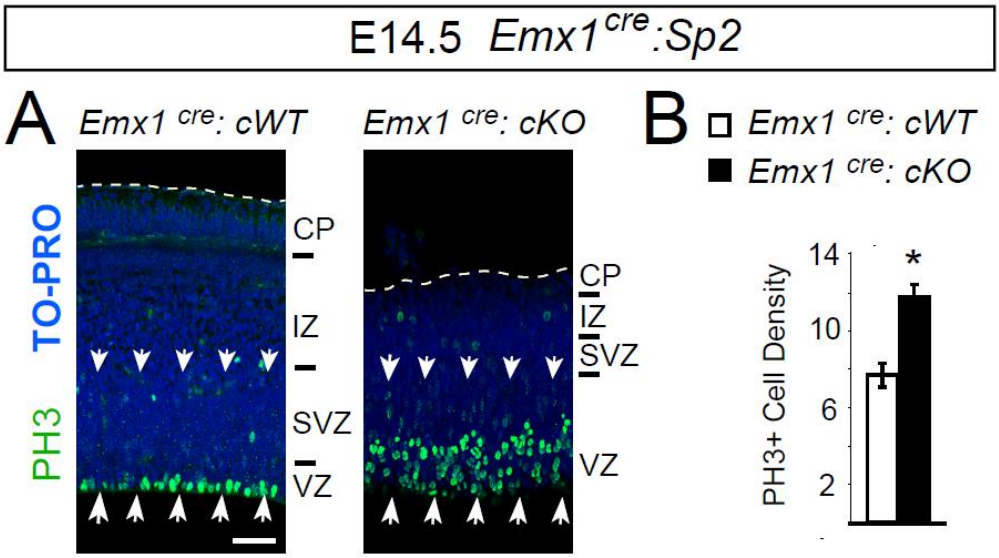

Figure 34. Expression pattern and density of PH3+ cells is disrupted in the Emx1:cKO cerebral cortex. (A) The laminar organization of PH3+ progenitors were disrupted the VZ and SVZ of the Emx1:cKO cerebral cortices at E14.5 (arrows). (B) The density of PH3+ Sp2-null progenitors was significantly higher compared to the cWT. Scale bar: 40 µm. *P<0.05, Student's t-test, n=3/age group.

2.2 Sp2 is required for timely progression from G2 to M phase

To determine if cycling progenitor cells were arrested in, or progressed more slowly through G2/M, a series of in vivo BrdU pulse-chase and in vitro flow cytometric experiments were conducted on postnatal NSCs and NPCs. To assess the acute effects of Sp2 deletion on the S-to-M transition, a single pulse of BrdU at P0 and P21 was followed by a one hour survival time (Fig. 35A). BrdU labeling was then combined with PH3

immunohistochemistry to detect cells that had undergone S-to-G2/M transition during the 1 hour chase period in both P0 and P21 brains (Fig. 35A). The percentage of BrdU+ cells colabeled with PH3+ was significantly higher in Nestin:cKO mice at P0 and P21 (Fig. 35B-C). Thus, BrdU incorporated nuclei appeared to rapidly transition into M, suggesting that the length of S-to-G2/M transition was shortened in the absence of Sp2.

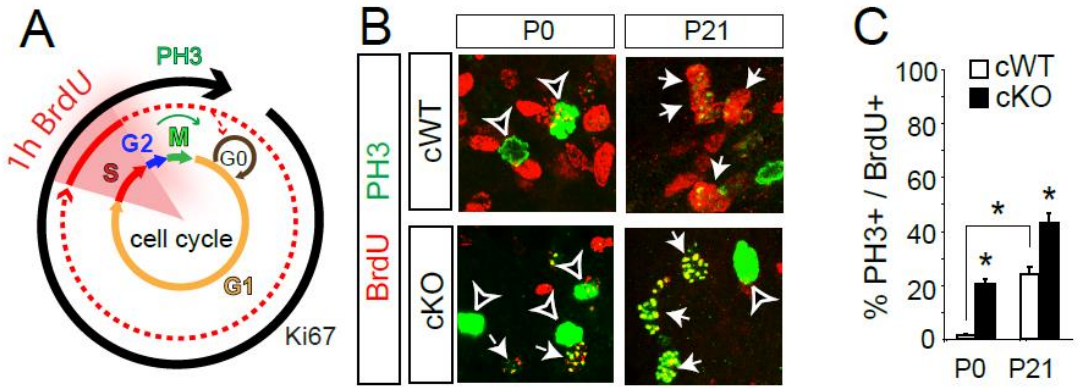

Figure 35. Transition from S-G2/M phase during 1 hour BrdU tracing in the P0 and P21 progenitors. (A) Cell cycle progression was assessed in vivo by means of administering pulses of BrdU followed by a 1-hour chase period prior to sacrifice. **(B)** S to M progression was quantified by co-labeling for BrdU (red) and PH3 (green; arrows). **(C)** Nestin:cKO progenitors had a consistent increase in percentage of BrdU+/PH3+ cells over total BrdU+ cells. *P<0.05, Student's t-test, n=3/age group.

Next, to determine if the transition defect in Sp2-null NSCs and NPCs was due to changes in S-phase duration or faulty G2/M progression, the length of S-phase was determined by a single pulse of IdU followed by a pulse of BrdU three hours later (Fig. 36B). Double labeling for BrdU and IdU and estimation of S-phase length failed to identify

significant changes in Nestin:cWT and Nestin:cKO NSCs and NPCs (Fig. 36C-D). This finding suggested that the duration of S phase was independent of Sp2 expression, and that the length of the G2-M transition was shortened.

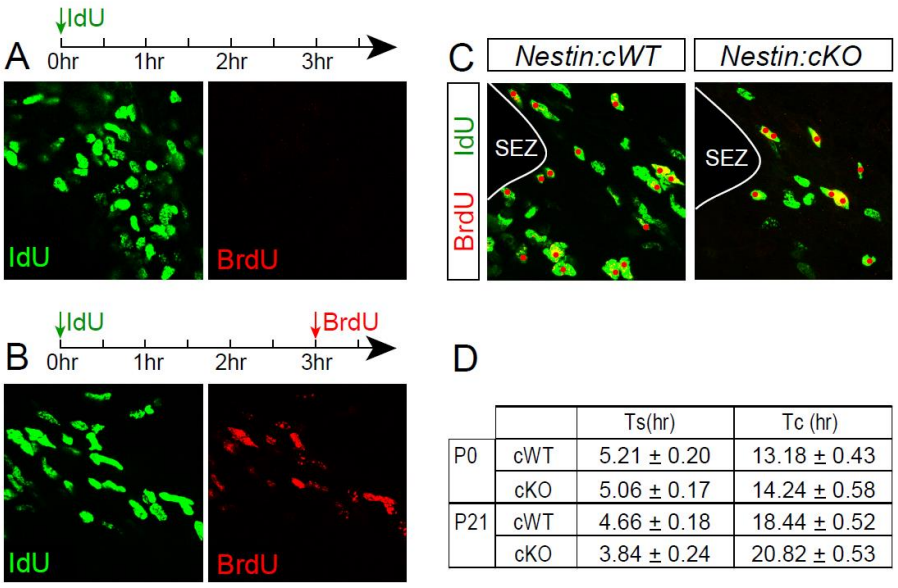

		Ts(hr)	Tc (hr)
P0	cWT	5.21 ± 0.20	13.18 ± 0.43
	cKO	5.06 ± 0.17	14.24 ± 0.58
P21	cWT	4.66 ± 0.18	18.44 ± 0.52
	cKO	3.84 ± 0.24	20.82 ± 0.53

Figure 36. IdU/BrdU dual labeling for estimation of the S-phase and total cell cycle length. (A) An antibody specific to BrdU failed to label IdU incorporated cells (green) in the absence of BrdU injection. **(B)** A pulse of IdU was followed by a pulse of BrdU 3 hours later which allowed for labeling using an antibody that recognizes both BrdU and IdU (green) and one that is specific to BrdU (red). **(C)** Representative confocal micrographs of IdU (green) and BrdU (red) in the P21 Nestin:cWT and Nestin:cKO SEZ. Red dots were added to highlight IdU+BrdU+ cells. **(D)** Estimated length of the S phase (Ts) and the total cell cycle (Tc) in the P0 and P21 wildtype and mutant SEZ progenitors.

To gain more insight into the fate of Sp2-null cycling cells that transitioned into M rapidly, we extended the survival time to four hours which still yielded a higher percentage

of BrdU+ PH3+ NSCs and NPCs in Nestin:cKO brains (Fig. 37A). In addition, a significant fraction of PH3+ cells in the Nestin:cKO SEZ and RMS remained BrdU-negative (Figs. 37B-C), suggesting that Sp2-null progenitors may be arrested in G2/M at the time of BrdU administration, and remained PH3+ throughout the four hour chase period.

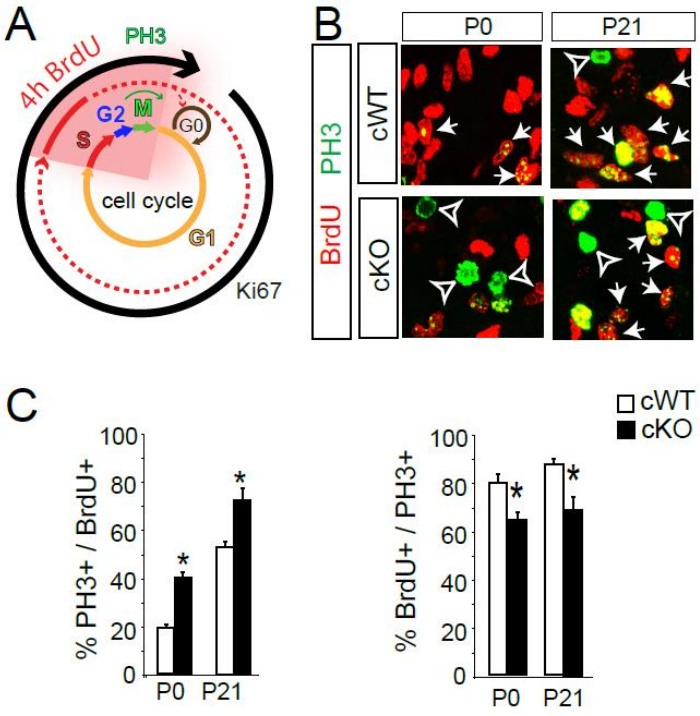

Figure 37. Transition from S-G2/M phase during 4-hour BrdU tracing in the P0 and P21 progenitors. (A) Cell cycle progression was assessed in vivo by means of administering pulses of BrdU followed by a 4-hour chase period prior to sacrifice. **(B)** S to M progression was quantified by co-labeling for BrdU (red) and PH3 (green; arrows). M-phase cells that did not incorporate BrdU were labeled as PH3+/ BrdU-negative (arrowheads). **(C)** Nestin:cKO progenitors had a consistent increase in percentage of BrdU+/PH3+ cells over total BrdU+ cells. Percentage of BrdU incorporated PH3+ cells significantly decreased in the Nestin:cKO progenitors. *P<0.05, Student's t-test, n=3/age group.

2.3 Sp2-null progenitors are arrested in M phase

To test the possibility of potential M phase arrest, we allowed longer survival after BrdU administration (12 hours) to quantify loss of PH3 immunoreactivity in BrdU+ cells (Fig. 38A). Again, the percentage of BrdU+PH3+ cells was significantly higher in the Nestin:cKO progenitors (Fig. 38B).

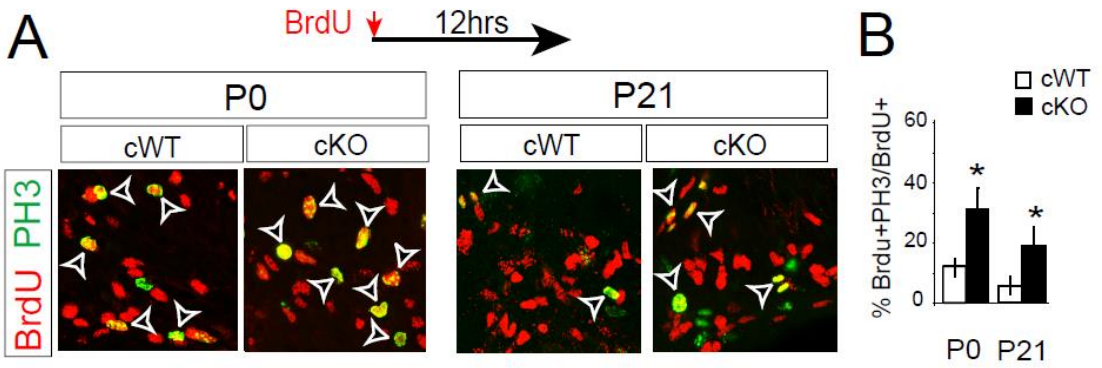

Figure 38. 12 hour BrdU tracing in the P0 and P21 progenitors. (A) Cell cycle progression was assessed in vivo by means of administering pulses of BrdU followed by a 12-hour chase period prior to sacrifice. BrdU + cells (red) that remained PH3+ (green) were indicated by arrows. **(B)** Nestin:cKO progenitors had a consistent increase in percentage of BrdU+/PH3+ cells over total BrdU+ cells. *P<0.05, Student's t-test, n=3/age group.

To assess the proportion of progenitors within distinct stages of the cell cycle, SEZ and RMS cells were isolated from P0 and P21 animals, labeled with propidium iodide, and subjected to flow cytometry. Normalization of flow data indicated significantly higher

proportions of Nestin:cKO cells in G2/M compared to wildtype at both P0 and P21 (Fig.39). These findings confirmed that NCSs and NPCs in Nestin:cKO brains were at least partially arrested in G2 and M phases of the cell cycle. Interestingly, we also identified a significant reduction in the proportion of cells in G1/G0 (Fig.39B), which may contribute toward a significant, yet moderate, increase in total cell cycle length in the cKO NSCs and NPCs in the postnatal brain (Fig. 36D).

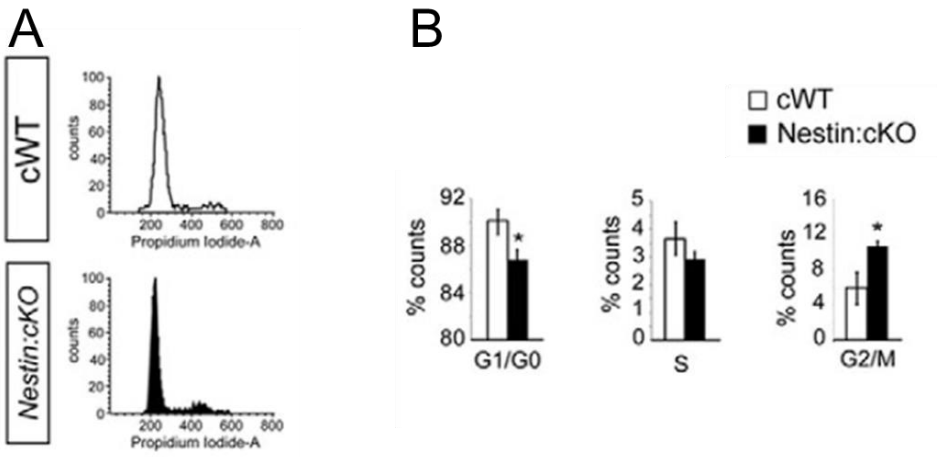

Figure 39. Flow cytometry for cell cycle analysis. (A) Flow cytometric data from cycling cells harvested from P21 cWT and Nestin:cKO SEZ and RMS. **(B)** There was a significantly higher proportion of cells in the G2/M phases and reduced proportion of G1/G0 phase. *P<0.05, Student's t-test, n=3/age group.

2.4 Cell cycle exiting is delayed in the absence of Sp2

The defect in G2/M transition in Sp2-null brains provoked us to determine whether Nestin:cKO cells were capable of exiting the cell cycle at a similar rate as wildtype

progenitors. To quantify cell cycle exiting, three pulses of BrdU were administered every two hours to P0 and P21 Nestin:cKO and cWT mice, followed by a 48 hour survival period (Fig. 40A). In this regimen, BrdU immunoreactivity was combined with Ki67 staining in order to distinguish progenitors that had remained in, or re-entered, the cell cycle after 48 hours (BrdU+/Ki67+), from cells that had exited the cell cycle (BrdU+/Ki67-negative). A significantly higher proportion of BrdU+ Nestin:cKO progenitors were Ki67+ compared to cWT progenitors, indicating a decline in cell cycle exiting (Fig. 40A-B).

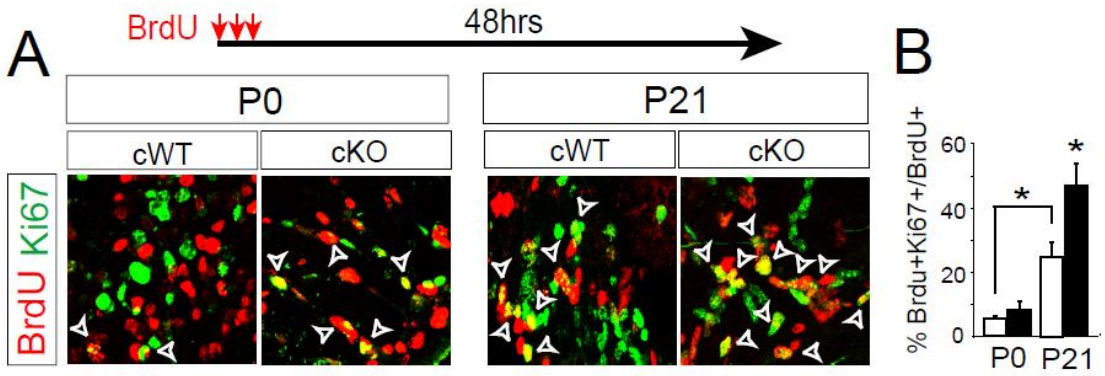

Figure 40. Cell cycle exiting is delayed in the Nestin:cKO progenitors. (A) For assessment of cell cycle exiting, 3 pulses of BrdU were administered at 2-hour intervals, and injected mice were perfused 48 hours after the last pulse. BrdU incroporatd cells that remained or reentered the cell cycle during the 48 hours chasing period were labeled as BrdU+/Ki67+ (arrowheds). **(B)** Percentage of cells remained or reentered the cell cycle (BrdU+/Ki67+ cells over total BrdU cells) during 48hrs chasing period was dramatically increased in Nestin:cKO progenitors. *P<0.05, Student's t-test, n=3/age group.

2.5 Sp2 is required for completion of cytokinesis

The extensive cell cycle analyses strongly indicated that Sp2-null NSCs and NPCs were partially arrested in M phase. To conclusively confirm the M phase defects and to identify specific sub-stages of M phase the Sp2-null cells were arrested in, we next performed time-lapse analysis to monitor progenitor cell division. We utilized the MADM11 system as described before and the cre-mediated mitotic recombination will be driven by either the *Nestin-cre* or *Emx1*^{cre} lines. Under this breeding scheme, MADM-cWT, MADM-cHET, and MADM-cKO cells can be clearly distinguished with fluorescent reporters (tdTom+= MADM-cWT; GFP+ tdTom+ = MADM-cHET; GFP+ = MADM-cKO). The power of the MADM system lies in the low levels of recombination in a small fraction of progenitors which allows for mosaic and clonal analysis of progenitor functions.

First, we harvested cells from P7 *Nestin-cre:Sp2 F/+:MADM-11* brains and fluorescent cells were subjected to time-lapse imaging. Neural progenitors from all three genotypes underwent mitotic round up and initiated cytokinesis (Fig. 41). However completion of cytokinesis was significantly retarded in Sp2-deficient cells, and often failed in Nestin:MADM-cKO cells (Fig. 41B). In the cKO dividing cell pairs that failed to complete cytokinesis, the intercellular bridge (ICB) elongated but persisted between the nascent daughter cells, indicating a specific defect in abscission at the terminal stage of cytokinesis. Within the small fraction of Sp2 mutant progenitors that completed cytokinesis its duration was significantly increased (Fig. 41C).

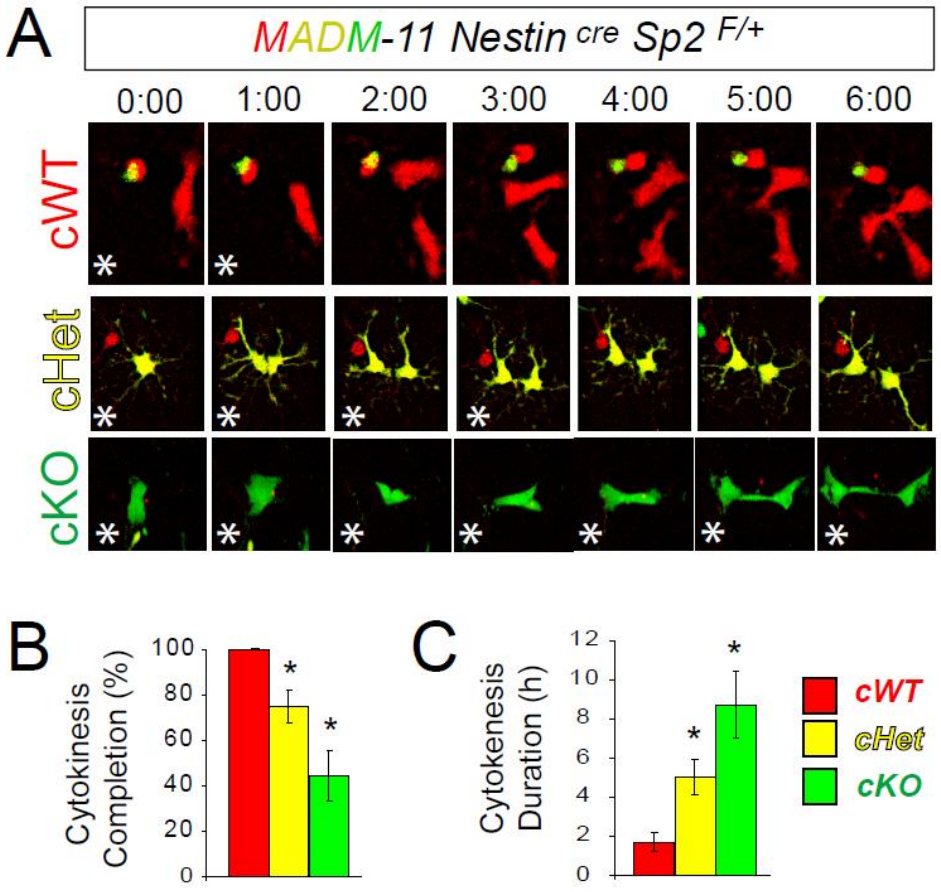

Figure 41. Nestin-cHET and Nestin-cKO progenitors fail to complete cytokinesis. (A) Time-lapse imaging of cultured neural progenitors harvested from *Nestin-cre:Sp2 F/+:MADM-11* mice. Duration of cytokinesis (labeled with asterisks) was consistently longer in both cHET (yellow) and cKO (green) progenitors than in the cWT (red) population. Time-lapse scale, hours:minutes. **(B)** Percentages of cWT, cHET, and cKO cells that completed cytokinesis over 12 hours of imaging. **(C)** Average duration of cytokinesis in cWT, cHET, and cKO cells. *P<0.05, Student's t-test. n=3/age group.

To confirm the cytokinesis defects *in vivo,* we next monitor progenitor divisions in the developing cerebral cortices. Organotypic brain slices were harvested from E14.5 *Emx1^{cre} /Sp2F+/MADM-11* mice followed by time-lapse imaging. For clarity we focused on apical radial glia cells (RGs) in the ventricular zone (VZ) of the cerebral cortices as they exhibit highly reliable temporal and spatial patterns of cellular divisions (Gotz and Huttner, 2005). Consistent to isolated postnatal progenitors, RGs from all three genotypes underwent mitotic round up and initiated cytokinesis, as judged by the appearance of the cleavage furrow (Fig. 42A). Cytokinesis often failed in Emx1: MADM-cHET and Emx1: MADM-cKO cells (Fig. 42B). Time to abscission was significantly longer in Emx1:MADM-cHET and Emx1:MADM-cKO cells that completed cytokinesis than in cWT cells (Fig. 42B) (1.9 ± 0.1 hrs in cWT; 5.2 ± 0.4 hrs in cHET; 8.3 ± 0.4 hrs in cKO; n=10 cells/genotype/animal, 3 animals total; $p<0.05$). The persistent duration of ICB was often found in Sp2 mutant dividing cell pairs that failed to complete abscission (Fig. 42A). Thus *in vivo* and *in vitro* time-lapse live imaging combined with the mosaic analysis system clearly demonstrated that Sp2 is cell-autonomously required for completion of abscission, the terminal stage of M phase.

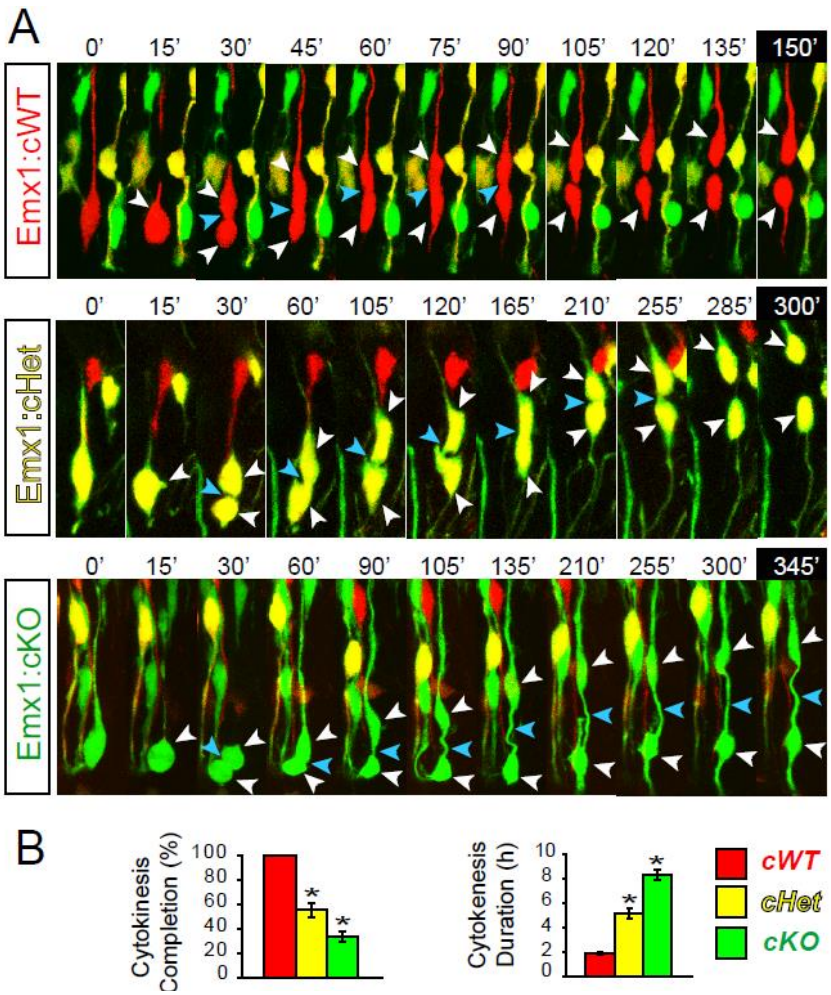

Figure 42. Emx1:Sp2-cKO NSCs exhibit defective cytokinesis and fail to complete abscission. (A) Time-lapse imaging of cultured cortical slice from E14.5 Emx1:Sp2 F/+:MADM-11 mice. White arrowheads indicate mother cells and the subsequent daughter cells they divided into. Blue arrowheads indicate cleavage furrow during cytokinesis initiation and the intercellular bridge (ICB) at later stage. Time lapse scale: minutes (nonlinear). **(B)** Percentages of Emx1:MADM-cWT, Emx1:MADM-cHET and Emx1:MADM-cKO cells that completed cytokinesis over 20 hours of imaging. Average duration of cytokinesis in Emx1:MADM-cWT, Emx1:MADM-cHET and Emx1:MADM-cKO cells is presented in hours. *P<0.05, Student's t-test. n=3/age group.

Consistent with the cytokinesis defects, MADM mutant progenitors possessing two or more nuclei were abundant in cultures fixed after three days (Fig. 43). The multinucleated cell formation indicates that mutant progenitors that failed to complete abscission often remain fused.

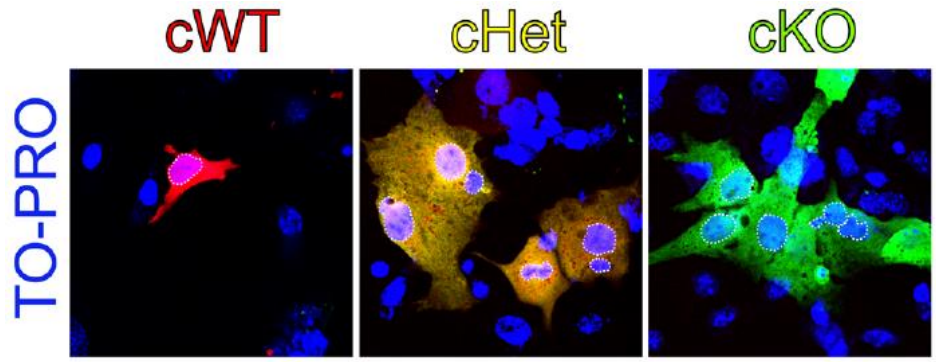

Figure 43. Multi-nucleated cell formation in the cultured MADM Nestin:cHET and MADM Nestin:cKO progenitors. TO-PRO stain (blue) was used to visualize nuclei.

2.6 Centrosome defects in Sp2-null NSCs

To gain more insights into the M phase defects, we next examined a potential disruption in the integrity of mitotic spindle apparatus assembly, centrosome duplication and motility during Sp2 mutant progenitor division. For visualization of centrosomes, neural progenitors were harvested from the transgenic mice expressing the centrosomal protein Centrin2 fused to GFP (CETN2::GFP). Quantification of centriole numbers revealed that the SEZ cKO population displayed significant increases in the incidence of cells containing more than a pair of centrioles (Fig. 44A-B). Thus, centrosomal numbers were disrupted in the

cKO population. Immunofluorescent staining using marker against α-tubulin was performed to label mitotic spindles. Misaligned mitotic spindle formation was frequently observed in the cKO cells (Fig. 44B). These data suggest that Sp2 is required for appropriate number of centrosomes and alignment of mitotic spindle during cellular division.

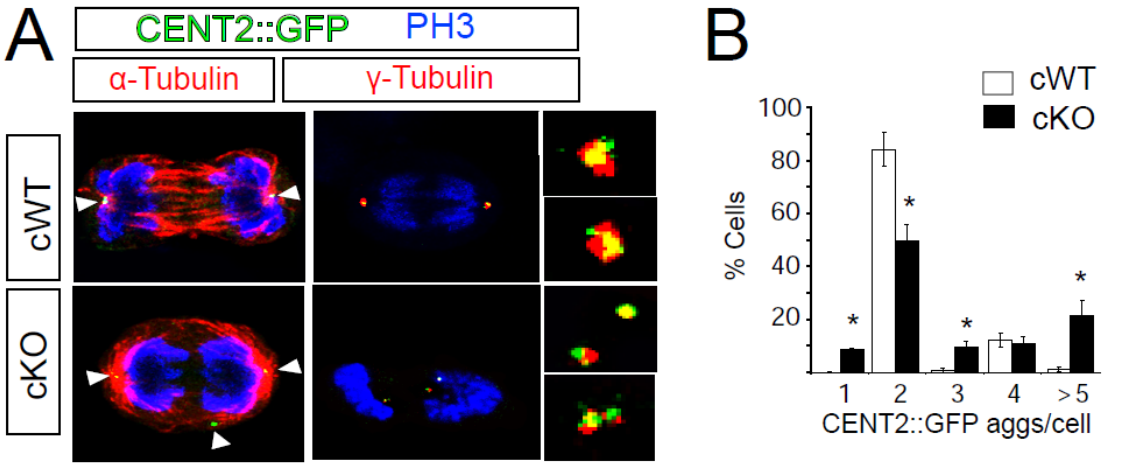

Figure 44. Centrosome number and mitotic spindle formation is disrupted in the cultured postnatal neural progenitors. (A) Cultured neural progenitors harvested from the SEZ of cWT and cKO mice on CETN2::GFP transgenic background. cKO cells consistently contained multiple CETN2::GFP + aggregates (green, arrowheads) and misaligned microtubles (red). Insets illustrate co-localization of CETN2::GFP with γ-tubulin+ peri-centrosomal complexes (red)**. (B)** Percentages cWT and cKO cells with multiple CETN2::GFP+ particles. *P<0.05, Student's t-test. n=3/age group.

To determine whether centrosome motility in dividing Sp2-null cells was dynamically defective, we subjected cKO and cWT cells on the CETN2::GFP background to time-lapse imaging. Centrosome movement was clearly present in cultured cKO cells during mitotic round-up (RU), furrow ingression (FI), and intercellular bridge formation (ICB; Fig. 45A).

During abscission, centrioles localized mostly near the nucleus of the nascent cWT daughter cells, whereas the centrioles in one or both cKO daughter cells remained in close proximity to the intercellular bridge (Fig. 45A). For the duration of ICB stage, when the daughter cells were still connected, the centrioles moved only once into the ICB in the majority of control cWT cells (90.0 + 8.3%). In contrast, centrosomal movement in and out of the ICB was significantly excessive in cytokinetic cKO cells (Fig. 45A,C). In many cKO cells, the abnormal centrosomal positioning was detected up to 10 hours after bridge formation. Consistent with these results, only 40 ± 11% of cKO cells completed cytokinesis (Fig. 45B). Interestingly, in the fraction of cKO cells that managed to complete cytokinesis, 67±14% contained centrioles that migrated into the ICB only once prior to abscission (n=30 cells from 3 independent mice).

The above findings suggested that the abscission defect in cKO progenitors may be directly associated with the subcellular pattern of centriole movement prior to abscission. In fact, the average time spent by cWT centrioles in the ICB was significantly shorter than the time spent by cKO centrioles (Fig. 45D). In turn, abscission occurred within minutes after cWT centrioles exited the ICB, whereas time to abscission was significantly longer in the few cKO cells that managed to undergo abscission (Fig. 45E). The disconnection between centriole movement and the timing of abscission indicated that a potential function of centriole movement into the ICB prior to abscission was defective in the absence of Sp2. In sum, results from series of BrdU tracings, flow cytometry analysis and time-lapse live imaging conclusively show that Sp2 is required for cell cycle progression of M phase in neural progenitors.

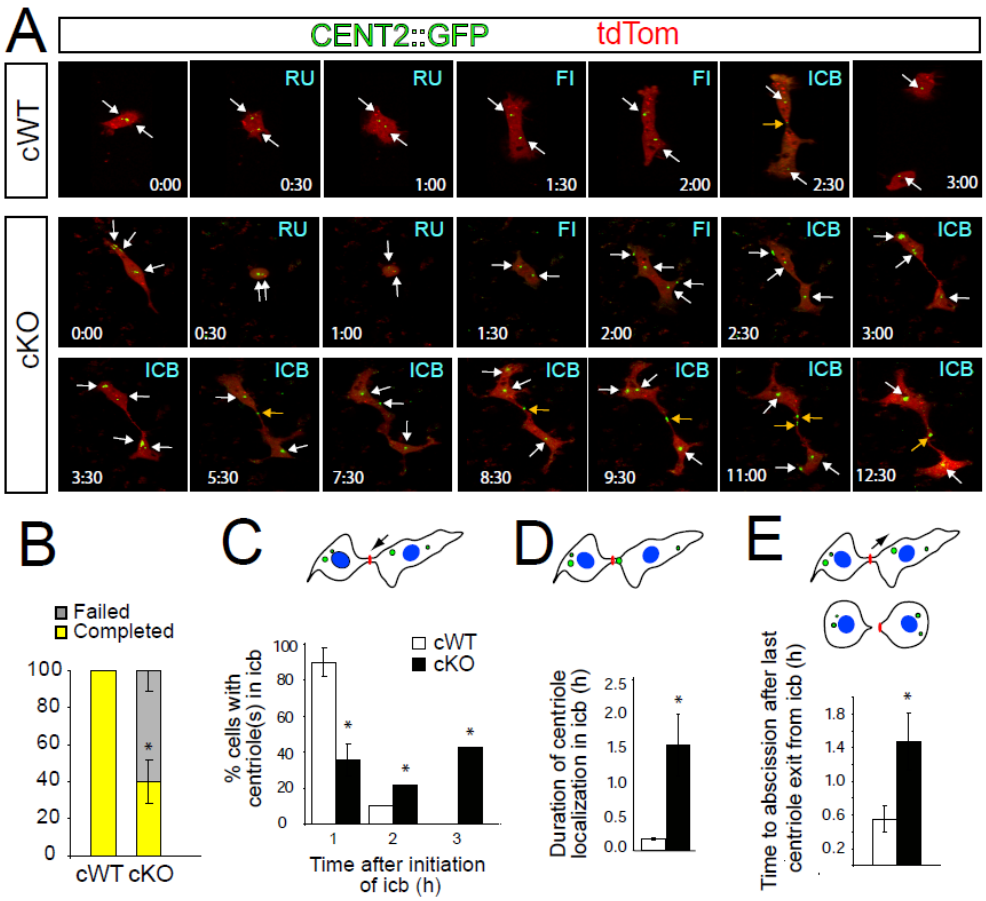

Figure 45. Centrosomal motility during cytokinesis of Sp2-null progenitors is disrupted. (A) Time-lapse imaging analysis of centrosomal dynamics during cytokenesis in CETN2::GFP+ cWT and cKO progenitors. Centrioles in cKO progenitors excessively shuttled between perinuclear locations (white arrows) and the intercellular bridge (orange arrows). Elapsed time is denoated by hours:minutes in each frame (nonlinear in cKO panels). **(B)** Percentage of cWT and cKO cells that completed abscission. **(C)** Percenage of cWT and cKO cells in which centriolar migration into the ICB occurred 1, 2, or 3 times following ICB formation during 12 hours of imaging. **(D)** Average duration of centriolar persistence in the ICB in cWT and cKO cells (in hours). **(E)** Average elapsed time to completion of abscission following centriolar exit from the ICB in cWT and the fraction of cKO cells that underwent abscission. *P<0.05, Student's t-test. n=3/age group.

CHAPTER 3

MECHANISM OF SP2 IN NEURAL PROGENITOR CELL CYCLE REGULATION

The findings in chapter 2 clearly demonstrated that Sp2 is a critical cell cycle regulator in neural progenitors during embryonic and postnatal periods. A combination of approaches led to identification of defective G2/M transition, M-phase arrest, whereas the S phase appears intact in Sp2-null NSCs and NPCs. Additional defects associated with centrosome number and motility during M phase were identified. These findings prompted us to begin investigating the mechanisms through which Sp2 exerts its role in cell cycle regulation. We addressed this issue by examining both transcription and potential non-transcription functions of Sp2. We postulated that Sp2-dependent mechanisms likely include its interaction with sub-cellular organelles and regulators implicated in cell cycle progression.

Results

3.1 Microarray analysis of Sp2-null NSCs

Based on the putative role of Sp2 as a potential transcription factor, we first conducted a transcriptome microarray analysis on Nestin-cWT and Nestin-cKO RNA extracted from microdissected SEZ and RMS tissue at P7, and P21. Results revealed significant changes in the levels of a multitude of transcripts in cKO samples relative to controls (n=6309 genes; one way ANOVA, $P<0.05$). However, only four genes exhibited changes in their level of expression of two fold or greater (all down-regulated in cKO SEZ and RMS relative to cWT). At this junction, it still remains to be determined whether or not the putative transcriptional function of Sp2 is compensated by other transcriptional

regulators. Differentially regulated genes with 1.5 and greater fold changes in their level of expression will be subjected for future analysis. Meanwhile Sp2 is likely a weak transcriptional regulator in vivo, which matches findings from previous reports by the Horowitz group which indicated weak DNA binding, and little if any transcriptional activity by Sp2 in various mammalian cell lines (Moorefield et al., 2004).

3.2 Sp2 is a nuclear and centrosomal associated protein

Despite lack of clear evidence for transcriptional function directly regulated by Sp2, we next postulated that Sp2 may perform alternative cell biological functions. To determine whether Sp2 exerts its role through structural mechanisms we set out to carefully document the dynamics of Sp2 protein during various stages of the cell cycle in cultured NSCs. To accomplish this goal, a construct that encoded for the full length Sp2 protein fused to EGFP under the ubiquitous chicken β-actin promoter (Sp2::EGFP) was cloned. The Sp2::EGFP construct was electroporated into embryonic cortical progenitors and its sub-cellular localization was examined. Sp2 was largely localized to the nucleus as reported previously (Moorefield et al., 2006); however, Sp2::EGFP also appeared in the perinuclear region resembling the microtubule organizing center in both NSCs and various cell lines (Fig. 46). To test this possibility, Sp2::EGFP was co-electroporated with a CETN::RFP construct to simultaneously visualize centrioles and Sp2 in neural progenitors. Confocal analysis confirmed co-localization of Sp2::EGFP with CETN::RFP (Fig. 46).

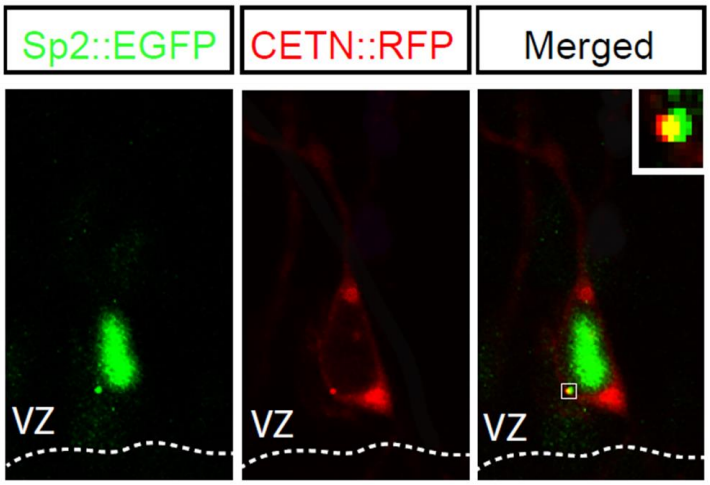

Figure 46. Sp2 is a nuclear and centrosome-associated protein in neural progenitors. RGs in E14.5 cortical slices were electroporated with constructs encoding Sp2::EGFP and CETN2::RFP. Sp2::EGFP colocalized with centrioles reported by CETN::RFP.

To confirm the nuclear and centrosome localization of Sp2, NIH-3T3 cells were lysed and subjected to a sucrose-gradient fractionation procedure to separate the nuclear and centrosomal fractions (Fig. 47). Confirming our subcellular co-localization data, both the centrosomal and nuclear fractions immunoblotted for Sp2. Thus, our findings for the first time revealed that Sp2 is both a nuclear and centrosome-associated protein (Fig. 47).

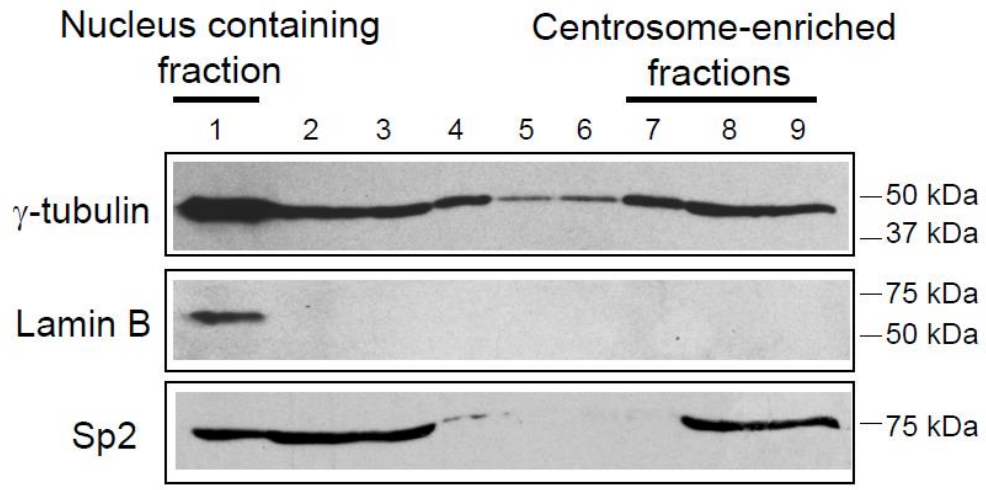

Figure 47. Co-sedimentation of Sp2 with the nucleus and centrosome- containing fractions. Cell fractionation experiments to determine Sp2 localization to both the nucleus and centrosomes. Lanes in each blot: 1, cell pellet; 2, lysate supernatant; 3, lysate in 20% sucrose cushion; 4, second fraction; 5, sixth fraction; 6, tenth fraction; 7, seventeenth fraction; 8, twenty first fraction; 9, twenty fourth fraction. Immunoblots were prepared against γ-tubulin, Lamin B, and Sp2 antibodies to determine specificity of each protein to distinct fractions.

Next, dynamic changes in subcellular localization of Sp2 during the cell cycle were revealed by time-lapse imaging of Sp2::EGFP transfected Cos7 cells. During interphase, Sp2::EGFP was confined to both subnuclear foci and the centrosomes (Fig. 48). At the onset of nuclear envelope breakdown during prophase the nuclear portion of Sp2::EGFP rapidly disappeared, likely due to diffusion in the cytoplasm (Fig. 48). The portion of Sp2::EGFP associated with the centrosomes remained intact and migrated toward the opposing poles of the cell as it proceeded into metaphase (Fig. 48). The nuclear portion of Sp2::EGFP

relocalized to the reforming nuclear envelope (Fig. 48). Following cleavage furrow ingression, a single speck of Sp2::EGFP appeared in the ICB connecting the two daughter cells during late telophase (Fig. 48), which was rapidly followed by abscission. This finding clearly illustrates that sub-cellular localization of Sp2 changes dynamically during cell division and motility of Sp2::EGFP into ICB prior to abscission matched our findings of centriole movement during neural progenitor cytokinesis.

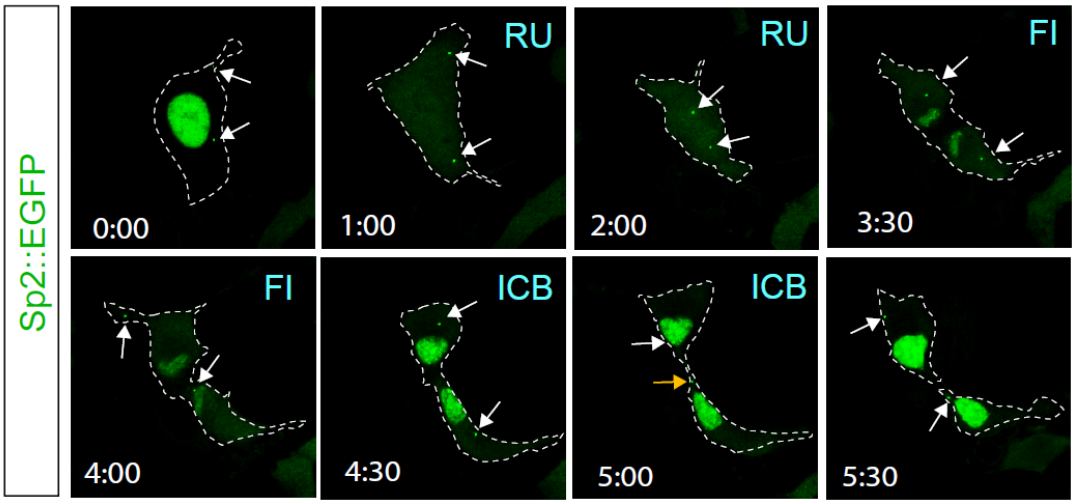

Figure 48. **Subcellular localization of Sp2 changes dynamically during cell division.** Time-lapse confocal scans of a mitotic Cos7cell electroporated with a pCAG:EGFP::SP2 construct. Sp2::EGFP remained bound to the centrosomes throughout cytokinesis (white arrows), whereas nuclear Sp2::EGFP diffused away during nuclear breakdown. A Sp2::EGFP bound centrosome from one of the daughter cells migrated into the intercellular bridge (ICB; yellow arrow) only once prior to abscission. Different stages of cytokinesis: RU, mitotic round up; FI, furrow ingression. Time-lapse scale, hours:minutes (nonlinear).

3.3 The amino- and carboxyl halves of Sp2 are uniquely required for the completion of cytokinesis in Cos7 cells

The newly identified dual localization of Sp2 in the nucleus and the centrosomes raised two important questions: 1) which domains of Sp2 are required for the nuclear/centrosomal localization, 2) whether nuclear and centrosomal localizing domains of Sp2 are collaboratively or uniquely required for Sp2-dependent mechanisms during cytokinesis. To address the first question, we performed domain analysis by generating each half of the full-length Sp2 protein. The domain that contains amino acids 1-381 of Sp2 was termed ΔC 382-612 (N-domain) and the domain that contained amino acids 382-612 was termed ΔN1-381 (C-domain) (Fig. 49A). The fluorescent reporter EGFP was fused to each domain to track their subcellular localization in Cos7 cells. 24 hours after transfection, we found that ΔC 382-612::EGFP displayed centrosomal localization as revealed by co-localization with CETN::RFP. However ΔC 382-612::EGFP failed to localize to nucleus as was expected in previously reported by the Horowitz group (Moorefield et al., 2006) (Fig. 49B). In contrast, ΔN1-381::EGFP displayed both centrosomal and nuclear localization (Fig. 49B). These data suggest that the amino-half of Sp2 contains one or multiple centrosomal localizing signals while its carboxyl-half contains both centrosomal and nuclear localizing signals.

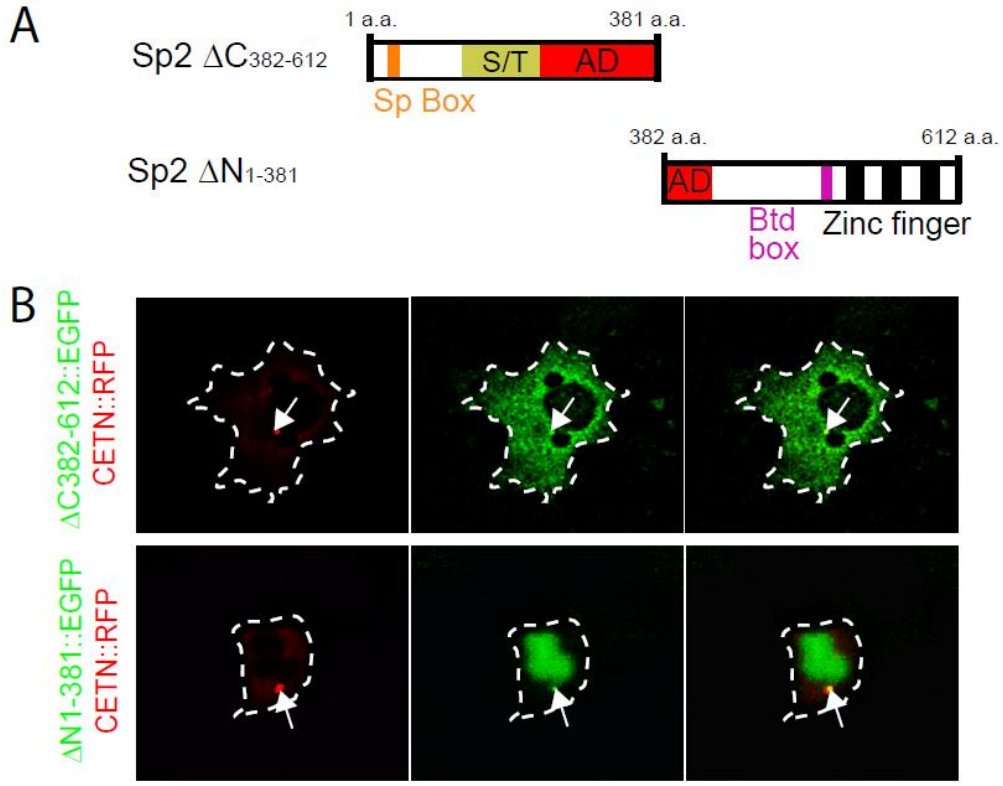

Figure 49. The N- and C-domains of Sp2 contain distinct subcellular localizing signals. (A) Diagram for Sp2 N- and C-domains containing 1-381 a.a. and 382-612 a.a. of Sp2, respectively. **(B)** The Δ C382-612::EGFP domain (green) exhibits centrosomal localization revealed by CETN::RFP (red), but not nuclear localization. The ΔN1-381::EGFP has both centrosomal and nuclear localization.

To gain more insight into the biological role of each domain in cell division, Cos7 cells transfected with each construct were time-lapse imaged for 48-72 hours post-transfection. We found that a significant percentage of ΔC 382-612::EGFP and ΔN1-

381::EGFP expressing cells exhibited defective cytokinesis compared to cells transfected with the control construct pCAG:EGFP (Fig. 50A-B). These data suggest that overexpression of Sp2 N- and C-domains causes dominant negative effects in completion of cytokinesis and both domains are likely to be required for completion of cytokinesis. Interestingly, expression of each domain appeared to arrest cytokinesis at different stages. Transfection of ΔC 382-612::EGFP induced a prolonged duration in ICB formation and the putative centrosome-bound EGFP fusion displayed an excessive shuffling within ICB (Fig. 50A). The defects in centriole motility accompanied with the abscission failure surprisingly mimicked the phenotype observed in the Sp2-null neural progenitors, indicating that N-domain expression potentially interfere with the function of endogenous Sp2 in abscission. Interestingly, expression of C-domain that was sufficient for both centrosomal and nuclear localization induced a prolonged duration in mitotic round-up stage and a failure in the early stage of cytokinesis, in which the cleavage furrows regressed followed by cytokinesis initiation (Fig. 50A). Together, these data indicate that both domains are likely to be cooperatively required for timely progression through different stages of cytokinesis.

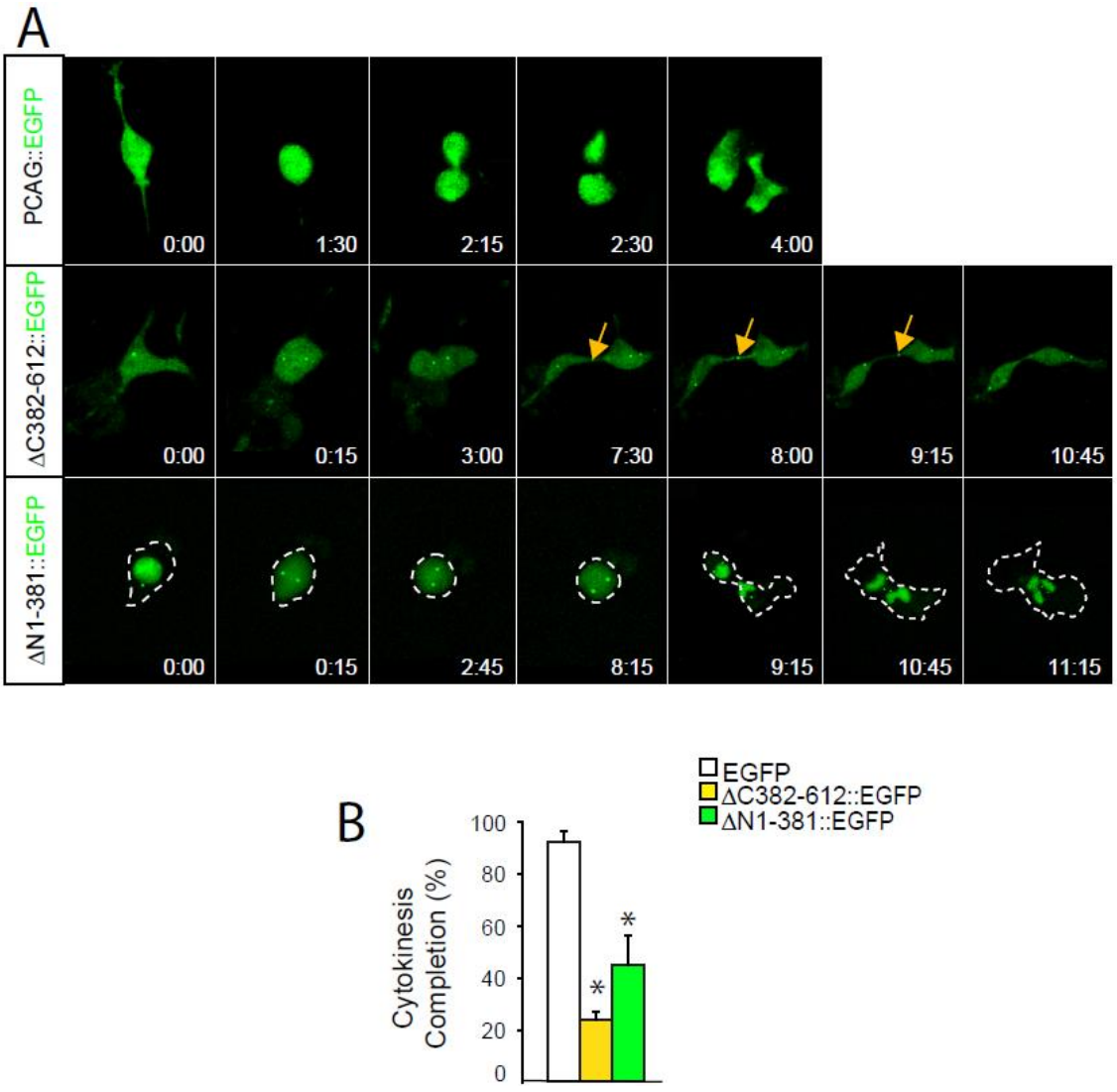

Figure 50. The N- and C-domains of Sp2 are both required for completion in cytokinesis. (A) Time-lapse imaging of dividing Cos7 cells transfected with EGFP only, D C382-612::EGFP or DN1-381::EGFP constructs. Prolonged duration of centrosome-bound EGFP in the ICB was found in the D C382-612::EGFP transfected cells (yellow arrows). Time-lapse scale, hours:minutes. **(B)** Transfection of both N- and C-domain of Sp2 significantly decreased percentage of cells with completed cytokinesis.

3.4 Identification of Sp2 interacting proteins

As previously mentioned, the centrosome has emerged as a critical regulatory site for CDK/cyclin complex (e.g., CDK1/cyclin B), activation and inactivation of which triggers subcellular events underlying cell cycle progression. Importantly, the centrosome also serves as an important docking site for regulatory proteins in cytokinesis. Thus the newly identified Sp2 centrosomal localization prompted us to investigate its protein interactome. A yeast two-hybrid screen yielded potential Sp2 interacting proteins that displayed the CDC25 homology domain shared by all members of the Cdc25 phosphatase family (Cdc25A, Cdc25B and Cdc25C). Additional biochemical analysis confirmed that Sp2 was in a complex associated with members of the Cdc25 family in the embryonic forebrains (Fig. 51).

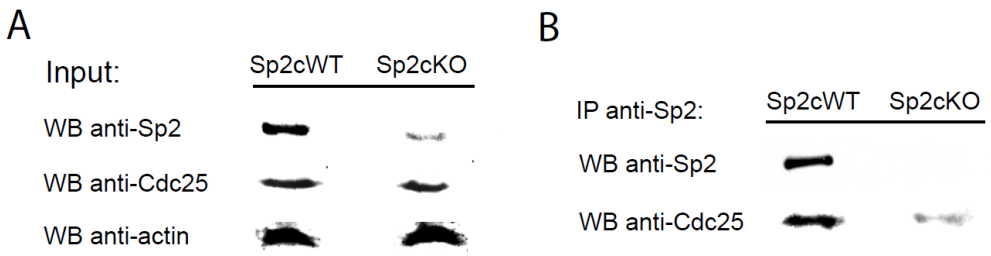

Figure 51. Sp2 interacts with members of the Cdc25 family. (A) Western blotting against Sp2 in protein extracts from P0 whole brains confirmed a near complete deletion of Sp2 from the Nestin:cKO mice. Western blotting using the pan-Cdc25 antibody demonstrated the presence of Cdc25 in both cWT and cKO protein extracts. **(B)** Immunoprecipitation against Sp2 was performed in proteins demonstrated in (A). Endogenous Sp2 coimmunoprecipitates with endogenous Cdc25 in cWT protein samples.

In addition, the potential function of Sp2 N- and C- domains in cell division prompted us to further investigate their interaction with Cdc25. Immunoprecipitation-western blot analysis was performed followed by transfection with a Myc-tagged Sp2 construct, N-domain and C-domain in Cos7 cells. Results demonstrated that Cdcd25 is part of a protein complex that associates with the Sp2, but not with the Sp2 N- or C-domains when expressed on their own (Fig. 52).

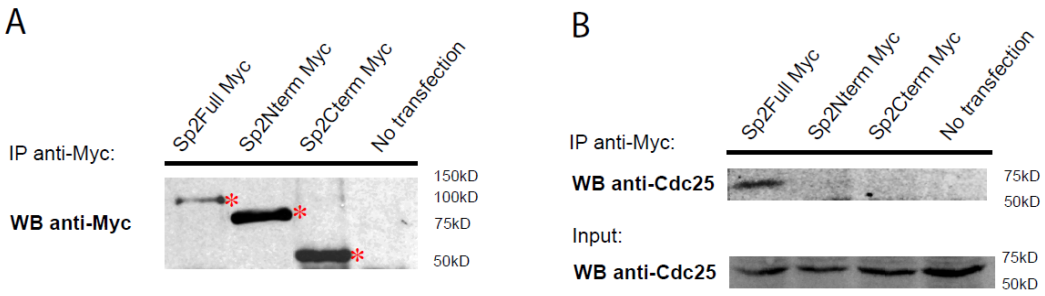

Figure 52. Sp2 full length but not Sp2 N- and C- domain interacts with members of the Cdc25 family. Constructs encoding a Myc tag fused to the Sp2 full length, N-domain and C-domain were transfected in Cos7 cells followed by immunoprecipitation-western blot analysis 24 hours post-transfection. **(A)** Immunoprecipitation against the Myc antibody pulled down corresponding Myc-tagged Sp2 domains at expected sizes (labeled with asterisks). **(B)** Endogenous Cdc25 coimmunoprecipitates with Myc-tagged Sp2 full length but not with Myc-tagged Sp2 N- and C-domain. Protein extracts from Cos7 cells with no transfection were demonstrated as negative controls in A and B.

In summary, our cell biological and molecular analysis of Sp2 has revealed a novel

dual-localization of Sp2 to the nucleus and centrosomes. The amino- and carboxyl halves of Sp2 contain distinct yet cooperative signals, both of which are required for successful completion of cytokinesis. Preliminary biochemical analyses have identified the Cdc25 phosphatase family as potential physical partners of Sp2 which raise exciting hypotheses regarding the mechanism of Sp2 function during cytokinesis specifically, and cell cycle progression in general.

CHAPTER 4

SP2 IS REQUIRED FOR CELL FATE DETERMINATION IN NEURAL PROGENITORS

In the previous chapters we demonstrated that Sp2 is a critical regulator of neural progenitor proliferation and cell cycle progression. Based on recently established paradigms described in my introduction regarding the impact of cell cycle regulators on fate-specification in neural progenitors, we next began to explore whether mechanisms regulated by Sp2 impact fate decisions in dividing NSCs. To address this issue we examined the production of NSCs, IPCs and neurons *in vivo* at various developmental time points. In addition, the neurosphere assay was utilized to assess the differentiation potential of neural precursors *in vitro.*

Results

4.1 Loss of Sp2 favors NSC cell fate and disrupts production of NPCs and neurons

We sought to identify the impact of Sp2 deletion on the fate of NSCs and NPCs. We first focused on the embryonic cerebral cortex, in which RGs serve as NSCs and give rise to neuronal IPCs. RGs express the transcription factor Pax6, which is required for RG self-renewal and multipotency (Sansom et al., 2009; Englund et al., 2005). During the transition from RGs to IPCs, downregulation of Pax6 associates with upregulation of Tbr2, a transcription factor required for neurogenesis in the SVZ (Arnold et al., 2008; Englund et al., 2005). Therefore Pax6 and Tbr2 will be utilized as the markers for RGs and IPCs, respectively. During the early stage of neurogenesis at E12.5, nearly the entire thickness of

the Emx1:cKO cerebral cortex was occupied by Pax6+ cells, whereas cWT Pax6+ NSCs are confined to the VZ (Fig. 53A). Moreover, TuJ1+ postmitotic neurons were significantly reduced (Fig. 52A) resulting in a severe reduction in the size of the preplate (Fig. 53B). Additionally, the percentage of Pax6+ NSCs within all PH3+ progenitors was elevated in the Emx1:cKO cerebral cortices compared to cWT controls (Fig. 53C).

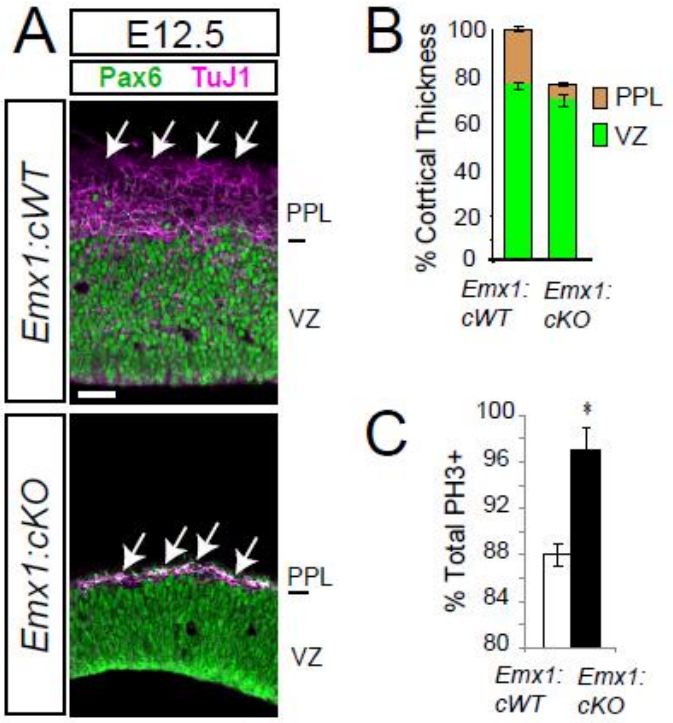

Figure 53. Disruption of neurogenesis in the E12.5 Emx1:cKO cerebral cortices. (A) Confocal micrographs of the embryonic cerebral cortex stained for Pax6 (green) and Tuj1 (purple) in the E12.5 (Arrows point to the pial surface of the cortex). **(B)** Percentage of total cortical thickness occupied by VZ and PPL at E12.5 (normalized to the average thickness of wildtype cortex). **(C)** Percentage of Pax6+ progenitors at E12.5 among all PH3+ cells in the wildtype and Sp2 mutant cerebral cortices. Scale bars: 20 µm. *P<0.05, Student's t-test. n=3/age group.

By E14.5, Tbr2+ IPCs were significantly less dense in the Emx1:cKO SVZ (Fig. 54A), resulting in significant disruption in apico- basal organization of the cortex (Fig. 54B). Additionally the percentage of PH3+ cells double labeled with Tbr2 was significantly retarded in the mutant basal VZ and SVZ at E14.5 (Fig. 54C). Thus, it appeared that in the Sp2-null cerebral cortex proliferating progenitors were arrested as Pax6+ NSCs at the expense of production in Tbr2+ NPCs and Tuj1+ neurons, suggesting defects in fate specification and differentiation in the early embryonic cortex.

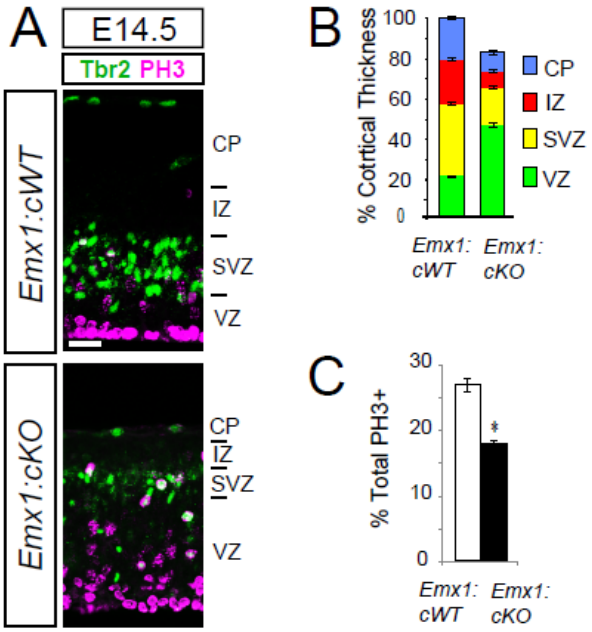

Figure 54. Disruption of intermediate progenitor production in the E14.5 Emx1:cKO cerebral cortices. (A) Confocal micrographs of the embryonic cerebral cortex stained for Tbr2 (green) and PH3 (purple) in the E14.5 cerebral cortices. **(B)** Percentage of total cortical thickness occupied by VZ, SVZ, IZ and CP at E14.5 (normalized to the average thickness of wildtype cortex). **(C)** Percentage of Tbr2 + progenitors at E14.5 among all PH3+ cells in the wildtype and Sp2 mutant cerebral cortices. Scale bars: 20 µm. *P<0.05, Student's t-test. n=3/age group.

As previously mentioned, during cortical development neurons are born and migrate to the cortical plates in an inside-out manner, which means early-born neurons are situated in deeper layers while late-born neurons are situated in upper layers. The defects of neurogenesis prompt us to further examine the impact of Sp2 deletion on neuronal differentiation and laminar organization in the P0 Emx1:cKO cortex. Expression of the transcription factor Ctip2 (COUP-TF interacting protein 2) selectively labels upper layer of cerebral cortex (layer V), and Cux1 (cut-like homeobox 1) selectively marks the deeper layers (layer II-IV) (Alcamo et al., 2008; Cubelos et al., 2008). Therefore, immunostaining against Cux1 and Ctip2 was performed to identify different layers of the cerebral cortex (Fig. 55B). Cux1+ cells in the mutant cortex were largely absent in the upper cortical layers and distribution of Ctip2+ cells failed to specify layer V as in cWT cortices (Fig. 55A, B). Additionally, ectopic and densely packed clusters of Ctip2+ cells were detected in the P0 cortex suggesting disruption of their differentiation or migration (Fig. 55A).

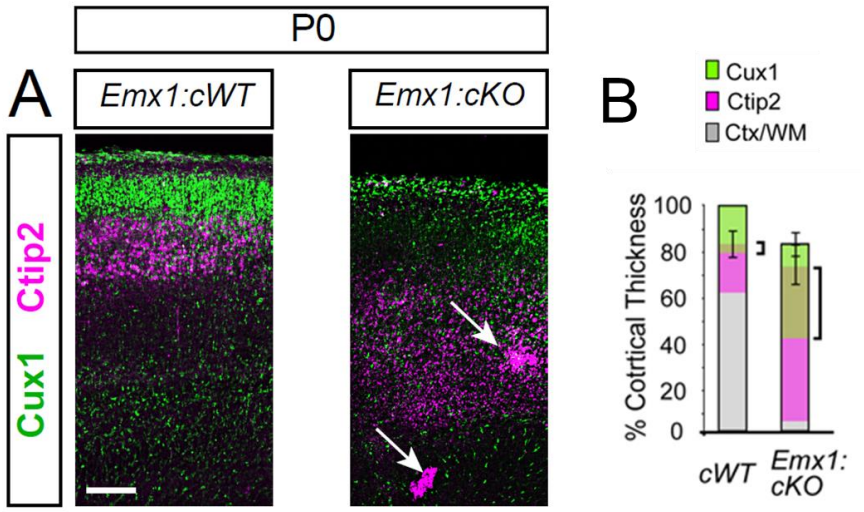

Figure 55. Organization of interneurons is disrupted in the P0 Emx1:cKO cerebral cortices. (A) Confocal micrographs of Cux1 (green) and Ctip2 (purple) in the P0 cWT and cKO cerebral cortex. **(B)** Percentage of total cortical and white matter thickness (gray) occupied by Cux1+ (green) and Ctip2+ (purple) projection neurons at P0 normalized to the average thickness of wild-type cortex. Brackets indicate degree of overlap between Cux1 and Ctip2 domains for each genotype. Scale bar: 50 µm.

4.2 Loss of Sp2 arrests NPCs in a Pax6 fate and disrupts neuronal and glial differentiation

To determine if perinatal deletion of Sp2 would similarly impact lineal relationships between postnatal NSCs and NPCs, we used Pax6, Dlx2, and Gsx2 staining in the Nestin:cKO SEZ and RMS. Remarkably, Sp2 deletion resulted in accumulation of Pax6+ cells concomitant with disruption of Gsx2+ or Dlx2+ progenitors and Dcx+ neuroblasts in the mutant SEZ and RMS (Fig.56).

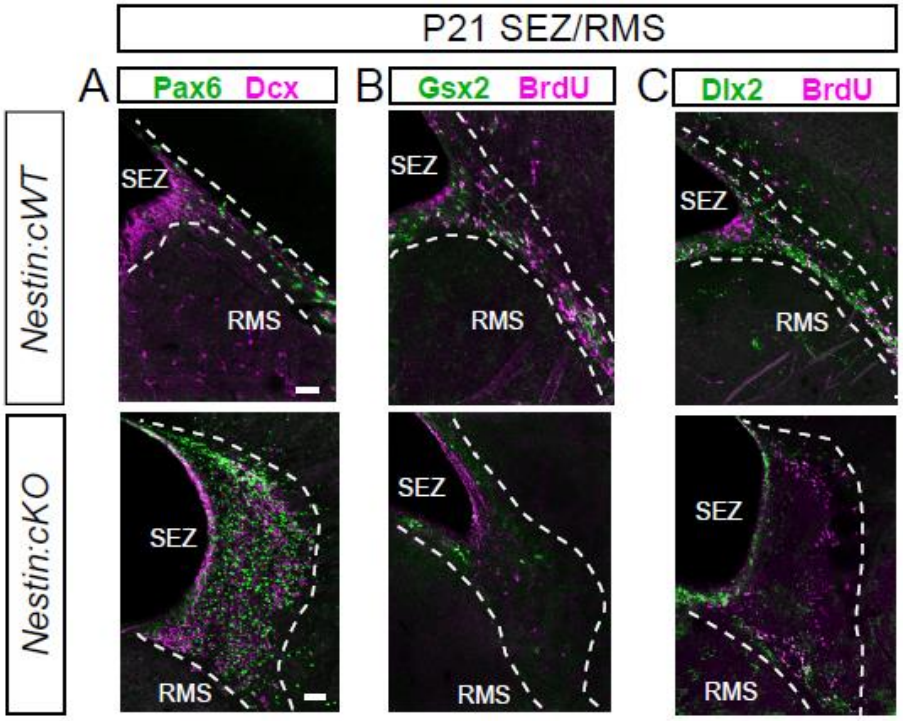

Figure 56. Expression pattern of the progenitor cell-type specific markers are disrupted in the Nestin:cKO stem cell niche. Confocal micrographs of Pax6+ (**A**, green), Gsx2 (**B**, green) and Dlx2+ (**C**, green) NSCs and NPCs in the P21 SEZ and RMS (outlined by dashed line). Tissues were costained for Dcx and BrdU (1 hour acute pulse) as labeled (purple). Scale bar: 20 µm.

Finally to assess the impact of Sp2 on the differentiation potential of postnatal NSCs and NPCs, P21 Nestin:cKO SEZ and RMS cells were cultured to generate neurospheres followed by plating for differentiation (Fig. 57). While cWT neurospheres generated astrocytes (GFAP+), oligodendrocytes (NG2+), and neurons (Tuj1+), cKO neurospheres were largely astrocytogenic, and their ability to differentiate into oligodendrocytes or neurons was significantly retarded (Fig. 57). Thus, these results suggest that Sp2-dependent

regulation of the cell cycle is required to drive the progeny of cycling NSCs and NPCs toward their programmed neuronal and glial fates during corticogenesis and postnatal neurogenesis. Disruption of Sp2-dependent cell cycle progression appears to favor the maintenance of an early NSC type in the developing and postnatal stem cell niches.

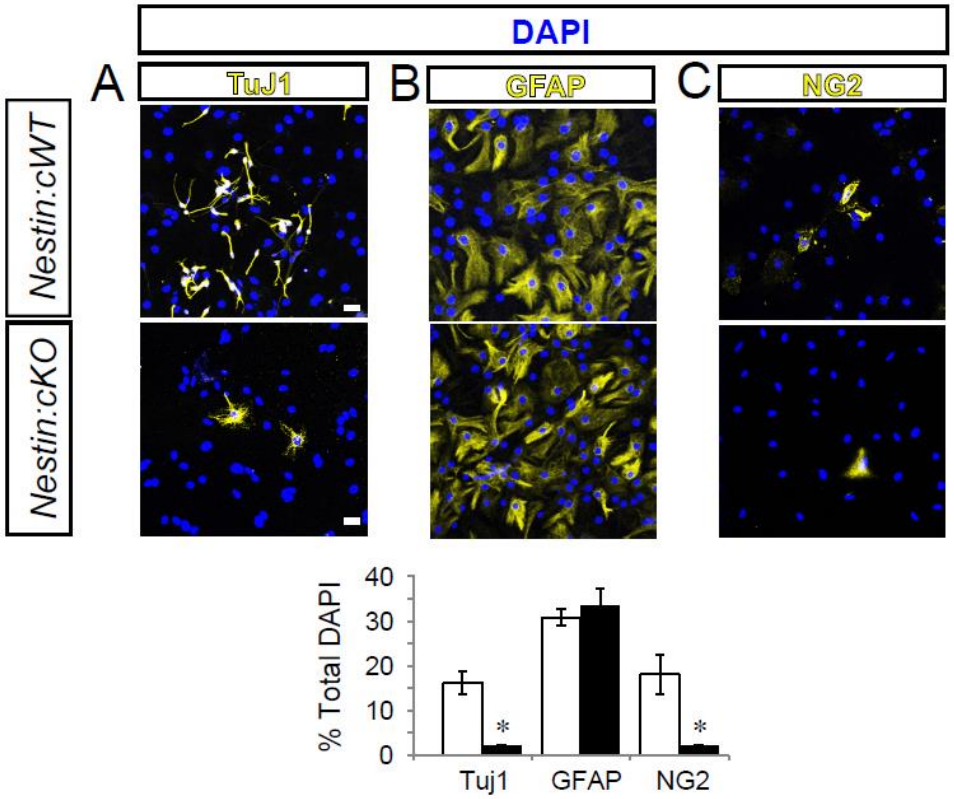

Figure 57. Differentiation potential of the Sp2-null neurosphere is compromised. Confocal micrographs of cultured Tuj1+ neurons (**A**, yellow), GFAP+ astrocytes (**B**, yellow), and NG2+ oligodendrocytes (**C**, yellow) obtained from cWT and Nestin:cKO SEZ and RMS progenitors and differentiated for 6 days following neurosphere plating. Percentages of each cell type among all DAPI labeled nuclei (blue).

In sum, conditional deletion of Sp2 favors arrest of progenitors in a Pax6+ NSC fate at the cost of generation of NPCs and neurons in the developing and postnatal brains. Our results indicate that Sp2 plays a critical role in cell fate determination in neural progenitors.

DISCUSSION

Sp2 is a novel regulator of cell cycle progression

In the first part of my thesis work I uncovered a novel role for the transcription factor Sp2 in cell cycle homeostasis within developing NSCs and NPCs. A combination of approaches led to identification of rapid G2/M transition, M phase arrest and shorter G1 while the S-phase appears intact in Sp2-null NSCs and NPCs. This function of Sp2 is not confined to a specific developmental stage, but equally impacts embryonic and postnatal NSCs and NPCs. M phase arrest in embryonic and postnatal Sp2-null NSCs and NPCs is concomitant with overall decline in the number of cycling cells, which is consistent with the notion that proper progression through mitosis is required for maintenance of neural progenitor pools during brain development (Feng and Walsh, 2004a; Gruber et al., 2011; Jacquet et al., 2009a; Lizarraga et al., 2010; Sakai et al., 2012; Silver et al., 2008). However, unlike the mitotic arrest due to deletion of Tcof1/Treakle (a centrosomal protein) which results in reduction of both apical and basal cortical progenitors (Sakai et al., 2012), our findings show that Sp2-dependent mitotic arrest may preferentially expand apical NSCs at the expense of basal NPCs. Since several M phase regulators such as Aurora A and Polo kinase can exert dual roles in cell cycle progression and fate determination (reviewed by Budirahardja and Gönczy, 2009), it is conceivable that potential cross talk between Sp2 functions and various cell cycle-active kinases may couple M progression with fate specification in NSCs and NPCs. Such coupling may differentially impact symmetric and asymmetric cell divisions in apical and basal progenitors of the cerebral cortex.

In addition to M-phase arrest in NSCs and NPCs, transition through G2/M is

accelerated in the absence of Sp2. In this context, the mitotic entry network involves upregulation of Cdk1/cyclin B complex and its activation through posttranscriptional modifications (Bollen et al., 2009; Fung and Poon, 2005; Lindqvist et al., 2009; White et al., 2009). Notably, many kinases and phosphatases that form the mitotic entry network are also required for progression through M (Bollen et al., 2009; Lindqvist et al., 2009; Pomerening et al., 2008), for example by coupling timely G2-M transition to centrosome maturation for appropriate mitotic spindle orientation in neural progenitors (Gruber et al., 2011). At this juncture it remains unclear how Sp2-dependent mechanisms regulate G2-M transition in parallel with M phase progression.

Our long term BrdU tracing experiments revealed a lower rate of cell cycle exiting in Sp2 mutant progenitors, which can be explained by arrest in M or by cell cycle re-entry instead of cell cycle exit. However, Sp2-null progenitors exhibit only a moderate increase in total cell cycle length which may at least in part be due to a simultaneous decline in G1 duration (indicated by flow data) combined with a prolonged M. Thus it appears that Sp2 null progenitors have shortened gap phases, a prolonged M phase, and likely re-enter the cell cycle constitutively, which is likely the root of the rapid decline in total NSCs and NPCs due to the absence of mechanisms for quiescence. In this situation, an intriguing parallel may be drawn regarding the lack of, or very brief G1 and G2 in early embryonic stem cells (Burdon et al., 2002; Stead et al., 2002). As development proceeds, the two gap phases emerge and progressively lengthen (especially G1) with a concomitant decline in the rate of stem cell divisions (He et al., 2009). By the time the neuroepithelium is specified the two gap phases are established in early NSCs, however the length of G1 is significantly shorter in cerebral

cortical progenitors at early (E11.5 in the mouse) versus late (E16.5 in the mouse) stages of development (Takahashi et al., 1996). Gap phase alterations are critical for prolonged maintenance of NSCs and NPCs as well as influencing the fate of their neuronal and glial progenies (Burns and Kuan, 2005; Cameron and McKay, 2001; Hayes and Nowakowski, 2002; Lu et al., 2007; Smith and Luskin, 1998). The perturbed duration of Gap phases in Sp2 null NSCs and NPCs at least partially resembles early stem cells, which suggests that Sp2-dependent mechanisms may be important regulators of cell cycle maturation in stem cells and progenitors during embryonic and postnatal development.

Sp2 is required for completion of cytokinesis

Time-lapse imaging combined with mosaic analysis with double markers (MADM) conclusively demonstrated that Sp2 is cell-autonomously required for completion of cytokinesis, which is why Sp2-null NSCs were found to be M-phase arrested in vivo. Interestingly, early stages of cytokinesis, including formation of the cleavage furrow and intercellular bridge (ICB), appear intact in the absence of Sp2. Instead Sp2-null progenitors failed in the cleavage of ICB, indicating that Sp2 may have a focused role in regulation of abscission, the final step of cytokinesis. Importantly, we demonstrated that in the control progenitor cell division, centrioles transiently moved into ICB once during the final stage of cytokinesis, and movement of the centriole away from the bridge correlates with induction of abscission. This unique centriolar motility during final stage of cytokinesis has been observed in mammalian cell lines for some time, and the centriole positioning into ICB were associated with narrowing of the bridge and depolymerization of microtubules within the central spindle (Piel, 2001). Subsequent functional studies have identified individual

centrosomal proteins including Centriolin and Cep55 with roles in abscission, whereby both proteins exhibit transient movements into the ICB. Both these proteins target membrane vesicle tethering complexes (exocysts) and membrane vesicle fusion complexes (SNAREs) to promote fusion of the plasma membrane at the abscission site (Gromley et al., 2005; Zhao et al., 2006). Therefore centriolar motility during late cytokinesis has been functionally linked to abscission in mammalian cell lines and our study for the first time indicates that Sp2-dependent mechanisms that need to be better defined impact the integrity of this abscission machinery in neural progenitor cell.

In the absence of Sp2 we found that an excessive shuffling of centriole movement into ICB is accompanied with abscission failure. This result suggests that while initiation of trafficking of centrioles to ICB is intact in the absence of Sp2, Sp2's physical trafficking to the ICB through its interaction with the centrosomes may provide important signals in initiation of abscission in the ICB. This hypothesis may be tested in future studies in the context of two possibilities: (1) Sp2 and its associated protein complexes at centrosomes might provide a signal to cellular machineries that drive abscission. For example, Sp2 transport may be required as a cofactor for enzymes involved in microtubule severing and plasma membrane fusion as described in the introduction of this thesis. (2) Sp2 may also function as a communicator between the nuclear matrix and the ICB to time nuclear reassembly following chromosome segregation with abscission at the ICB. In this possibility, centrosomes may function as transport portals that allow Sp2 to be shuttled between the nuclear matrix and the ICB. Sp2 may signal through recruitment of several kinases with known localization to the ICB and the midbody precisely during the same

period when Sp2 null defects are so prevalent. In fact, several centrosomal proteins are subject to phosphorylation by a number of kinases active during cytokinesis, and these phosphorylation events have been shown to be critical to the integrity of abscission (Bastos and Barr, 2010; Fabbro et al., 2005). For example, Cep55 is phosphorylated by CDK1, and ectopic expression of Cep55 with a mutant phosphorylation site causes abscission failure and a surprisingly elevated localization of Cep55 to the ICB (Fabbro et al., 2005). Although the question of how centrosome proteins (e.g., Cep55) are temporally and spatially regulated by cell cycle regulators (e.g., CDK1) for abscission still remains unanswered, these studies present a possibility that a master regulatory machinery governing CDK1 activity could in turn regulate the timing of abscission. Excitingly, based on the biochemistry analysis we begin to identify a potential interaction of Sp2 with family of the Cdc25 phosphatases, two members of which (Cdc25A and Cdc25B) are well-established regulators of CDK1/Cyclin B activation at the onset of mitosis (Timofeev et al., 2010). Thus future direction of our studies using Sp2 signaling as a model will determine the specific Cdc25 isoforms that interact with Sp2, and how these interactions affect CDK1 activity during mitosis and abscission.

Finally our study provides the first model of abscission failure in neural progenitors to this date. Thus far only few proteins have been implicated in regulation of cytokinesis in neural progenitor. The best characterized player is the Rho-effector citron kinase (CitK), deletion of which causes cytokinesis failure in cortical neural progenitors (Sarkisian et al., 2002). However, identification of binucleated cells was the sole tool adopted in defining cytokinesis failure and the dynamic of mutant progenitor cell division was not further investigated in that study. Moreover deletion of Citk, as demonstrated in mammalian cell

lines, causes cleavage furrow and midbody regression suggesting a defect in early cytokinesis, unlike the results we have obtained from Sp2 deletion. Similar to our study, mutation in CitK causes a decrease in the thickness of the cerebral cortex and compromised neuronal production (Anastas et al., 2011; Sarkisian et al., 2002). However the massive cell apoptosis observed in the CitK mutant progenitors were not found prominent in the Sp2 mutant cortical progenitors. This discrepancy might suggest a different sensitivity in apoptosis when cells fail at different stages of cytokinesis. In addition, CitK is required for cytokinesis in neuronal precursors but not for glial precursor cytokinesis, indicating that different cytokinetic machinery might be employed by precursors that are committed to different cell linage (Sarkisian et al., 2002). At this junction, further investigations are needed to determine if Sp2 is required for progenitor division in all stem and progenitor cells. Moreover, it will be critical to determine whether Sp2 functions impact both symmetric and asymmetric divisions equally. These future studies will further shed light on how Sp2 might couple cell division with cell fate determination.

Sp2 deletion impacts the fate of NSC and NPC progenies

Numerous studies have illustrated changes in cell cycle compartments that impact neurogenesis and the differentiation potential of NSCs and NPCs. For example, the total length of the cell cycle and the duration of G1 clearly impact neurogenic NPCs compared to early proliferative NSCs(Calegari et al., 2005; Salomoni and Calegari, 2010). Furthermore, lengthening of G1 is highly correlated with the transition from apical NSCs to basal NPCs in the developing cortex (Arai et al., 2011). Similarly, lengthening the cell cycle promotes expansion of the NPC pool and enhances neuronal production in human neural progenitors

(García-García et al., 2012). Moreover, as G2 lengthens during embryonic development it slows the rate of S-G2-M transition in basal NPCs, but not in apical NSCs (Calegari et al., 2005). Thus, the normal maintenance of a stem cell niche entails preservation of some progenitors with characteristics of developmentally early NSCs, as is also evident in the presence of slow-dividing NSCs in the adult mouse SEZ (Doetsch et al., 1999b, 1999c).

Disruption of the cell cycle in the absence of Sp2 severely impacts fate specification in NSCs and NPCs, where a significant expansion of Pax6+ NSCs is in conjunction with depletion of Tbr2+ NPCs, and correlates with near absence of postmitotic neurons in the cortical plate, a lineage that is well established (Englund et al., 2005; Sessa et al., 2008). A conceptually similar phenotype was apparent in the SEZ/RMS of *Nestin-cre* deleted Sp2 brains where presumptive Pax6+ NSCs were expanded, whereas the Gsx2+ and Dlx2+ NSCs and NPCs were relatively unaffected in the mutant SEZ. This observation is in sync with a past report that Pax6 deletion leads to ectopic upregulation of Dlx2 in the dorsal telencephalon (Toresson et al., 2000). However, these findings must be interpreted cautiously as the lineal relationships among Pax6, Gsx2, and Dlx2 expressing populations in the postnatal SEZ and RMS are complex, partially overlapping, and likely nonlinear (Brill et al., 2008). Whether the misregulated timing of NPC expansion as well as neuronal production directly contribute to the defects in the cortical progenitor organization still remains to be determined. In addition, Sp2-dependent cell cycle regulation appears to be required for differentiation of both postnatal neuronal and oligodendroglial lineages by functioning as a key regulator of the switch from proliferation to differentiation in NSCs and NPCs. How the timing of cell cycle progression regulates programmed fate decisions during

neurogenesis and gliogenesis remains largely unknown.

SUMMARY OF DISSERTATION

In summary, our study for the first time reveals that Sp2-dependent regulation of transitions through distinct cell cycle phases is critical for developmental maturation of early embryonic NSCs into neurogenic and gliogenic NPCs in the cortex and the postnatal stem cell niche. How Sp2 carries out these important functions is the subject of future studies. Molecular mechanisms of Sp2 as a putative transcription factor have remained largely enigmatic; while a recent study implicates Sp2 as a global transcriptional regulator (Terrados et al., 2012), a number of past studies failed to identify strong DNA-binding or transcriptional activity by Sp2 suggesting these functions of Sp2 may be negatively regulated in mammalian cells (Moorefield et al., 2004). At this juncture it is tempting to speculate that loss of Sp2 may severely impact symmetric and asymmetric decisions in NSCs and NPCs through misregulation of cell cycle progression and in particular G2/M progression. An important future direction of the current work is to determine whether or not Sp2 directly participates in symmetric and asymmetric division of NSCs and NPCs in the developing and postnatal brains as a putative transcription factor or through alternative cell biological roles. Conditional deletion of Sp2 will provide a suitable model for studying the link between cell cycle regulation and fate specification in NSCs and NPCs in these future studies.

REFERENCE LIST

Alcamo, E.A., Chirivella, L., Dautzenberg, M., Dobreva, G., Fariñas, I., Grosschedl, R., and McConnell, S.K. (2008). Satb2 Regulates Callosal Projection Neuron Identity in the Developing Cerebral Cortex. Neuron *57*, 364–377.

Ali, F., Hindley, C., McDowell, G., Deibler, R., Jones, A., Kirschner, M., Guillemot, F., and Philpott, A. (2011). Cell cycle-regulated multi-site phosphorylation of Neurogenin 2 coordinates cell cycling with differentiation during neurogenesis. Development *138*, 4267–4277.

Alsop, G.B., and Zhang, D. (2003). Microtubules are the only structural constituent of the spindle apparatus required for induction of cell cleavage. The Journal of Cell Biology *162*, 383–390.

Anastas, S.B., Mueller, D., Semple-Rowland, S.L., Breunig, J.J., and Sarkisian, M.R. (2011). Failed cytokinesis of neural progenitors in citron kinase-deficient rats leads to multiciliated neurons. Cerebral Cortex (New York, N.Y. : 1991) *21*, 338–344.

Anderson, C.T., and Stearns, T. (2009). Centriole age underlies asynchronous primary cilium growth in mammalian cells. Current Biology: CB *19*, 1498–1502.

Anthony, T.E., Klein, C., Fishell, G., and Heintz, N. (2004). Radial glia serve as neuronal progenitors in all regions of the central nervous system. Neuron *41*, 881–890.

Arai, Y., Pulvers, J.N., Haffner, C., Schilling, B., Nüsslein, I., Calegari, F., and Huttner, W.B. (2011). Neural stem and progenitor cells shorten S-phase on commitment to neuron production. Nature Communications *2*, 154.

Arnold, S.J., Huang, G.-J., Cheung, A.F.P., Era, T., Nishikawa, S.-I., Bikoff, E.K., Molnár, Z., Robertson, E.J., and Groszer, M. (2008). The T-box transcription factor Eomes/Tbr2 regulates neurogenesis in the cortical subventricular zone. Genes & Development *22*, 2479–2484.

Astrinidis, A., Kim, J., Kelly, C.M., Olofsson, B.A., Torabi, B., Sorokina, E.M., and Azizkhan-Clifford, J. (2010). The transcription factor SP1 regulates centriole function and chromosomal stability through a functional interaction with the mammalian target of rapamycin/raptor complex. Genes, Chromosomes & Cancer *49*, 282–297.

Bassi, Z.I., Audusseau, M., Riparbelli, M.G., Callaini, G., and D'Avino, P.P. (2013). Citron kinase controls a molecular network required for midbody formation in cytokinesis. Proceedings of the National Academy of Sciences of the United States of America 1–6.

Bastos, R.N., and Barr, F.A. (2010). Plk1 negatively regulates Cep55 recruitment to the midbody to ensure orderly abscission. The Journal of Cell Biology *191*, 751–760.

Baur, F., Nau, K., Sadic, D., Allweiss, L., Elsässer, H.-P., Gillemans, N., De Wit, T., Krüger, I., Vollmer, M., Philipsen, S., et al. (2010). Specificity protein 2 (Sp2) is essential for mouse development and autonomous proliferation of mouse embryonic fibroblasts. PloS One *5*, e9587.

Beaudouin, J., Gerlich, D., Daigle, N., Eils, R., and Ellenberg, J. (2002). Nuclear envelope breakdown proceeds by microtubule-induced tearing of the lamina. Cell *108*, 83–96.

Black, A.R., Black, J.D., and Azizkhan-Clifford, J. (2001). Sp1 and krüppel-like factor family of transcription factors in cell growth regulation and cancer. Journal of Cellular Physiology *188*, 143–160.

Bollen, M., Gerlich, D.W., and Lesage, B. (2009). Mitotic phosphatases: from entry guards to exit guides. Trends in Cell Biology *19*, 531–541.

Bornens, M. (2002). Centrosome composition and microtubule anchoring mechanisms. Current Opinion in Cell Biology *14*, 25–34.

Bouwman, P., Göllner, H., Elsässer, H.P., Eckhoff, G., Karis, A., Grosveld, F., Philipsen, S., and Suske, G. (2000). Transcription factor Sp3 is essential for post-natal survival and late tooth development. The EMBO Journal *19*, 655–661.

Brill, M.S., Snapyan, M., Wohlfrom, H., Ninkovic, J., Jawerka, M., Mastick, G.S., Ashery-Padan, R., Saghatelyan, A., Berninger, B., and Götz, M. (2008). A Dlx2- and Pax6-Dependent Transcriptional Code for Periglomerular Neuron Specification in the Adult Olfactory Bulb. The Journal of Neuroscience *28*, 6439–6452.

Budirahardja, Y., and Gönczy, P. (2009). Coupling the cell cycle to development. Development *136*, 2861–2872.

Burdon, T., Smith, A., and Savatier, P. (2002). Signalling, cell cycle and pluripotency in embryonic stem cells. Trends in Cell Biology *12*, 432–438.

Burns, K.A., and Kuan, C.-Y. (2005). Low doses of bromo- and iododeoxyuridine produce near-saturation labeling of adult proliferative populations in the dentate gyrus. The European Journal of Neuroscience *21*, 803–807.

Calegari, F., and Huttner, W.B. (2003). An inhibition of cyclin-dependent kinases that lengthens, but does not arrest, neuroepithelial cell cycle induces premature neurogenesis. Journal of Cell Science *116*, 4947–4955.

Calegari, F., Haubensak, W., Haffner, C., and Huttner, W.B. (2005). Selective lengthening of the cell cycle in the neurogenic subpopulation of neural progenitor cells during mouse brain development. The Journal of Neuroscience : the Official Journal of the Society for Neuroscience *25*, 6533–6538.

Cameron, H.A., and McKay, R.D. (2001). Adult neurogenesis produces a large pool of new granule cells in the dentate gyrus. The Journal of Comparative Neurology *435*, 406–417.

Canman, J.C., Hoffman, D.B., and Salmon, E.D. (2000). The role of pre- and post-anaphase microtubules in the cytokinesis phase of the cell cycle. Current Biology: CB *10*, 611–614.

Cayouette, M. (2003). The orientation of cell division influences cell-fate choice in the developing mammalian retina. Development *130*, 2329–2339.

Chee, M.K., and Haase, S.B. (2010). B-cyclin/CDKs regulate mitotic spindle assembly by phosphorylating kinesins-5 in budding yeast. PLoS Genetics *6*, e1000935.

Chen, C.-T., Hehnly, H., and Doxsey, S.J. (2012). Orchestrating vesicle transport, ESCRTs and kinase surveillance during abscission. Nature Reviews Molecular Cell Biology *13*, 483–488.

Chen, J.-S., Lu, L.X., Ohi, M.D., Creamer, K.M., English, C., Partridge, J.F., Ohi, R., and Gould, K.L. (2011). Cdk1 phosphorylation of the kinetochore protein Nsk1 prevents error-prone chromosome segregation. The Journal of Cell Biology *195*, 583–593.

Connell, J.W., Lindon, C., Luzio, J.P., and Reid, E. (2009). Spastin couples microtubule severing to membrane traffic in completion of cytokinesis and secretion. Traffic (Copenhagen, Denmark) *10*, 42–56.

Costa, M.R., Ortega, F., Brill, M.S., Beckervordersandforth, R., Petrone, C., Schroeder, T., Götz, M., and Berninger, B. (2011). Continuous live imaging of adult neural stem cell division and lineage progression in vitro. Development (Cambridge, England) *138*, 1057–1068.

Cremisi, F., Philpott, A., and Ohnuma, S. (2003). Cell cycle and cell fate interactions in neural development. Current Opinion in Neurobiology *13*, 26–33.

Cubelos, B., Sebastián-Serrano, A., Kim, S., Redondo, J.M., Walsh, C., and Nieto, M. (2008). *Cux-1* and *Cux-2* control the development of Reelin expressing cortical interneurons. Developmental Neurobiology *68*, 917–925.

Curtis, M. a, Kam, M., Nannmark, U., Anderson, M.F., Axell, M.Z., Wikkelso, C., Holtås, S., Van Roon-Mom, W.M.C., Björk-Eriksson, T., Nordborg, C., et al. (2007). Human

neuroblasts migrate to the olfactory bulb via a lateral ventricular extension. Science (New York, N.Y.) *315*, 1243–1249.

Dehay, C., and Kennedy, H. (2007). Cell-cycle control and cortical development. Nature Reviews. Neuroscience *8*, 438–450.

Doetsch, F., Caillé, I., Lim, D. a, García-Verdugo, J.M., and Alvarez-Buylla, a (1999a). Subventricular zone astrocytes are neural stem cells in the adult mammalian brain. Cell *97*, 703–716.

Doetsch, F., García-Verdugo, J.M., and Alvarez-Buylla, a (1999b). Regeneration of a germinal layer in the adult mammalian brain. Proceedings of the National Academy of Sciences of the United States of America *96*, 11619–11624.

Doetsch, F., Caillé, I., Lim, D. a, García-Verdugo, J.M., and Alvarez-Buylla, a (1999c). Subventricular zone astrocytes are neural stem cells in the adult mammalian brain. Cell *97*, 703–716.

Dubreuil, V., Marzesco, A.-M., Corbeil, D., Huttner, W.B., and Wilsch-Bräuninger, M. (2007). Midbody and primary cilium of neural progenitors release extracellular membrane particles enriched in the stem cell marker prominin-1. The Journal of Cell Biology *176*, 483–495.

Englund, C., Fink, A., Lau, C., Pham, D., Daza, R.A.M., Bulfone, A., Kowalczyk, T., and Hevner, R.F. (2005). Pax6, Tbr2, and Tbr1 Are Expressed Sequentially by Radial Glia, Intermediate Progenitor Cells, and Postmitotic Neurons in Developing Neocortex. The Journal of Neuroscience *25*, 247–251.

Errico, A., Deshmukh, K., Tanaka, Y., Pozniakovsky, A., and Hunt, T. (2010). Identification of substrates for cyclin dependent kinases. Advances in Enzyme Regulation *50*, 375–399.

Evans, T., Rosenthal, E.T., Youngblom, J., Distel, D., and Hunt, T. (1983). Cyclin: a protein specified by maternal mRNA in sea urchin eggs that is destroyed at each cleavage division. Cell *33*, 389–396.

Fabbro, M., Zhou, B.-B., Takahashi, M., Sarcevic, B., Lal, P., Graham, M.E., Gabrielli, B.G., Robinson, P.J., Nigg, E.A., Ono, Y., et al. (2005). Cdk1/Erk2- and Plk1-dependent phosphorylation of a centrosome protein, Cep55, is required for its recruitment to midbody and cytokinesis. Developmental Cell *9*, 477–488.

Fan, Y., Abrahamsen, G., McGrath, J.J., and Mackay-Sim, A. (2012). Altered cell cycle dynamics in schizophrenia. Biological Psychiatry *71*, 129–135.

Farkas, L.M., and Huttner, W.B. (2008). The cell biology of neural stem and progenitor cells and its significance for their proliferation versus differentiation during mammalian brain development. Current Opinion in Cell Biology *20*, 707–715.

Faulkner, N.E., Dujardin, D.L., Tai, C.Y., Vaughan, K.T., O'Connell, C.B., Wang, Y., and Vallee, R.B. (2000). A role for the lissencephaly gene LIS1 in mitosis and cytoplasmic dynein function. Nature Cell Biology *2*, 784–791.

Fededa, J.P., and Gerlich, D.W. (2012). Molecular control of animal cell cytokinesis. Nature Cell Biology *14*, 440–447.

Feng, Y., and Walsh, C.A. (2004a). Mitotic spindle regulation by Nde1 controls cerebral cortical size. Neuron *44*, 279–293.

Fielding, A.B., Schonteich, E., Matheson, J., Wilson, G., Yu, X., Hickson, G.R.X., Srivastava, S., Baldwin, S. a, Prekeris, R., and Gould, G.W. (2005). Rab11-FIP3 and FIP4 interact with Arf6 and the exocyst to control membrane traffic in cytokinesis. The EMBO Journal *24*, 3389–3399.

Fish, J.L., Kosodo, Y., Enard, W., Pääbo, S., and Huttner, W.B. (2006). Aspm specifically maintains symmetric proliferative divisions of neuroepithelial cells. Proceedings of the National Academy of Sciences of the United States of America *103*, 10438–10443.

Foster, D. a, Yellen, P., Xu, L., and Saqcena, M. (2010). Regulation of G1 Cell Cycle Progression: Distinguishing the Restriction Point from a Nutrient-Sensing Cell Growth Checkpoint(s). Genes & Cancer *1*, 1124–1131.

Franco, S.J., Gil-Sanz, C., Martinez-Garay, I., Espinosa, A., Harkins-Perry, S.R., Ramos, C., and Müller, U. (2012). Fate-restricted neural progenitors in the mammalian cerebral cortex. Science *337*, 746–749.

Frantz, G.D., and McConnell, S.K. (1996). Restriction of Late Cerebral Cortical Progenitors to an Upper-Layer Fate. Neuron *17*, 55–61.

FUJITA, S. (1960). Mitotic pattern and histogenesis of the central nervous system. Nature *185*, 702–703.

Fung, T.K., and Poon, R.Y.C. (2005). A roller coaster ride with the mitotic cyclins. Seminars in Cell & Developmental Biology *16*, 335–342.

Furutachi, S., Matsumoto, A., Nakayama, K.I., and Gotoh, Y. (2013). P57 Controls Adult Neural Stem Cell Quiescence and Modulates the Pace of Lifelong Neurogenesis. The EMBO Journal *32*, 970–981.

Garcia, a D.R., Doan, N.B., Imura, T., Bush, T.G., and Sofroniew, M. V (2004). GFAP-expressing progenitors are the principal source of constitutive neurogenesis in adult mouse forebrain. Nature Neuroscience *7*, 1233–1241.

García-García, E., Pino-Barrio, M.J., López-Medina, L., and Martínez-Serrano, A. (2012). Intermediate progenitors are increased by lengthening of the cell cycle through calcium signaling and p53 expression in human neural progenitors. Molecular Biology of the Cell *23*, 1167–1180.

Gautier, J., Solomon, M.J., Booher, R.N., Bazan, J.F., and Kirschner, M.W. (1991). Cdc25 Is a Specific Tyrosine Phosphatase That Directly Activates P34Cdc2. Cell *67*, 197–211.

Gavet, O., and Pines, J. (2010). Progressive activation of CyclinB1-Cdk1 coordinates entry to mitosis. Developmental Cell *18*, 533–543.

Georgatos, S.D., Pyrpasopoulou, a, and Theodoropoulos, P. a (1997). Nuclear envelope breakdown in mammalian cells involves stepwise lamina disassembly and microtubule-drive deformation of the nuclear membrane. Journal of Cell Science *110 (Pt 17)*, 2129–2140.

Ghashghaei, H.T., Lai, C., and Anton, E.S. (2007). Neuronal migration in the adult brain: are we there yet? Nature Reviews Neuroscience *8*, 141–151.

Glotzer, M. (2009). The 3Ms of central spindle assembly: microtubules, motors and MAPs. Nature Reviews. Molecular Cell Biology *10*, 9–20.

Göllner, H., Bouwman, P., Mangold, M., Karis, A., Braun, H., Rohner, I., Del Rey, A., Besedovsky, H.O., Meinhardt, A., Van den Broek, M., et al. (2001). Complex phenotype of mice homozygous for a null mutation in the Sp4 transcription factor gene. Genes to Cells: Devoted to Molecular & Cellular Mechanisms *6*, 689–697.

Gorr, I.H., Reis, A., Boos, D., Wühr, M., Madgwick, S., Jones, K.T., and Stemmann, O. (2006). Essential CDK1-inhibitory role for separase during meiosis I in vertebrate oocytes. Nature Cell Biology *8*, 1035–1037.

Gorski, J. a, Talley, T., Qiu, M., Puelles, L., Rubenstein, J.L.R., and Jones, K.R. (2002). Cortical excitatory neurons and glia, but not GABAergic neurons, are produced in the Emx1-expressing lineage. The Journal of Neuroscience *22*, 6309–6314.

Goss, J.W., and Toomre, D.K. (2008). Both daughter cells traffic and exocytose membrane at the cleavage furrow during mammalian cytokinesis. The Journal of Cell Biology *181*, 1047–1054.

Götz, M., Hartfuss, E., and Malatesta, P. (2002). Radial glial cells as neuronal precursors: a new perspective on the correlation of morphology and lineage restriction in the developing cerebral cortex of mice. Brain Research Bulletin *57*, 777–788.

Green, R.A., Paluch, E., and Oegema, K. (2012). Cytokinesis in animal cells. Annual Review of Cell and Developmental Biology *28*, 29–58.

Gromley, A., Yeaman, C., Rosa, J., Redick, S., Chen, C.-T., Mirabelle, S., Guha, M., Sillibourne, J., and Doxsey, S.J. (2005). Centriolin anchoring of exocyst and SNARE complexes at the midbody is required for secretory-vesicle-mediated abscission. Cell *123*, 75–87.

Gruber, R., Zhou, Z., Sukchev, M., Joerss, T., Frappart, P.-O., and Wang, Z.-Q. (2011). MCPH1 regulates the neuroprogenitor division mode by coupling the centrosomal cycle with mitotic entry through the Chk1-Cdc25 pathway. Nature Cell Biology *13*, 1325–1334.

Guse, A., Mishima, M., and Glotzer, M. (2005). Phosphorylation of ZEN-4/MKLP1 by aurora B regulates completion of cytokinesis. Current Biology : CB *15*, 778–786.

Güttinger, S., Laurell, E., and Kutay, U. (2009). Orchestrating nuclear envelope disassembly and reassembly during mitosis. Nature Reviews. Molecular Cell Biology *10*, 178–191.

Hand, R., Bortone, D., Mattar, P., Nguyen, L., Heng, J.I.-T., Guerrier, S., Boutt, E., Peters, E., Barnes, A.P., Parras, C., et al. (2005). Phosphorylation of Neurogenin2 specifies the migration properties and the dendritic morphology of pyramidal neurons in the neocortex. Neuron *48*, 45–62.

Harbour, J.W., Luo, R.X., Dei Santi, A., Postigo, A.A., and Dean, D.C. (1999). Cdk phosphorylation triggers sequential intramolecular interactions that progressively block Rb functions as cells move through G1. Cell *98*, 859–869.

Hartfuss, E., Galli, R., Heins, N., and Götz, M. (2001). Characterization of CNS precursor subtypes and radial glia. Developmental Biology *229*, 15–30.

Hatten, M.E. (1999). Central nervous system neuronal migration. Annual Review of Neuroscience *22*, 511–539.

Haubensak, W., Attardo, A., Denk, W., and Huttner, W.B. (2004). Neurons arise in the basal neuroepithelium of the early mammalian telencephalon: a major site of neurogenesis. Proceedings of the National Academy of Sciences of the United States of America *101*, 3196–3201.

Hayes, N.L., and Nowakowski, R.S. (2002). Dynamics of cell proliferation in the adult dentate gyrus of two inbred strains of mice. Brain Research. Developmental Brain Research *134*, 77–85.

He, S., Nakada, D., and Morrison, S.J. (2009). Mechanisms of stem cell self-renewal. Annual Review of Cell and Developmental Biology *25*, 377–406.

Hebbar, S., Mesngon, M.T., Guillotte, A.M., Desai, B., Ayala, R., and Smith, D.S. (2008). Lis1 and Ndel1 influence the timing of nuclear envelope breakdown in neural stem cells. The Journal of Cell Biology *182*, 1063–1071.

Hershko, a, Ganoth, D., Sudakin, V., Dahan, a, Cohen, L.H., Luca, F.C., Ruderman, J. V, and Eytan, E. (1994). Components of a system that ligates cyclin to ubiquitin and their regulation by the protein kinase cdc2. The Journal of Biological Chemistry *269*, 4940–4946.

Hesse, M., Raulf, A., Pilz, G.-A., Haberlandt, C., Klein, A.M., Jabs, R., Zaehres, H., Fügemann, C.J., Zimmermann, K., Trebicka, J., et al. (2012). Direct visualization of cell division using high-resolution imaging of M-phase of the cell cycle. Nature Communications *3*, 1076.

Hickson, G.R.X., and O'Farrell, P.H. (2008). Rho-dependent control of anillin behavior during cytokinesis. The Journal of Cell Biology *180*, 285–294.

Hinds, J.W., and Ruffett, T.L. (1971). Cell proliferation in the neural tube: an electron microscopic and golgi analysis in the mouse cerebral vesicle. Zeitschrift Für Zellforschung Und Mikroskopische Anatomie (Vienna, Austria : 1948) *115*, 226–264.

Hippenmeyer, S., Youn, Y.H., Moon, H.M., Miyamichi, K., Zong, H., Wynshaw-Boris, A., and Luo, L. (2010). Genetic mosaic dissection of Lis1 and Ndel1 in neuronal migration. Neuron *68*, 695–709.

Holland, A.J., and Taylor, S.S. (2006). Cyclin-B1-mediated inhibition of excess separase is required for timely chromosome disjunction. Journal of Cell Science *119*, 3325–3336.

Holloway, S.L., Glotzer, M., King, R.W., and Murray, A.W. (1993). Anaphase is initiated by proteolysis rather than by the inactivation of maturation-promoting factor. Cell *73*, 1393–1402.

Irniger, S., Piatti, S., Michaelis, C., and Nasmyth, K. (1995). Genes involved in sister chromatid separation are needed for B-type cyclin proteolysis in budding yeast. Cell *81*, 269–278.

Ito, N., and Rubin, G.M. (1999). gigas, a Drosophila Homolog of Tuberous Sclerosis Gene Product-2, Regulates the Cell Cycle. Cell *96*, 529–539.

Jackman, M., Lindon, C., Nigg, E. a, and Pines, J. (2003). Active cyclin B1-Cdk1 first appears on centrosomes in prophase. Nature Cell Biology *5*, 143–148.

Jacquet, B. V, Patel, M., Iyengar, M., Liang, H., Therit, B., Salinas-Mondragon, R., Lai, C., Olsen, J.C., Anton, E.S., and Ghashghaei, H.T. (2009a). Analysis of neuronal proliferation, migration and differentiation in the postnatal brain using equine infectious anemia virus-based lentiviral vectors. Gene Therapy *16*, 1021–1033.

Jacquet, B. V, Salinas-Mondragon, R., Liang, H., Therit, B., Buie, J.D., Dykstra, M., Campbell, K., Ostrowski, L.E., Brody, S.L., and Ghashghaei, H.T. (2009b). FoxJ1-dependent gene expression is required for differentiation of radial glia into ependymal cells and a subset of astrocytes in the postnatal brain. Development *136*, 4021–4031.

Jiang, W., Jimenez, G., Wells, N.J., Hope, T.J., Wahl, G.M., Hunter, T., and Fukunaga, R. (1998). PRC1: a human mitotic spindle-associated CDK substrate protein required for cytokinesis. Molecular Cell *2*, 877–885.

Katsel, P., Davis, K.L., Li, C., Tan, W., Greenstein, E., Kleiner Hoffman, L.B., and Haroutunian, V. (2008). Abnormal Indices of Cell Cycle Activity in Schizophrenia and their Potential Association with Oligodendrocytes. Neuropsychopharmacology *33*, 2993–3009.

Kelly, A.E., and Funabiki, H. (2009). Correcting aberrant kinetochore microtubule attachments: an Aurora B-centric view. Current Opinion in Cell Biology *21*, 51–58.

Kim, T.-H., Chiera, S.L., Linder, K.E., Trempus, C.S., Smart, R.C., and Horowitz, J.M. (2010). Overexpression of Transcription Factor Sp2 Inhibits Epidermal Differentiation and Increases Susceptibility to Wound- and Carcinogen-Induced Tumorigenesis. Cancer Research *70*, 8507–8516.

Kimura, K., Tsuji, T., Takada, Y., Miki, T., and Narumiya, S. (2000). Accumulation of GTP-bound RhoA during Cytokinesis and a Critical Role of ECT2 in This Accumulation. Journal of Biological Chemistry *275*, 17233–17236.

King, R.W., Deshaies, R.J., Peters, J.M., and Kirschner, M.W. (1996). How proteolysis drives the cell cycle. Science *274*, 1652–1659.

Kohwi, M., Osumi, N., Rubenstein, J.L.R., and Alvarez-Buylla, A. (2005). Pax6 Is Required for Making Specific Subpopulations of Granule and Periglomerular Neurons in the Olfactory Bulb. The Journal of Neuroscience *25*, 6997–7003.

Kohwi, M., Petryniak, M. a, Long, J.E., Ekker, M., Obata, K., Yanagawa, Y., Rubenstein, J.L.R., and Alvarez-Buylla, A. (2007). A subpopulation of olfactory bulb GABAergic interneurons is derived from Emx1- and Dlx5/6-expressing progenitors. The Journal of Neuroscience *27*, 6878–6891.

Kosodo, Y., Röper, K., Haubensak, W., Marzesco, A.-M., Corbeil, D., and Huttner, W.B. (2004). Asymmetric distribution of the apical plasma membrane during neurogenic divisions of mammalian neuroepithelial cells. The EMBO Journal *23*, 2314–2324.

Kosodo, Y., Toida, K., Dubreuil, V., Alexandre, P., Schenk, J., Kiyokage, E., Attardo, A., Mora-Bermúdez, F., Arii, T., Clarke, J.D.W., et al. (2008). Cytokinesis of neuroepithelial cells can divide their basal process before anaphase. The EMBO Journal *27*, 3151–3163.

Kriegstein, A., and Alvarez-Buylla, A. (2009). The glial nature of embryonic and adult neural stem cells. Annual Review of Neuroscience *32*, 149–184.

Kriegstein, A., Noctor, S., and Martínez-cerdeño, V. (2006). Patterns of neural stem and progenitor cell division may underlie evolutionary cortical expansion. Nature Reviews. Neuroscience *7*, 883–890.

Krüger, I., Vollmer, M., Simmons, D.G., Simmons, D., Elsässer, H.-P., Philipsen, S., and Suske, G. (2007). Sp1/Sp3 compound heterozygous mice are not viable: impaired erythropoiesis and severe placental defects. Developmental Dynamics: An Official Publication of the American Association of Anatomists *236*, 2235–2244.

Kurtz, a, Zimmer, a, Schnütgen, F., Brüning, G., Spener, F., and Müller, T. (1994). The expression pattern of a novel gene encoding brain-fatty acid binding protein correlates with neuronal and glial cell development. Development *120*, 2637–2649.

Laan, L., Pavin, N., Husson, J., Romet-Lemonne, G., Van Duijn, M., López, M.P., Vale, R.D., Jülicher, F., Reck-Peterson, S.L., and Dogterom, M. (2012). Cortical dynein controls microtubule dynamics to generate pulling forces that position microtubule asters. Cell *148*, 502–514.

Lange, C., Huttner, W.B., and Calegari, F. (2009). Article Cdk4 / CyclinD1 Overexpression in Neural Stem Cells Shortens G1 , Delays Neurogenesis , and Promotes the Generation and Expansion of Basal Progenitors. Stem Cell *5*, 320–331.

Lendahl, U., Zimmerman, L.B., and McKay, R.D. (1990). CNS stem cells express a new class of intermediate filament protein. Cell *60*, 585–595.

Li, A., Saito, M., Chuang, J.-Z., Tseng, Y.-Y., Dedesma, C., Tomizawa, K., Kaitsuka, T., and Sung, C.-H. (2011). Ciliary transition zone activation of phosphorylated Tctex-1 controls

ciliary resorption, S-phase entry and fate of neural progenitors. Nature Cell Biology *13*, 402–411.

Lindqvist, A., Källström, H., Lundgren, A., Barsoum, E., and Rosenthal, C.K. (2005). Cdc25B cooperates with Cdc25A to induce mitosis but has a unique role in activating cyclin B1-Cdk1 at the centrosome. The Journal of Cell Biology *171*, 35–45.

Lindqvist, A., Rodríguez-Bravo, V., and Medema, R.H. (2009). The decision to enter mitosis: feedback and redundancy in the mitotic entry network. The Journal of Cell Biology *185*, 193–202.

Lizarraga, S.B., Margossian, S.P., Harris, M.H., Campagna, D.R., Han, A.-P., Blevins, S., Mudbhary, R., Barker, J.E., Walsh, C.A., and Fleming, M.D. (2010). Cdk5rap2 regulates centrosome function and chromosome segregation in neuronal progenitors. Development *137*, 1907–1917.

Löffler, H., Fechter, A., Matuszewska, M., Saffrich, R., Mistrik, M., Marhold, J., Hornung, C., Westermann, F., Bartek, J., and Krämer, A. (2011). Cep63 recruits Cdk1 to the centrosome: implications for regulation of mitotic entry, centrosome amplification, and genome maintenance. Cancer Research *71*, 2129–2139.

Lois, C., García-Verdugo, J.M., and Alvarez-Buylla, a (1996). Chain migration of neuronal precursors. Science *271*, 978–981.

Loo, P.F. van, Bouwman, P., Ling, K.-W., Middendorp, S., Suske, G., Grosveld, F., Dzierzak, E., Philipsen, S., and Hendriks, R.W. (2003). Impaired hematopoiesis in mice lacking the transcription factor Sp3. Blood *102*, 858–866.

Louvi, A., and Grove, E.A. (2011). Cilia in the CNS: the quiet organelle claims center stage. Neuron *69*, 1046–1060.

Lu, M., Zhang, R.L., Zhang, Z.G., Yang, J.J., and Chopp, M. (2007). Linkage of cell cycle kinetics between embryonic and adult stroke models: an analytical approach. Journal of Neuroscience Methods *161*, 323–330.

Lui, J.H., Hansen, D. V, and Kriegstein, A.R. (2011). Development and evolution of the human neocortex. Cell *146*, 18–36.

Lundberg, a S., and Weinberg, R. a (1998). Functional inactivation of the retinoblastoma protein requires sequential modification by at least two distinct cyclin-cdk complexes. Molecular and Cellular Biology *18*, 753–761.

Lüscher, B., Brizuela, L., Beach, D., and Eisenman, R.N. (1991). A role for the p34cdc2 kinase and phosphatases in the regulation of phosphorylation and disassembly of lamin B2 during the cell cycle. The EMBO Journal *10*, 865–875.

Luskin, M.B. (1993). Restricted proliferation and migration of postnatally generated neurons derived from the forebrain subventricular zone. Neuron *11*, 173–189.

Malatesta, P., Hartfuss, E., and Götz, M. (2000). Isolation of radial glial cells by fluorescent-activated cell sorting reveals a neuronal lineage. Development *127*, 5253–5263.

Malumbres, M., and Barbacid, M. (2009). Cell cycle, CDKs and cancer: a changing paradigm. Nature Reviews. Cancer *9*, 153–166.

Marin, M., Karis, A., Visser, P., Grosveld, F., and Philipsen, S. (1997). Transcription factor Sp1 is essential for early embryonic development but dispensable for cell growth and differentiation. Cell *89*, 619–628.

Martynoga, B., Morrison, H., Price, D.J., and Mason, J.O. (2005). Foxg1 is required for specification of ventral telencephalon and region-specific regulation of dorsal telencephalic precursor proliferation and apoptosis. Developmental Biology *283*, 113–127.

Matsumura, F. (2005). Regulation of myosin II during cytokinesis in higher eukaryotes. Trends in Cell Biology *15*, 371–377.

McCollum, D. (2004). Cytokinesis: the central spindle takes center stage. Current Biology : CB *14*, R953–5.

McConnell, S.K., and Kaznowski, C.E. (1991). Cell cycle dependence of laminar determination in developing neocortex. Science *254*, 282–285.

McGowan, C.H., and Russell, P. (1993). Human Wee1 kinase inhibits cell division by phosphorylating p34cdc2 exclusively on Tyr15. The EMBO Journal *12*, 75–85.

Merkle, F.T., Tramontin, A.D., García-Verdugo, J.M., and Alvarez-Buylla, A. (2004). Radial glia give rise to adult neural stem cells in the subventricular zone. Proceedings of the National Academy of Sciences of the United States of America *101*, 17528–17532.

Ming, G.-L., and Song, H. (2011). Adult neurogenesis in the mammalian brain: significant answers and significant questions. Neuron *70*, 687–702.

Mishima, M., Kaitna, S., and Glotzer, M. (2002). Central spindle assembly and cytokinesis require a kinesin-like protein/RhoGAP complex with microtubule bundling activity. Developmental Cell *2*, 41–54.

Mishima, M., Pavicic, V., Grüneberg, U., Nigg, E.A., and Glotzer, M. (2004). Cell cycle regulation of central spindle assembly. Nature *430*, 908–913.

Miyata, T., Kawaguchi, a, Okano, H., and Ogawa, M. (2001). Asymmetric inheritance of radial glial fibers by cortical neurons. Neuron *31*, 727–741.

Miyata, T., Kawaguchi, A., Saito, K., Kawano, M., Muto, T., and Ogawa, M. (2004). Asymmetric production of surface-dividing and non-surface-dividing cortical progenitor cells. Development *131*, 3133–3145.

Mizutani, K., and Saito, T. (2005). Progenitors resume generating neurons after temporary inhibition of neurogenesis by Notch activation in the mammalian cerebral cortex. Development *132*, 1295–1304.

Mollinari, C., Kleman, J.-P., Jiang, W., Schoehn, G., Hunter, T., and Margolis, R.L. (2002). PRC1 is a microtubule binding and bundling protein essential to maintain the mitotic spindle midzone. The Journal of Cell Biology *157*, 1175–1186.

Molyneaux, B.J., Arlotta, P., Menezes, J.R.L., and Macklis, J.D. (2007). Neuronal subtype specification in the cerebral cortex. Nature Reviews. Neuroscience *8*, 427–437.

Moorefield, K.S., Fry, S.J., and Horowitz, J.M. (2004). Sp2 DNA Binding Activity and trans-Activation Are Negatively Regulated in Mammalian Cells. Journal of Biological Chemistry *279*, 13911–13924.

Moorefield, K.S., Yin, H., Nichols, T.D., Cathcart, C., Simmons, S.O., and Horowitz, J.M. (2006). Sp2 Localizes to Subnuclear Foci Associated with the Nuclear Matrix. Molecular Biology of the Cell *17*, 1711–1722.

Nagy, A., Gertsenstein, M., Vintersten, K., and Behringer, R. (2007). Staining Whole Mouse Embryos for β-Galactosidase (lacZ) Activity. Cold Spring Harbor Protocols *2007*, pdb.prot4725.

Nasmyth, K., and Haering, C.H. (2009). Cohesin: its roles and mechanisms. Annual Review of Genetics *43*, 525–558.

Nguyen-Ngoc, T., Afshar, K., and Gönczy, P. (2007). Coupling of cortical dynein and G alpha proteins mediates spindle positioning in Caenorhabditis elegans. Nature Cell Biology *9*, 1294–1302.

Nguyên-Trân, V.T., Kubalak, S.W., Minamisawa, S., Fiset, C., Wollert, K.C., Brown, A.B., Ruiz-Lozano, P., Barrere-Lemaire, S., Kondo, R., Norman, L.W., et al. (2000). A novel

genetic pathway for sudden cardiac death via defects in the transition between ventricular and conduction system cell lineages. Cell *102*, 671–682.

Nigg, E.A. (2001). Mitotic kinases as regulators of cell division and its checkpoints. Nature Reviews. Molecular Cell Biology *2*, 21–32.

Nigg, E.A., and Stearns, T. (2011). The centrosome cycle: Centriole biogenesis, duplication and inherent asymmetries. Nature Cell Biology *13*, 1154–1160.

Niiya, F., Xie, X., Lee, K.S., Inoue, H., and Miki, T. (2005). Inhibition of cyclin-dependent kinase 1 induces cytokinesis without chromosome segregation in an ECT2 and MgcRacGAP-dependent manner. J. Biol. Chem. *280*, 36502–36509.

Nishimura, Y., and Yonemura, S. (2006). Centralspindlin regulates ECT2 and RhoA accumulation at the equatorial cortex during cytokinesis. J. Cell Sci. *119*, 104–114.

Noctor, S.C., Flint, a C., Weissman, T. a, Dammerman, R.S., and Kriegstein, a R. (2001). Neurons derived from radial glial cells establish radial units in neocortex. Nature *409*, 714–720.

Noctor, S.C., Flint, A.C., Weissman, T. a, Wong, W.S., Clinton, B.K., and Kriegstein, A.R. (2002). Dividing precursor cells of the embryonic cortical ventricular zone have morphological and molecular characteristics of radial glia. The Journal of Neuroscience *22*, 3161–3173.

Noctor, S.C., Martínez-Cerdeño, V., Ivic, L., and Kriegstein, A.R. (2004). Cortical neurons arise in symmetric and asymmetric division zones and migrate through specific phases. Nature Neuroscience *7*, 136–144.

Noctor, S.C., Martínez-Cerdeño, V., and Kriegstein, A.R. (2008). Distinct behaviors of neural stem and progenitor cells underlie cortical neurogenesis. The Journal of Comparative Neurology *508*, 28–44.

O'Farrell, P.H. (2001). Triggering the all-or-nothing switch into mitosis. Trends in Cell Biology *11*, 512–519.

Ohnuma, S., Hopper, S., Wang, K.C., Philpott, A., and Harris, W. a (2002). Co-ordinating retinal histogenesis: early cell cycle exit enhances early cell fate determination in the Xenopus retina. Development *129*, 2435–2446.

Oliveira, R. a, Hamilton, R.S., Pauli, A., Davis, I., and Nasmyth, K. (2010). Cohesin cleavage and Cdk inhibition trigger formation of daughter nuclei. Nature Cell Biology *12*, 185–192.

Pauli, A., Althoff, F., Oliveira, R. a, Heidmann, S., Schuldiner, O., Lehner, C.F., Dickson, B.J., and Nasmyth, K. (2008). Cell-type-specific TEV protease cleavage reveals cohesin functions in Drosophila neurons. Developmental Cell *14*, 239–251.

Pavicic-Kaltenbrunner, V., Mishima, M., and Glotzer, M. (2007). Cooperative assembly of CYK-4/MgcRacGAP and ZEN-4/MKLP1 to form the centralspindlin complex. Molecular Biology of the Cell *18*, 4992–5003.

Pazour, G.J., and Witman, G.B. (2003). The vertebrate primary cilium is a sensory organelle. Current Opinion in Cell Biology *15*, 105–110.

Peco, E., Escude, T., Agius, E., Sabado, V., Medevielle, F., Ducommun, B., and Pituello, F. (2012). The CDC25B phosphatase shortens the G2 phase of neural progenitors and promotes efficient neuron production. Development *139*, 1095–1104.

Peter, M., Nakagawa, J., Dorée, M., Labbé, J.C., and Nigg, E. a (1990). In vitro disassembly of the nuclear lamina and M phase-specific phosphorylation of lamins by cdc2 kinase. Cell *61*, 591–602.

Piekny, A.J., and Glotzer, M. (2008). Anillin Is a Scaffold Protein That Links RhoA, Actin, and Myosin during Cytokinesis. Current Biology *18*, 30–36.

Piel, M. (2001). Centrosome-Dependent Exit of Cytokinesis in Animal Cells. Science *291*, 1550–1553.

Pilaz, L.J., Patti, D., Marcy, G., Ollier, E., Pfister, S., Douglas, R.J., Betizeau, M., Gautier, E., Cortay, V., Doerflinger, N., et al. (2009). Forced G1-phase reduction alters mode of division, neuron number, and laminar phenotype in the cerebral cortex. Proceedings of the National Academy of Sciences of the United States of America *106*, 21924–21929.

Pines, J. (1995). Cyclins and cyclin-dependent kinases: a biochemical view. The Biochemical Journal *308 (Pt 3)*, 697–711.

Pomerening, J.R., Ubersax, J.A., and Ferrell, J.E. (2008). Rapid Cycling and Precocious Termination of G1 Phase in Cells Expressing CDK1AF. Molecular Biology of the Cell *19*, 3426–3441.

Ponti, G., Obernier, K., Guinto, C., Jose, L., Bonfanti, L., and Alvarez-Buylla, A. (2013). Cell cycle and lineage progression of neural progenitors in the ventricular-subventricular zones of adult mice. Proceedings of the National Academy of Sciences of the United States of America *110*, E1045–54.

Qian, X., Goderie, S.K., Shen, Q., Stern, J.H., and Temple, S. (1998). Intrinsic programs of patterned cell lineages in isolated vertebrate CNS ventricular zone cells. Development *125*, 3143–3152.

Qian, X., Shen, Q., Goderie, S.K., He, W., Capela, a, Davis, a a, and Temple, S. (2000). Timing of CNS cell generation: a programmed sequence of neuron and glial cell production from isolated murine cortical stem cells. Neuron *28*, 69–80.

Raaijmakers, J. a, Van Heesbeen, R.G.H.P., Meaders, J.L., Geers, E.F., Fernandez-Garcia, B., Medema, R.H., and Tanenbaum, M.E. (2012). Nuclear envelope-associated dynein drives prophase centrosome separation and enables Eg5-independent bipolar spindle formation. The EMBO Journal *31*, 4179–4190.

Rakic, P. (1974). Neurons in rhesus monkey visual cortex: systematic relation between time of origin and eventual disposition. Science *183*, 425–427.

Reynolds, B. a, and Weiss, S. (1992). Generation of neurons and astrocytes from isolated cells of the adult mammalian central nervous system. Science *255*, 1707–1710.

ROBBINS, E., and GONATAS, N.K. (1964). THE ULTRASTRUCTURE OF A MAMMALIAN CELL DURING THE MITOTIC CYCLE. The Journal of Cell Biology *21*, 429–463.

Rusan, N.M., Fagerstrom, C.J., Yvon, a M., and Wadsworth, P. (2001). Cell cycle-dependent changes in microtubule dynamics in living cells expressing green fluorescent protein-alpha tubulin. Molecular Biology of the Cell *12*, 971–980.

Russell, P., and Nurse, P. (1987). Negative regulation of mitosis by wee1+, a gene encoding a protein kinase homolog. Cell *49*, 559–567.

Sadler, T. w. (2005). Embryology of neural tube development. American Journal of Medical Genetics Part C: Seminars in Medical Genetics *135C*, 2–8.

Saito, K., Kawaguchi, A., Kashiwagi, S., Yasugi, S., Ogawa, M., and Miyata, T. (2003). Morphological asymmetry in dividing retinal progenitor cells. Development, Growth & Differentiation *45*, 219–229.

Sakai, D., Dixon, J., Dixon, M.J., and Trainor, P.A. (2012). Mammalian neurogenesis requires Treacle-Plk1 for precise control of spindle orientation, mitotic progression, and maintenance of neural progenitor cells. PLoS Genetics *8*, e1002566.

Salina, D., Bodoor, K., Eckley, D.M., Schroer, T.A., Rattner, J.B., and Burke, B. (2002). Cytoplasmic dynein as a facilitator of nuclear envelope breakdown. Cell *108*, 97–107.

Salomoni, P., and Calegari, F. (2010). Cell cycle control of mammalian neural stem cells: putting a speed limit on G1. Trends in Cell Biology *20*, 233–243.

Sansom, S.N., Griffiths, D.S., Faedo, A., Kleinjan, D.J., Ruan, Y., Smith, J., Van Heyningen, V., Rubenstein, J.L., and Livesey, F.J. (2009). The level of the transcription factor Pax6 is essential for controlling the balance between neural stem cell self-renewal and neurogenesis. PLoS Genetics *5*, e1000511.

Sarkisian, M.R., Li, W., Cunto, F. Di, D'Mello, S.R., and LoTurco, J.J. (2002). Citron-Kinase, A Protein Essential to Cytokinesis in Neuronal Progenitors, Is Deleted in the FlatheadMutant Rat. The Journal of Neuroscience *22*, RC217–RC217.

Satterwhite, L.L., and Pollard, T.D. (1992). Cytokinesis. Current Opinion in Cell Biology *4*, 43–52.

Sauer, F.C. (1935). Mitosis in the neural tube. The Journal of Comparative Neurology *62*, 377–405.

Schiel, J. a., Park, K., Morphew, M.K., Reid, E., Hoenger, a., and Prekeris, R. (2011). Endocytic membrane fusion and buckling-induced microtubule severing mediate cell abscission. Journal of Cell Science *124*, 1769–1769.

Schmid, R.S., Shelton, S., Stanco, A., Yokota, Y., Kreidberg, J. a, and Anton, E.S. (2004). Alpha3Beta1 Integrin Modulates Neuronal Migration and Placement During Early Stages of Cerebral Cortical Development. Development *131*, 6023–6031.

Seeley, E.S., and Nachury, M. V (2010). The perennial organelle: assembly and disassembly of the primary cilium. Journal of Cell Science *123*, 511–518.

Sessa, A., Mao, C.-A., Hadjantonakis, A.-K., Klein, W.H., and Broccoli, V. (2008). Tbr2 directs conversion of radial glia into basal precursors and guides neuronal amplification by indirect neurogenesis in the developing neocortex. Neuron *60*, 56–69.

Sharp, D.J., Rogers, G.C., and Scholey, J.M. (2000). Microtubule motors in mitosis. Nature *407*, 41–47.

Shen, Q., Zhong, W., Jan, Y.N., and Temple, S. (2002). Asymmetric Numb distribution is critical for asymmetric cell division of mouse cerebral cortical stem cells and neuroblasts. Development *129*, 4843–4853.

Silver, D.L., Hou, L., Somerville, R., Young, M.E., Apte, S.S., and Pavan, W.J. (2008). The secreted metalloprotease ADAMTS20 is required for melanoblast survival. PLoS Genetics *4*, e1000003.

Silver, D.L., Watkins-Chow, D.E., Schreck, K.C., Pierfelice, T.J., Larson, D.M., Burnetti, A.J., Liaw, H.-J., Myung, K., Walsh, C.A., Gaiano, N., et al. (2010). The exon junction complex component Magoh controls brain size by regulating neural stem cell division. Nature Neuroscience *13*, 551–558.

Smart, I.H. (1972). Proliferative characteristics of the ependymal layer during the early development of the spinal cord in the mouse. Journal of Anatomy *111*, 365–380.

Smart, I.H.M. (1973). Proliferative characteristics of the ependymal layer during the early development of the mouse neocortex : a pilot study based on recording the number , location and plane of cleavage of mitotic figures. Journal of Anatomy *116*, 67–91.

Smith, C.M., and Luskin, M.B. (1998). Cell cycle length of olfactory bulb neuronal progenitors in the rostral migratory stream. Developmental Dynamics: An Official Publication of the American Association of Anatomists *213*, 220–227.

Spear, P.C., and Erickson, C. a (2012). Apical movement during interkinetic nuclear migration is a two-step process. Developmental Biology *370*, 33–41.

Stead, E., White, J., Faast, R., Conn, S., Goldstone, S., Rathjen, J., Dhingra, U., Rathjen, P., Walker, D., and Dalton, S. (2002). Pluripotent cell division cycles are driven by ectopic Cdk2, cyclin A/E and E2F activities. Oncogene *21*, 8320–8333.

Stenman, J., Toresson, H., and Campbell, K. (2003). Identification of two distinct progenitor populations in the lateral ganglionic eminence: implications for striatal and olfactory bulb neurogenesis. The Journal of Neuroscience *23*, 167–174.

Su, K.-C., Takaki, T., and Petronczki, M. (2011). Targeting of the RhoGEF Ect2 to the equatorial membrane controls cleavage furrow formation during cytokinesis. Developmental Cell *21*, 1104–1115.

Sullivan, M., and Morgan, D.O. (2007). Finishing mitosis, one step at a time. Nature Reviews. Molecular Cell Biology *8*, 894–903.

Supp, D.M., Witte, D.P., Branford, W.W., Smith, E.P., and Potter, S.S. (1996). Sp4, a member of the Sp1-family of zinc finger transcription factors, is required for normal murine growth, viability, and male fertility. Developmental Biology *176*, 284–299.

Takahashi, T., Nowakowski, R.S., and Caviness, V.S., Jr (1995). The cell cycle of the pseudostratified ventricular epithelium of the embryonic murine cerebral wall. The Journal of Neuroscience *15*, 6046–6057.

Takeda, D.Y., and Dutta, A. (2005). DNA replication and progression through S phase. Oncogene *24*, 2827–2843.

Terrados, G., Finkernagel, F., Stielow, B., Sadic, D., Neubert, J., Herdt, O., Krause, M., Scharfe, M., Jarek, M., and Suske, G. (2012). Genome-wide localization and expression profiling establish Sp2 as a sequence-specific transcription factor regulating vitally important genes. Nucleic Acids Research *40*, 7844–7857.

Timofeev, O., Cizmecioglu, O., Settele, F., Kempf, T., and Hoffmann, I. (2010). Cdc25 phosphatases are required for timely assembly of CDK1-cyclin B at the G2/M transition. The Journal of Biological Chemistry *285*, 16978–16990.

Toresson, H., Potter, S.S., and Campbell, K. (2000). Genetic control of dorsal-ventral identity in the telencephalon: opposing roles for Pax6 and Gsh2. Development *127*, 4361–4371.

Tseng, L.-C., and Chen, R.-H. (2011). Temporal control of nuclear envelope assembly by phosphorylation of lamin B receptor. Molecular Biology of the Cell *22*, 3306–3317.

Vernon, A.E., Devine, C., and Philpott, A. (2003). The cdk inhibitor p27Xic1 is required for differentiation of primary neurones in Xenopus. Development *130*, 85–92.

Waclaw, R.R., Allen, Z.J., Bell, S.M., Erdélyi, F., Szabó, G., Potter, S.S., and Campbell, K. (2006). The zinc finger transcription factor Sp8 regulates the generation and diversity of olfactory bulb interneurons. Neuron *49*, 503–516.

Walczak, C.E., Cai, S., and Khodjakov, A. (2010). Mechanisms of chromosome behaviour during mitosis. Nature Reviews. Molecular Cell Biology *11*, 91–102.

Wang, W., Bu, B., Xie, M., Zhang, M., Yu, Z., and Tao, D. (2009a). Neural cell cycle dysregulation and central nervous system diseases. Progress in Neurobiology *89*, 1–17.

Wang, Y., Ji, P., Liu, J., Broaddus, R.R., Xue, F., and Zhang, W. (2009b). Centrosome-associated regulators of the G(2)/M checkpoint as targets for cancer therapy. Molecular Cancer *8*, 8.

Weissman, T., Noctor, S.C., Clinton, B.K., Honig, L.S., and Kriegstein, A.R. (2003). Neurogenic radial glial cells in reptile, rodent and human: from mitosis to migration. Cerebral Cortex *13*, 550–559.

Wheatley, S.P., Hinchcliffe, E.H., Glotzer, M., Hyman, a a, Sluder, G., and Wang, Y.L. (1997). CDK1 inactivation regulates anaphase spindle dynamics and cytokinesis in vivo. The Journal of Cell Biology *138*, 385–393.

White, M.A., Riles, L., and Cohen, B.A. (2009). A systematic screen for transcriptional regulators of the yeast cell cycle. Genetics *181*, 435–446.

Wolf, F., Wandke, C., Isenberg, N., and Geley, S. (2006). Dose-dependent effects of stable cyclin B1 on progression through mitosis in human cells. The EMBO Journal *25*, 2802–2813.

Woods, C.G., Bond, J., and Enard, W. (2005). Autosomal recessive primary microcephaly (MCPH): a review of clinical, molecular, and evolutionary findings. American Journal of Human Genetics *76*, 717–728.

Wu, S.-X., Goebbels, S., Nakamura, K., Nakamura, K., Kometani, K., Minato, N., Kaneko, T., Nave, K.-A., and Tamamaki, N. (2005). Pyramidal neurons of upper cortical layers generated by NEX-positive progenitor cells in the subventricular zone. Proceedings of the National Academy of Sciences of the United States of America *102*, 17172–17177.

Xie, J., Yin, H., Nichols, T.D., Yoder, J.A., and Horowitz, J.M. (2010). Sp2 Is a Maternally Inherited Transcription Factor Required for Embryonic Development. Journal of Biological Chemistry *285*, 4153–4164.

Yang, D., Rismanchi, N., Renvoisé, B., Lippincott-Schwartz, J., Blackstone, C., and Hurley, J.H. (2008). Structural basis for midbody targeting of spastin by the ESCRT-III protein CHMP1B. Nature Structural & Molecular Biology *15*, 1278–1286.

Yin, H., Nichols, T.D., and Horowitz, J.M. (2010). Transcription of mouse Sp2 yields alternatively spliced and sub-genomic mRNAs in a tissue- and cell-type-specific fashion. Biochimica Et Biophysica Acta *1799*, 520–531.

Yingling, J., Youn, Y.H., Darling, D., Toyo-Oka, K., Pramparo, T., Hirotsune, S., and Wynshaw-Boris, A. (2008). Neuroepithelial stem cell proliferation requires LIS1 for precise spindle orientation and symmetric division. Cell *132*, 474–486.

Young, K.M., Fogarty, M., Kessaris, N., and Richardson, W.D. (2007). Subventricular zone stem cells are heterogeneous with respect to their embryonic origins and neurogenic fates in the adult olfactory bulb. The Journal of Neuroscience *27*, 8286–8296.

Yüce, O., Piekny, A., and Glotzer, M. (2005). An ECT2-centralspindlin complex regulates the localization and function of RhoA. The Journal of Cell Biology *170*, 571–582.

Zetterberg, a, Larsson, O., and Wiman, K.G. (1995). What is the restriction point? Current Opinion in Cell Biology *7*, 835–842.

Zhang, X., Chen, Q., Feng, J., Hou, J., Yang, F., Liu, J., Jiang, Q., and Zhang, C. (2009). Sequential phosphorylation of Nedd1 by Cdk1 and Plk1 is required for targeting of the gammaTuRC to the centrosome. Journal of Cell Science *122*, 2240–2251.

Zhao, W., Seki, A., and Fang, G. (2006). Cep55, a microtubule-bundling protein, associates with centralspindlin to control the midbody integrity and cell abscission during cytokinesis. Molecular Biology of the Cell *17*, 3881–3896.

Zhu, C., and Jiang, W. (2005). Cell cycle-dependent translocation of PRC1 on the spindle by Kif4 is essential for midzone formation and cytokinesis. Proceedings of the National Academy of Sciences of the United States of America *102*, 343–348.